UNIVERSIDAD NACIONAL DE INGENIERÍA

FACULTAD DE CIENCIAS

TESIS

"DEVELOPMENT IN C++ AND PYTHON OF A TIME STRUCTURE ANALYSIS TOOL FOR PARTICLE BEAM ANALYSIS FOR THE MINERvA TEST BEAM EXPERIMENT"

PARA OBTENER EL GRADO ACADÉMICO DE MAESTRO EN CIENCIAS CON MENCION EN FÍSICA

ELABORADO POR:

GERALD FERNANDO SALAZAR QUIROZ

ASESOR:

Dr. CARLOS JAVIER SOLANO SALINAS

LIMA – PERÚ

2016

Dedicado a Fisher, Arnold, Ana, Nataly, Abel y Carmen.

Do not go gentle into that good night,
Old age should burn and rave at close of day;
Rage, rage against the dying of the light.

Though wise men at their end know dark is right,
Because their words had forked no lightning they
Do not go gentle into that good night.

Dylan Thomas, 1914 - 1953

Acknowledgments

How can anyone resume all the time, help, advice and support received over the time that this thesis was done in a couple of lines?. For all of them thanks, even the tiny hint was useful and well taken. However, there are some important persons and institutions that I do want to thanks.

To my advisor Dr. Javier Solano for his support and advice during all the time I spent at Fermilab, as well to Dr. Jorge Morfin: great listener and even greater physicist. To all the MINERvA Collaboration and specially to Deborah for their kindest support. From the very first moment in the experiment I was able to see by myself that science is truly a hard, colaborative and open endeavour in the pursue of knowledge.

To the Test Beam crew: Leo Bellatoni for all the guidance, Aaron Bercellie, Rob Fine, Anne Norrick and Geoff Savage, as well to Howard Budd for the countless hours teaching me the basis of how to be a Detector Expert. To Edgar Valencia, from who I receive my first hints in the painful walk of learning ROOT, which by the way it is not as hard as once appered specially when my code was crashing even that, minutes before it was working okey. Of course I know the answer to that: bad use of pointers.

To Paola from who I am still learning a lot of great things. To my 5 Sauk Circle's friends: Aaron, Anu, Anna and Maya. During the time I was writing this thesis my mind was driven gently to the awesome time we spent together, and finally to Mayra (#FA's for the win).

Abstract

We present in this thesis the results of the design and programming of a temporal analysis tool for experiment data MINERVA Test Beam (TbTaTool), which receives pions and electrons in the energy range corresponding to the end of the interactions of neutrinos energy states with MINERvA detector. The TbTaTool is independent, flexible and adaptable to other contexts where we need to analyze the distribution of events over time, because it has separated datasets' production from the tool itself. Our tool has been applied to the data (Run 2 and Run 3) that the experiment has obtained in MTest at Fermilab, focusing on the variables of frequency of spill of the particles (MI's spill frequency), duration of spill (MI's spill duration) and the profile over time of packets corresponding to the delivery of the particles (time profile). Our calculations show 0.01% of difference for the frequency of spill of the particles and 9.34%, for the second variable, compared to the values indicated by the Fermilab's Accelerators Division. Furthermore, this tool had set the basis for constructing a real time DAQ visualizator of the measurement process.

Resumen

Se presenta los resultados del diseño y programación de una herramienta de análisis temporal para los datos del experimento MINERvA Test Beam (TbTaTool), que recibe piones y electrones en el rango de energía correspondiente a los estados energéticos finales de las interacciones de neutrinos con el detector MINERvA. El TbTaTool es independiente, flexible y adaptable a otros contextos donde se quiera analizar la distribución de eventos respecto al tiempo. Nuestra herramienta ha sido aplicada a los datos (Run 2 y Run 3) que el experimento ha obtenido en el MTest en el Fermilab, enfocándonos en las variables de frequencia de entrega de las partículas (MI's spill frequency), duración de la entrega (MI's spill duration) y el perfil en el tiempo de los paquetes correspondientes a la entrega de las partículas (Time Profile). Nuestros cálculos muestran un 0.01% de diferencia para la frecuencia de entrega de las partículas y 9.34%, para la segunda variable, frente a los valores indicados por la División de Aceleradores de Fermilab. Además esta herramienta ha establecido el fundamento para la construcción de visualizador del proceso de adquisicion de datos en tiempo real.

Contents

List of Figures

List of Tables

Introduction

In **Chapter 1**, a theoretical review of weak interactions is done in order to describe the weak sector of the Standard Model (sec. 1.1) and introduce the neutrino oscillation research (sec. 1.2). By now we know that the deficit in the solar and atmospheric neutrinos reaching the earth is due to neutrino non-zero mass which express in neutrino flavour oscillations. However in order to confirm the value of masses between the three neutrinos more precise experiments are needed in the reduction of systematic erros due to neutrino interactions with the detectors. This is the motivation of the neutrino experiments like MINERvA **Chapter 2 and 3**. The improve of detection models between neutrinos and nucleus, since modern experiments are and will rely more on heavy nucleus detectors like argon or lead. The calorimetric response and the fine detection of last product pions by the detector allows to reconstruct the incoming neutrino energy. MINERvA face this challenge by setting up a small scale replica detector called Test Beam Detector **Chapter 4** where we receive particles of knwo momenta and type in order to improve the models detection of pions, muons and electrons of the main detector.

But, as important of knowing the composition of the beam, it is important to know the time structure of it, in order to set up timing resolution of your detection system. That is what this analysis has carried out, a comprobation of the timing in the scale of Main Injector time space: the spill. In **Chapter 4** and **Appendix C** a review of the Time Structure of the Beam and the Electromagnetic theory of Radio Frequency Cavities are stated. Section 4.3 describe why the beam that we received have a specific structure in time.

In **Chapter 6**, we describe the Analysis Tool developed in C++ and ROOT that allow us to analysis the scale of spill. Its features and how the tool works close that chapter. Finally in **Chapter 7**, **Appendix A** and **Chapter 8** we present the results and conclusions fo this work.

I must mention that I had a small contribution in two publications of MINERvA:

(a) **Physical Review D** Vol 92 (2015) 9, 092008

Título: Charge pion production in interactions on hydrocarbon at <E>!= 4.0GeV

Autores: G. Salazar, A. Zegarra, C. J. Solano Salinas and the MINERvA Colaboration

(b) Physical Review Letters Vol 116 (2016) 081802

Title: Measurement of Electron Neutrino Quasielastic and Quasielasti-clike Scattering on Hydrocarbon at <E>!= 3.6GeV

Authors: G. Salazar, A. Zegarra, C. J. Solano Salinas and the MINERvA colaboration)

Finally in Appendix B, a review of other activities during the intership at Fermilab has been described. In the **Appendix D** we present the documentantion and in **Appendix E** the parts of the code. **The final tool can be found in a public repository at github**[1].

[1] https://github.com/gsalazarq/TbTaTool/tree/master/TbTaTool

Chapter 1

Theoretical Framework

One of the greatest achievements in science, is the formulation of the Standard Model of Particle Physics, a quantum field theoretical framework which has the most complete description of the fundamental process in nature.

As a quantum field theory, the Standard Model (SM) has been formulated in terms of Lagrangians, with three fields: Gauge fields (bosons of spin 1 whose mediate forces), Weyl fermions (which outline massless neutrinos) and a spin 0 scalar field which describe the Higgs boson. These SU(3)xSU(2)xU(1) gauge fields portray what types of particles and interactions are allowed, where the SU(3) gives rise to the strong interactions, SU(2) and U(1) describe the weak and electromagnetic interactions.

The success of this model, has been stated because the predictions of new phenomena and particles in a very precise way while the technology started to reach the values of energies required. For example: in 1974, the discovery of the J/psi (c quark); in 1977, the b quark; in 1981/82, W+- and Z bosons were discovered. The appear of the Higgs boson in 2012 is probably one of the most important milestones achieve by the Standard Model.

But, as impressive the predictions of the SM are, also the gaps and new findings that do not fit in the theoretical framework. The baryon asymmetry of the Universe ([23, p. 9]), the identity of dark matter, for how long the proton lives? or the neutrino's masses are a couple of flags inside the model. It is the neutrino oscillations and the related neutrino cross-section scattering research that give experiments like MINERνA the fuel to look deeper into the nature of interactions of neutrinos with matter.

One of the most impressive feature of the neutrino is that is not massless, in contradiction with the Standard Model. Neutrinos research is one of the most interesting, growing and intensive area of research in particle physics, with future experiments that involve billions of investment as is the case of the DUNE experiment.[1] [2]

It is worth to mention that the 2015 Physics' Nobel Prize went to T. Kajita and A. McDonald for the neutrino's oscillations research in Super-Kamiokande (Japan) and the SNO Experiment (Canada) (fig. (1.1)):

> "For the discovery of neutrino oscillation which shows that neutrinos have mass"[3]

Other neutrino Nobel Prizes have been awarded in **1988** to L. M. Lederman, M. Schwartz and J. Steinberger "for the neutrino beam method and the demonstration of the doublet structure of the leptons through the discovery of the muon neutrino"; in **1995** to M. L. Perl "for the discovery of the tau lepton" and F. Reines "for the detection of the neutrino"; in **2002** to R. Davis Jr. and M. Koshiba "for pioneering contributions to astrophysics, in particular for the detection of cosmic neutrinos" and R. "for pioneering contributions to astrophysics, which have led to the discovery of cosmic X-ray sources"[4]. For sure, those Nobel Prizes will not be the last one to be awarded to neutrino research.

1.1 Weak Interactions

Decays of μ and τ decays' and natural radioactivity are due to weak interactions. Even that unified weak and electromagnetic theory was proposed by S. Weinberg

[1] The Deep Underground Neutrino Experiment (DUNE) is a proposed experiment with a near detector at Fermilab and a far detector at the Sanford Underground Research Facility at South Dakota. This international mega-science project is designed to discover, for example, if neutrinos exhibit matter-antimatter asymmetries. More information at http://www.dunescience.org/

[2] Ghosh, Pallab (15 February 2014). "UK backs huge US neutrino plan". BBC News. Retrieved 15 February 2014.

[3] http://www.nobelprize.org/nobel_prizes/physics/laureates/2015/

[4] The quotations have been reviewed from the official page of the Nobel Prize Foundation http://www.nobelprize.org/nobel_prizes/physics/laureates/

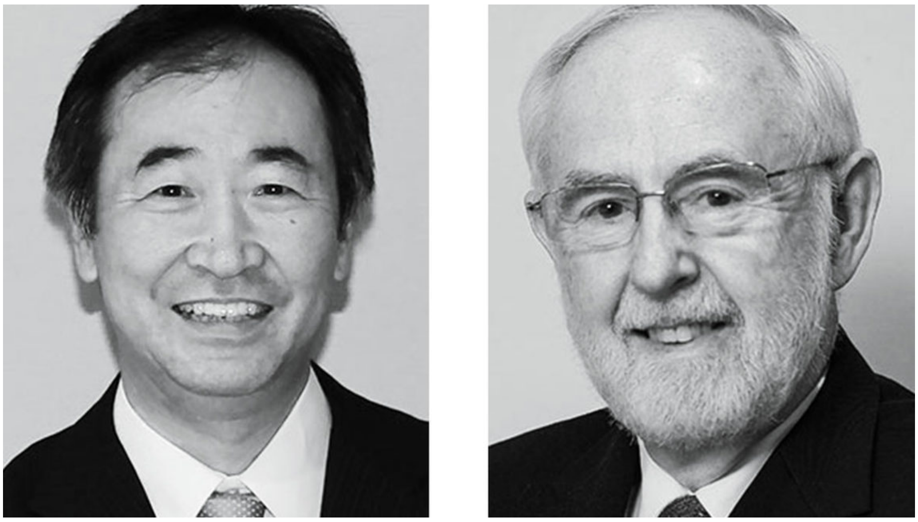

Figure 1.1: The 2015 Nobel Prize in Physics winners: Takaaki Kajita (left) and Arthur B. McDonald (right)

and A. Salam in the late sixties, the actual discovery of the mediators did not happen until January of 1983.

During the decade 1964-1974 ([16, p. 42]), the particle physics theoretical framework was incomplete and full of new discoveries that did not fit on it. In the summer of 1974, the ψ meson was first observed at Brookhaven Laboratory by a group under C.C. Ting, with a lifetime of 1000 times greater than any particle; by next year it was a new lepton: the tau[30]. In 1983, the W was discovered by Carlo Rubbia's group at CERN[5] (at $81 \pm 5GeV/c^2$ and five months after, the Z^0 (at $95 \pm 3GeV/c^2$)[6].

Now we know that matter is made out of three kind of elementary particles: leptons, quarks and mediators. There are three generations of leptons, according to their charge (Q), electron number (L_e), muon number (L_μ) and tau number (L_τ), each of these numbers define a generation or a family, composed by a lepton and its corresponding neutrino. The classification ends considering the particles and antiparticles, the weak force having two mediators for charge currents ($W^\pm$) and one for neutral current (Z^0).

These three mediators ($W^\pm, Z^0$) correspond to the triplet for $SU(2)_L$ and a single, for $U(1)_Y$ The symmetry breaking in the $SU(2)L \times U(1)Y$ sector gives the

[5] G. Arnison, Physics Letters B, Volume 122, Issue 1, 1983, Pages 103-116.

[6] G. Arnison, UA1 Collaboration. Physics Letters B, Volume 126, Issue 5, 1983, Pages 398-410.

three SU(2) mediators mass thought the interactions with the Higgs Boson. The photon, though stay massless.

Since the three mediators have positive, negative and no charge, the interactions can be ordered into charged currents interactions and neutral currents interactions.

The fundamental charged vertex is presented in the fig. (1.2). A neutrino is produced by its corresponding lepton, with the emission of a W^- (or absorption of W^+)

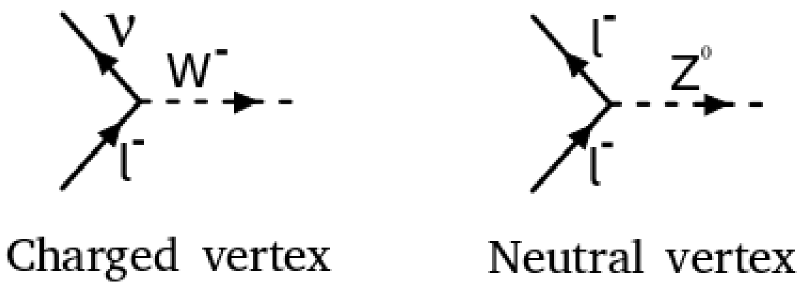

Figure 1.2: Fundamental vertex for weak interactions.

A more complicated reactions can be produce if the primitive diagram is combined, as for example for the reactions:

$$\begin{aligned} \mu^- + \nu_e \rightarrow e^- + \nu_\mu \\ \bar{\nu_e} + p \rightarrow n + e^+ \end{aligned} \tag{1.1}$$

If the target is a nucleon and with the necessary energy of the income neutrino, we can resolve the nucleus as a one (CCQE - Quasielastic Interactions) or as a quarks (DIS - Deep Inelastic Scattering). For example, the reaction (1.1) is called inverse neutron decay and was used by C. Reins and F. Cowan in the discovery of the antineutrino. Also, weak charged current can change lepton and quark flavours.The fundamental neutral current (fig.2.2) was first suggested in 1958 by Bludman[7], that preserves the three leptonic numbers.

The 1973 CERN's bubble chamber, revealed that in the reaction $\bar{\nu_\mu} + e^- \rightarrow \bar{\nu_\mu} + e^-$, a neutral Z^0 was the mediator[8]. The same experiment saw the mediation

[7]C. D. Anderson. "Early Work on the Positron and Muon " American Journal of Physics December 1961 Volume 29, Issue 12, pp. 825

[8]DESY found unmistakable evidence of the contribution of Z^0 by studied the reaction $e^- +$

of this boson in neutrino-nucleon scattering (1.2), with values of three times large as those related with charged events [16, p. 323].

$$\nu_\mu + N \to \nu_\mu + N \tag{1.2}$$

From the values of decay lifetimes we can be inferred the forces that produces and the strength of the interaction. Pions and muons decays' lifetimes (1.3) are considerably longer than particles that decay only by strong and electromagnetic forces. The difference in the order of magnitudes are evidence of the existence of another type of interaction, beside the strong interaction.

$$\pi^- \to \mu^- \bar{\nu}_\mu, \text{ with } \tau = 2.6 \times 10^{-8} sec,$$
$$\mu^- \to^- \bar{\nu}_e \nu_\mu, \text{ with } \tau = 2.2 \times 10^{-8} sec, \tag{1.3}$$

Finally we recall that the lifetimes are inversely related to the coupling strength of this interactions, that means that this new interaction is has weaker coupling than electromagnetism.

Table 1.1: Range of interaction of the four fundamental forces.

Interaction	Range	Lifetime (sec)	Cross Section (mb)	Coupling α_i
Strong	1F $\simeq \frac{1}{m_\pi}$ Color confinement range	10^{-23} e.g. $\Delta \to p\pi$	10 e.g. $\pi p \to \pi p$	1
Electromagnetic	∞	$10^{-20} \sim 10^{-16}$ e.g., $\pi^0 \to \gamma\gamma$ $\Sigma \to \Lambda\gamma$	10^{-3} e.g., $\gamma p \to p\pi^0$	10^{-2}
Weak	$\frac{1}{M_W}$ with $M_W \simeq 100 m_p$	10^{-12} or longer e.g., $\Sigma^- \to n\pi^-$ $\pi^- \to \mu^-\bar{\nu}$	10^{-11} e.g., $\nu p \to \nu p$ $\nu p \to \mu^- p \pi^+$	10^{-6}

$e^+ \to \mu^- + \mu^+$

1.2 Neutrino Physics

Neutrino was proposed by Wolfgang Pauli in 1930 to hold up the energy-momentum conservation law and Fermi's statistics in β-nuclei decay (eq. 1.4). This new particle had to have: no charge, should not interact with matter, or in the other case interact very weakly and almost no mass. For the same problem Bohr, proposed a statistical version of the energy conservation law. Experiments showed that Pauli was right.

$$n^0 \to p^+ + e^- + \bar{\nu}_e \tag{1.4}$$

In 1932, a more massive neutral particle was discovered by Chadwick([8]), and was named neutron. Pauli's name of the unknown particle was turned into neutrinos (little neutron one) by Enrico Fermi, who used it in 1932.

In 1956, the antineutrino was discovered experimentally by F. Reines an C.L. Cowan allowing the interaction of protons with electron antineutrinos' fluxes[9] created in nuclear reactions (eq. 1.5):

$$\bar{\nu}_e + p^+ \to n^0 + e^+ \tag{1.5}$$

The detection was made since a positron quickly finds an electron producing two opposite 0.5 MeV γ rays which are detectable, but not necessarily the indication of the antineutrino existence. Another gamma ray is detected due to capture of the neutron by the nucleus ($n +^{108} Cd \to^{109} Cd^* \to^{109} Cd + \gamma$). This two events configure the signature of an antineutrino interaction looked.

Neutrinos are elementary particles with spin $1/2$, electrically neutral and obey Fermi-Dirac statistics. The Standard Model consider three **Weyl massless neutrino flavors**: ν_e, ν_μ, ν_τ, each one corresponding to three different leptons, the electron e^-, the muon μ^- and the tau τ, each doublet has their antiparticles.

However the nature of neutrino is still open, for sure they are not Weyl's massless fermions. Two plus one options arise: neutrinos can be Majorana neutrinos,

[9] By that time they were expecting $10^{12} - 10^{13}$ neutrinos per second per m^2. They did not know that they were using electronic antineutrinos.

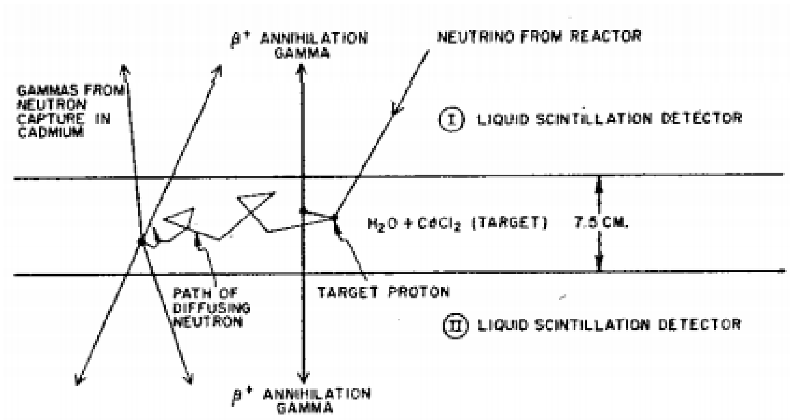

Figure 1.3: Schematic diagram of neutrino detector as appeared in the original paper of Reines and Cowan[10].

Dirac neutrinos or a mix between both where the seesaw mechanics plays an important role.

Parity and CP invariance

Parity is violated in weak interactions as Goldhaber observed, neutrinos have spin antiparallel to their momentum (left-handed) and antineutrinos have it parallel (right-handed).[11]

Not only the parity is violated, but also the charge conjugation invariance, where Γ is the lifetime of process. For instance,

$$\begin{aligned} \Gamma(\pi^+ \to \mu^+ \nu_L) \neq \Gamma(\pi^+ \to \mu^+ \nu_R) \text{ P violation,} \\ \Gamma(\pi^+ \to \mu^+ \nu_L) \neq \Gamma(\pi^- \to \mu^- \bar{\nu_L}) \text{ C violation,} \end{aligned} \tag{1.6}$$

but the CP variance is conserved. Future experiments have as main objective the comprobation of the CP invariance or its violation by neutrinos.

$$\Gamma(\pi^+ \to \mu^+ \nu_L) = \Gamma(\pi^- \to \mu^- \bar{\nu_R}) \text{ CP invariance.} \tag{1.7}$$

1.2.1 Solar and Atmospheric Neutrinos

The **neutrino mass**, is one of the most important discoveries from the last decade outside the framework of the Standard Model[12].

[11] The historic experiment for testing this, was with β-transitions of polarized cobalt nuclei. $^{60}C \to ^{60} Ni^* + e^- + \bar{\nu_e}$

[12] A good review of the physics beyond the Standard Model is made by N. Mihoko in [24]

Solar Neutrinos

The Solar Neutrinos problem was first formulated in 1964 by Ray Davis's and John N. Bahcall from the Homestake Experiment[13], who were the first to look a deficit in the flux of neutrinos from the Sun. Their final results, published in 1998[10], showed that the experimental value, 2.56 ± 0.16 (stat) ± 0.16 (sys) was over 30% of the theoretically flux value 8.5 ± 0.9 SNU [28].[14]

So why the experimental flux that reaches the earth is anomalously low? This is the core question of the Solar Neutrino Problem[1, p. 10].

We are able to distinguish the solar neutrinos, since we know the sun's processes that generate them: fusion of hydrogen to helium: $p + p \rightarrow 2H + e^{+} + \nu_e$, the pp-chain $4p \rightarrow^4 He + 2e^{+} + 2\nu_e$ and the CNO-cycle are process that produce neutrinos[21, p. 9-7].

While measurements of the different solar neutrinos' chains were improved, in the flux did not change. The Sudbury Neutrino Observatory (SNO) with a Cerenkow detector of 1000ton ultra-pure heavy water (D_2O) in an acrylic sphere of 12 m diameter, clearly state that the deficit was not a technical problem, instead the conversion between ν_e and ν_μ was a physical event, later confirmed by KamLAND reactor experiment.[15]

Atmospheric neutrinos

As we know, cosmic rays from outer space interact with the atmosphere generating particles that come into the earth's surface. Through these decays processes (eq. 1.8), we are able to study the flux atmospheric of electron and muon neutrinos putting the detectors underground, shielding them from the muons and electrons generated.

[13] A lot of information about the experiment and the papers can be found on the web page http://www.nu.to.infn.it/exp/all/homestake/

[14] A SNU is the solar neutrino unit (SNU). It is equal to the neutrino flux producing 10^{-36} captures per target atom per second.

[15] As mentioned before, with the Super-Kamiokande Collaboration won the 2015 Physics Nobel Prize.

$$\pi^{\pm} \rightarrow \mu^{\pm} + \nu_{\mu}(\bar{\nu_{\mu}})$$
$$\mu^{\pm} \rightarrow e^{\pm} + \nu_{e}(\bar{\nu_{e}}) + \bar{\nu_{\mu}}(\nu_{\mu}) \tag{1.8}$$

At low energies ($\leq 1GeV$), the ratio between the flux of muon-neutrinos to electron-neutrinos was around ~ 2[15][16]. A better ration index was later improved defining R as the ratio of data to theoretical expectation fluxes. The IMB experiment [17] reported $R \sim 0.54$[19] and Kamiokande$R \sim 0.60$[18].

Later, T. Kajita from Super-Kamiokande experiment[18] presented compelling evidence in favour of neutrino oscillations in the neutrino conference Neutrino'98[14].

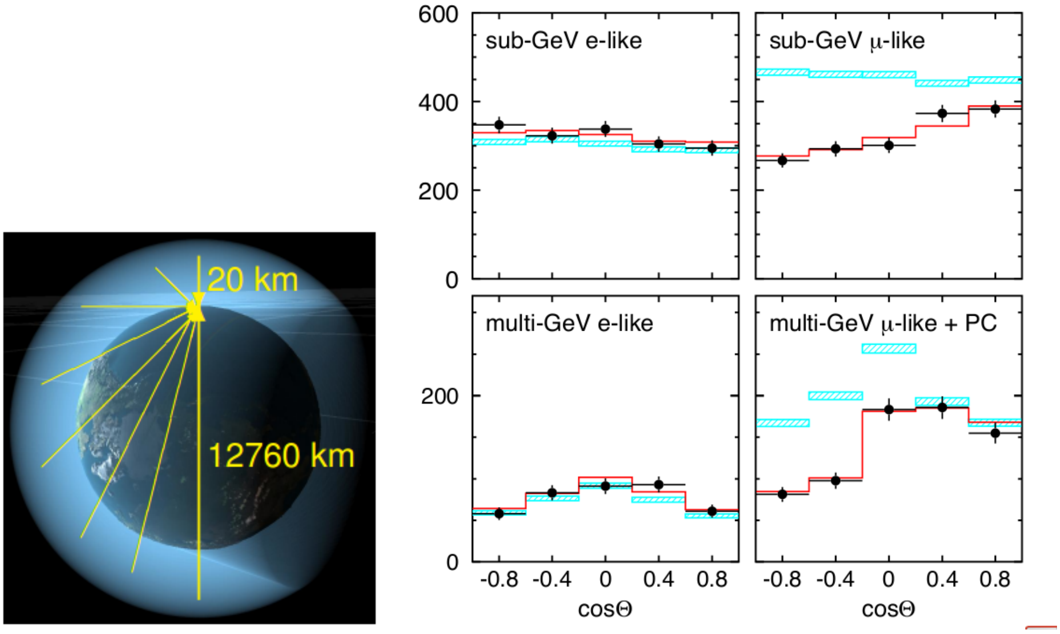

(a) (b)

Figure 1.4: (a) Path of the atmospheric neutrinos during its travels through the earth. (b) Zenith angle events distribution of e-like and μ-like events in Super-Kamiokande in the range of energy below 1.33GeV[11]. The red line, indicates the best fit for the data points, while the boxes show the Monte Carlo events expectation considering no oscillations.

If the flux of neutrinos coming from the atmosphere is expected to be isotropic, independent of the zenith, a question raised, why the observed fluxes of up-going

[16]The ratio is defined as $R = (N_{\mu}/N_{e})_{DATA}/(N_{\mu}/N_{e})_{MC}$

[17]The Irvine-Michigan-Brookhaven Water-Cerenkov detectors (Ohio, USA) `http://www-personal.umich.edu/~jcv/imb/imb.html`

[18]Super-Kamiokande Collaboration a 50000t water Cerenkov detector, 10 times larger than its predecessor Kamiokande in the Mozimu zinc mine, Japan.

and down-going neutrinos in an underground detector are not the same?. While the flux of e-neutrinos has almost no zenith angle dependece (right plots from fig. 1.4), the μ-neutrinos's flux of down-going ($cos\theta = 1$) exceeds the flux of up-going ν_μ.

The most simple explanation was accepted: neutrino flavour oscillation. Neutrinos moving upward through the detector are created in the atmosphere at the opposite side of the Earth, and travel thousand of kilometers before interaction.

Apparently muon-neutrinos disappear on the way whereas electron-neutrinos do not. Down-going muon-neutrinos, produced in the atmosphere directly above the detector, only travel a few dozen kilometers and are detected at the level expected. No indication of an increased electron-neutrino flux, the missing muon-neutrinos must have oscillated into tau-neutrinos.

After 1998, neutrino oscillations started to open a new set of question that needed to be answered through the design of new experiments focus on neutrino oscillations, and as we will mention, a shears experiments started to work in the improvement of the models of neutrino-nucleus interaction, like MINERνA (sec. 3.1). In the next section, a brief review of the oscillation of only two flavours are made.

1.2.2 Neutrino oscillations

Consider for simplicity that two of the known neutrinos ν_e and ν_μ are eigenstates with *no well defined masses* but they are a linear composition of the *neutrino mass eigenstates* ν_1 and ν_2 with masses m_1 and m_2, respectively:

$$\begin{aligned} |\nu_e\rangle &= |\nu_1\rangle cos\theta + |\nu_2\rangle sin\theta \\ |\nu_\mu\rangle &= -|\nu_1\rangle sin\theta + |\nu_2\rangle cos\theta, \end{aligned} \tag{1.9}$$

where θ is the neutrino mixing angle. We will get the dependece of the oscillation probability with the energy and the difference of masses. Following the rules of quantum mechanics, we can construct the state at any time t, and then get the probability of transformation from a state to another.

First, lets consider that at time $t = 0$. We have a pure weak eigenstate

$|\nu(0)\rangle = |\nu_\mu\rangle$, the propagation of this state in time is dictated by the free non-time dependent Hamiltonian.

$$|\nu_t\rangle = -|\nu_1\rangle e^{-iE_1 t} sin\theta + |\nu_2\rangle e^{-iE_2 t} cos\theta, \tag{1.10}$$

where $E_{1,2} = \sqrt{p^2 + m_{1,2}^2} \approx p + \frac{m_{1,2}^2}{2p}$. The probability of finding a neutrino with electron flavor is then:

$$\begin{aligned} P(\nu_\mu \to \nu_e; t) &= |\langle \nu_e | \nu(t) \rangle|^2 \\ &= sin^2\theta cos^2\theta | - e^{-E_1 t + e^{-iE_2 t}}|^2 \\ &= sin^2 2\theta sin^2(\frac{\Delta m^2 t}{4E}) \\ &= sin^2 2\theta sin^2(\frac{\Delta m^2 L}{4E}) \end{aligned} \tag{1.11}$$

Here $\Delta m^2 = m_2^2 - m_1^2$ is the squared mass difference and $E = p$. The last line is valid for relativistics particles ($L = t$) with L being the traveled distance, which in practice allow us to construct tunels of decays in order to observe the oscillation, or in turn place the far and near detector in an oscillation experiment at a fixed distance.

As it can be seem the mass difference is present in the form of a squared difference, hence the measuring oscillation probabilities will not give absolute values of the masses. In the table (1.2), different sources of neutrinos and the minimum value that can reach the measurement of min(Δm^2)[eV^2].

This model with two flavors, can be extended to one with three flavor mixing and three angles, three squared massess differences Δm_{12}^2, Δm_{13}^2 and Δm_{23}^2. [20]

Table 1.2: Sensitivity of different oscillation experiments.[32, p. 11]

Source	Type of ν	E[MeV]	L[km]	min(Δm^2)[eV^2]
Reactor	$\bar{\nu_e}$	~ 1	1	$\sim 10^{-3}$
Reactor	$\bar{\nu_e}$	~ 1	100	$\sim 10^{-5}$
Accelerator	$\bar{\nu_{mu}}, \nu_\mu$	$\sim 10^3$	1	~ 1
Accelerator	$\bar{\nu_{mu}}, \nu_\mu$	$\sim 10^3$	1000	$\sim 10^{-3}$
Atmospheric ν's'	$\bar{\nu_{e,\mu}}, \bar{\nu_{\mu,e}}$	$\sim 10^3$	10^4	$\sim 10^{-4}$
Sun	ν_e	~ 1	1.5×10^8	$\sim 10^{-11}$

Chapter 2

Neutrino Experiments

In recent years, many experiments[1] have been setup in order to improve the models of interaction between detectors and neutrinos due to requirement of neutrino oscillation experiments.

Neutrino interaction's models need to predict not only the signal and background of mass neutrino oscillation, but also how the energy is transfered to the observable particles, while reducing the uncertainties[2]. As mentioned by D. Harris: [17, p- 1]

"Future oscillation experiments such as DUNE [9] depend on the ability to predict far detector signal's (background) spectra at the 1% (5%) level (...), the particle physics community is still at the level of measuring cross sections and making far detector predictions at the $7-10\%$ level."

New oscillation experiments need to expand the models for other nucleus than hydrogen or deuterium, since the far and near detectors are made of targets of carbon, water, argon or iron. Another requirement for neutrino cross-section experiments is to focus energy region of few hundred MeV to a hand full of GeV, since oscillation probabilities are function of the inverse of the neutrino energy.

It is worth to mention that MINERνA has a 15% constrain from a CCQE measurements and 10% in the flux uncertainties "[17].

[1] Only for mention some of them: MINERνA, T2K (Tokai to Kamioka), NOνA, MINOS and MicroBooNE

[2] Another source of uncertainty comes from the incoming neutrino flux which is now at 8% to 10%.

MINERνA[3] is a cross-sections precision studies experiment of (anti)neutrino-nucleus scattering in the range of 1-20GeV at the NuMI Beam at Fermilab. The tracking region is made purely by scintillators which recognize the particle by the energy loss per unit length (dE/dx) after the neutrinos had interacted with the targets (carbon, iron and lead) interleaved between the scintillator planes. Technical details of the experiment will be describe in sec. 3.1.

This chapter state the principal concepts of neutrino interactions with matter (sec. 2.1), the different regions of cross-section interaction ν-A regarding the energy (sec. 2.2) and experiments that perform measurements of neutrino's properties (sec. 2.3).

2.1 Neutrino interaction with matter

The cross-section (σ) quantify the interactions between particles and targets, regarding energy, flux and type of interactions taking place (if it is a strong, electromagnetic or a weak interaction).

Defined as the rate (sec. 2.1) of interactions between incoming particles that are scattered due to the interaction with the targets over a known energy and flux of incoming particles,

$$\sigma = \frac{\text{Number of reactions of a given type per unit time}}{\text{(Incoming flux)(Number of target particles)}} \tag{2.1}$$

σ is a number that has dimensions of area and is usually expressed in cm^2 or in barns (1barn $= 10^{-24}cm^2$)[45].

Differential cross-sections ($d\sigma/dA$) is a distribution of probability, which give us the dependence of the cross-sections to an specific variable (A), for example the angle range $d\theta$ around some direction θ.

An **elastic cross-sections**, is a type of interaction where neither beam particle or the target has been disintegrated, the opposite is called an **inelastic cross-**

[3]Main INjector ExpeRiment ν-A

[4]The proton-proton cross-sections is 40mb

[5]For each cross-section corresponding to a particular type of interaction, the term partial is added.

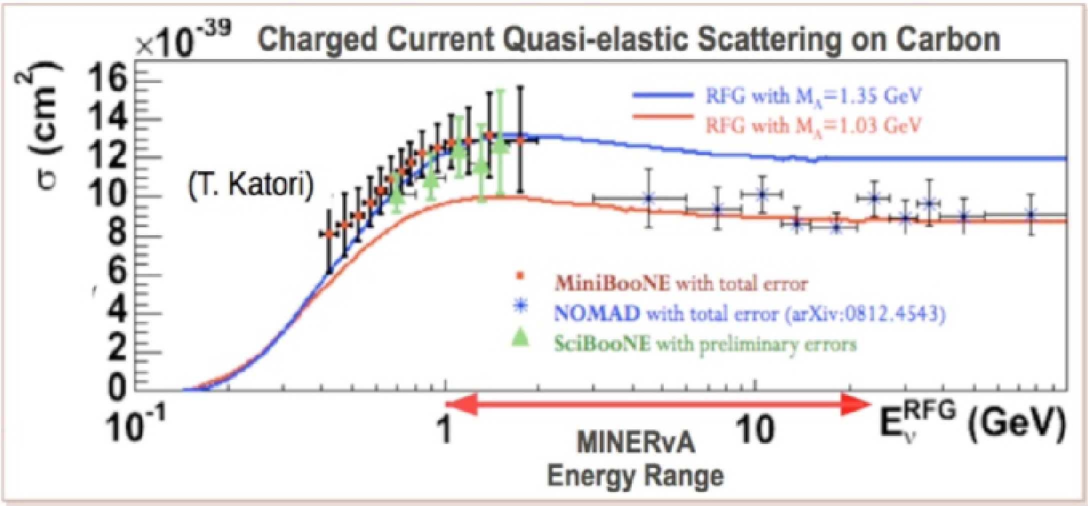

Figure 2.1: Total cross-sections for Charge Current Quasi-elastic Scattering on Carbon measured by different experiments. This figure has been taken from the Conference MINERνA 101 by C. Patrick [27]

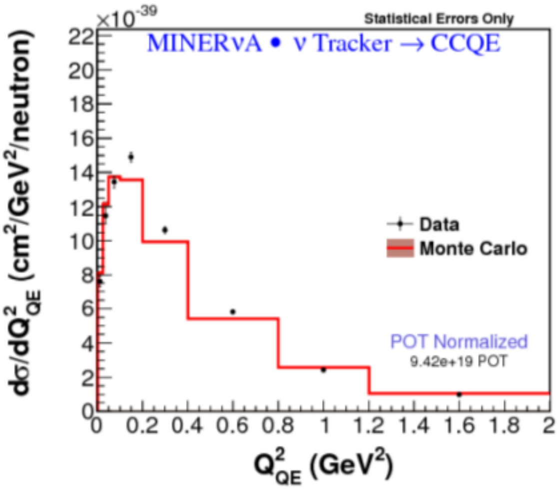

Figure 2.2: Fundamental vertex. This figure has been taken from the Conference MINERνA 101 by C. Patrick [27]

sections. When we sum the inelastic and elastic interaction, the cross-sections is called **total cross-sections**, while the **inclusive cross-sections** is referred to all the process that contains at least one π^+ in the final state (e.g., $p + p \rightarrow \pi^+$) an **exclusive cross-section** is when the final stated is exclusively defined with no extras (e.g., $p + p \rightarrow p + p + \pi^0$).

In the next section, it will be described the three most important process of this intermediate energy region[6].

2.1.1 Intermediate Energy Cross Sections

In the range of $E_\nu \sim 0.1 - 20$GeV three main categories in neutrino scattering are: elastic and quasi-elastic, resonance production and deep inelastic scattering.

The ***elastic and quasi-elastic scattering*** is produce when a neutrino elastically scatter off a nucleon target, liberating a nucleon (or many of them) from it. Quasi-elastic scattering is also referred as charged current neutrino scattering (CCQE), while neutral current scattering is traditional named as elastic scattering.

The next region is the ***resonance production region*** going up in the range of energy, neutrinos can excite nucleon's target into a baryonic resonance state (Δ, N^*), and decay into many mesonic final states producing combinations of nucleons and mesons.

Finally, the ***deep inelastic scattering's*** energy allows the neutrino resolve the individual quark constituents of the nucleon, that usually is expressed with the creation of hadronic showers. Nuclear effects have more impact in the cross-section scattering in the subregion. The fig. (2.3) summarizes the total neutrino and antineutrino per nucleon in the CC Cross Section (charged current interactions).

[6] The complete classification made by J. A. Formaggio and G.P. Zeller [13] is: (1) Thresholdless processes ($E_\nu \sim 0 - 1$MeV), (2) Low Energy Nuclear Processes ($E_\nu \sim 1 - 100$MeV), (3) Intermediate Energy Cross Section ($E_\nu \sim 0.1 - 20$GeV), (4) High Energy Cross Section ($E_\nu \sim 20 - 500$GeV) and (5) Ultra High Energy Neutrinos ($E_\nu \sim 0.5$TeV -1EeV)

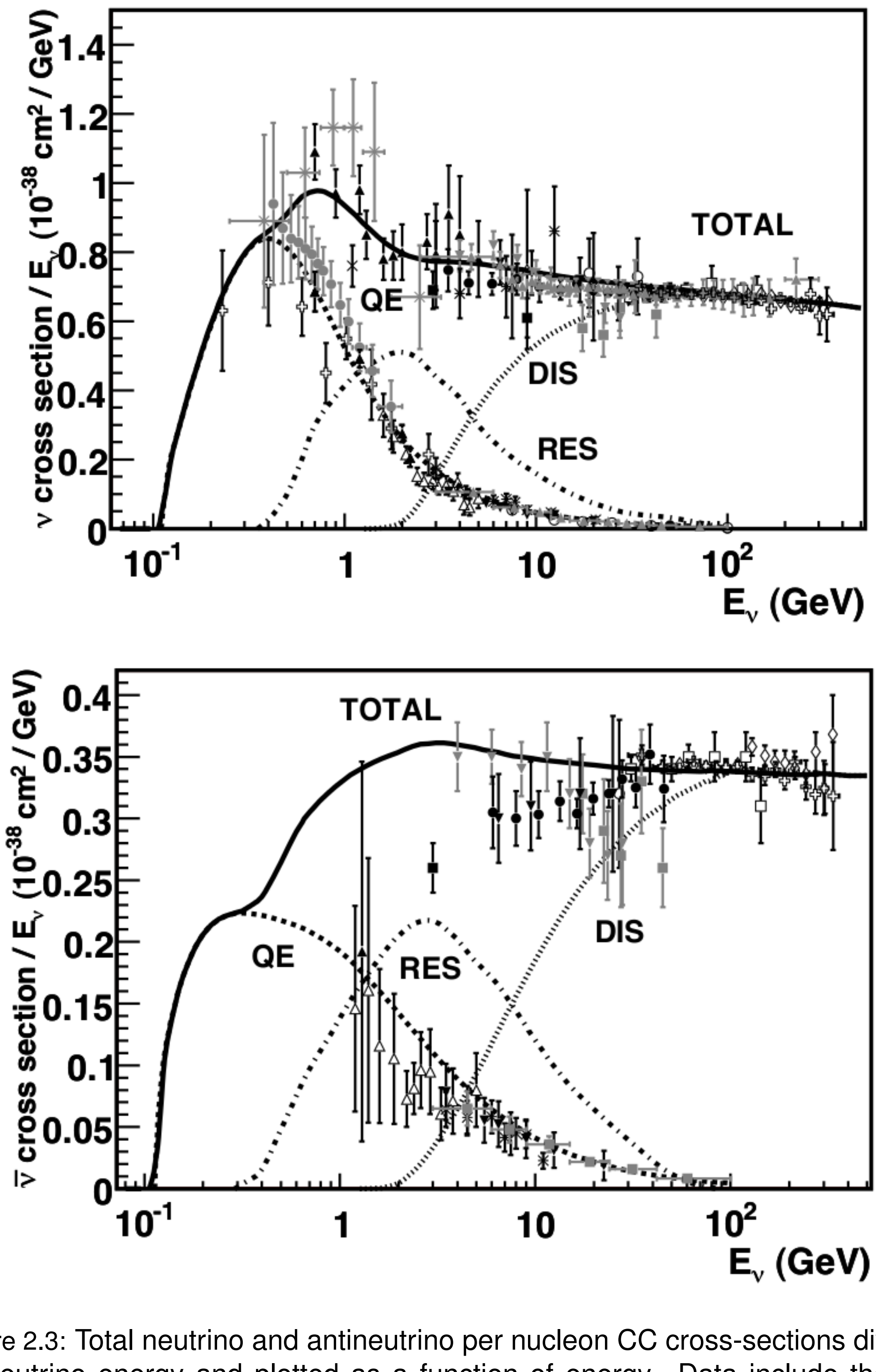

Figure 2.3: Total neutrino and antineutrino per nucleon CC cross-sections divided by neutrino energy and plotted as a function of energy. Data include the low energy data from ▲ ([6]), ∗ ([]), ■ ([]), and ⋆ ([]). The three main regions are ploted as quasi-elastic (dashed), resonance production (dot-dash), and deep inelastic scattering (dotted). The predicitions for each region are provided by the NUANCE generator ([7])

Quasi-elastic Scattering

Quasi-elastic (QE) interactions are produced when a neutrino scatter off a nucleon and create a charged lepton. A typical reaction (eq. 2.2) produce a proton, a neutron and the corresponding charged muon. If the energy of the neutrino is less $\sim$ 2GeV, is more likely to have a CCQE event. These events are the dominant signal mechanics for T2K and a large fractions for NOvA experiment.

$$\begin{aligned} \nu_\mu + n \rightarrow \mu^- + p, \\ \bar{\nu_\mu} + p \rightarrow \mu^+ + n \end{aligned} \tag{2.2}$$

For quasielastic interactions, the cross section is given by the Llewellyn Smith formalism[7]

$$\frac{d\sigma}{dQ^2} = \frac{G_F^2 M^2 |V_{ud}|^2}{8_\nu^2}[A \pm \frac{(s-u)}{M^2} + \frac{(s-u)^2}{M^4}C], \tag{2.3}$$

where $\pm$ referes to (anti)neutrino scattering, G_F is Fermi's coupling constant, Q^2 is the squared four-momentum transfer ($Q^2 = -q^2 > 0$) M is the nucleon mass, m is the lepton mass, E_ν is the incident neutrino energy, and $(s-u) = 4ME_\nu - Q^2 - m^2$. The factors A, B and C are functions of the familiar vector (F_1 and F_2), axial-vector (F_A), V_{ud} is element of CKM-Matrix[8] for quark mixing, and the pseudoscalar (F_P).

With CCQE interactions we can study the weak nucleon form-factors and fully reconstruct the incoming energy neutrino[9] which is critical for measuring the oscillation parameters. However, the uses for CCQE are complicated with heavier targets.

It can be seen from the fig. (2.4) that the predicted values are bellow the experimental data, this comes from the fact that nucleon-nucleon correlations and two-body exchange currents must be included for improving the accuracy of

[7]C.H. Llewellyn Smith, Phys. Rep. 3, 261 (1972).

[8]N. Cabibbo (1963). "Unitary Symmetry and Leptonic Decays". Physical Review Letters 10 (12): 531–533 M. Kobayashi, T. Maskawa; Maskawa (1973).
"CP-Violation in the Renormalizable Theory of Weak Interaction". Progress of Theoretical Physics 49 (2): 652–657

[9]The initial nucleon is at rest and by reconstructing the momentum transfer simply by measuring the outgoing muon's momentum and angle and assuming conservation of total momentum and energy.

neutrino-nucleus QE scattering.[17].

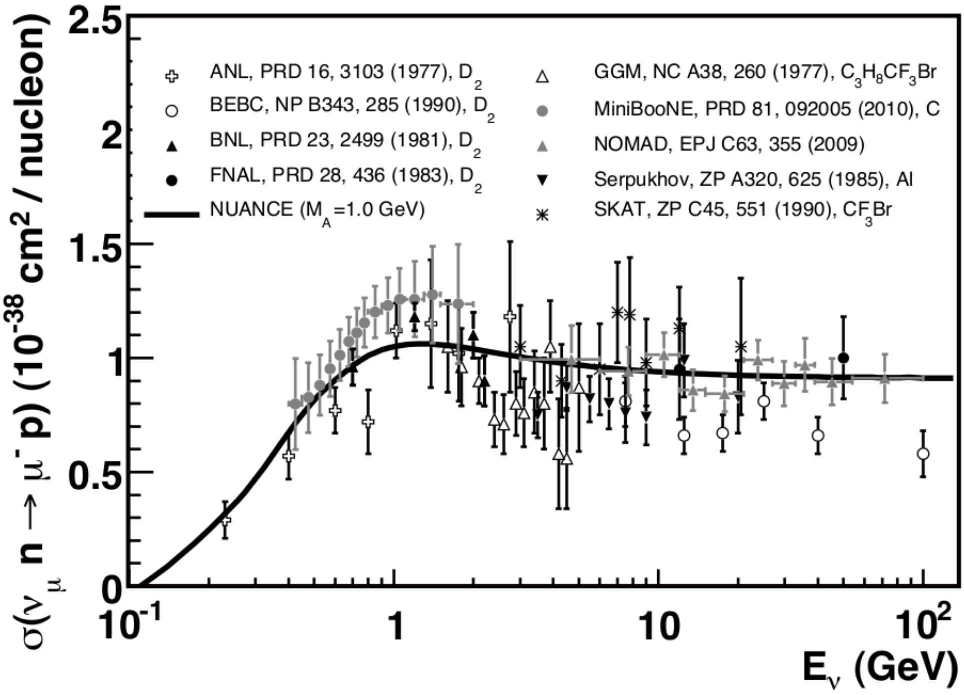

Figure 2.4: All ν_μ quasi-elastic scattering cross-sections, $\nu_\mu n \rightarrow \mu^- p$ measurements until the year 2002 by [7] as a function of neutrino energy for different nuclear targets.

Neutral Charge Elastic Scattering

According with the Glashow-Weinberg-Salam theory, the weak interaction has also a neutral boson Z^0 bosons, that are responsible for neutral current interactions like:

$$\begin{aligned} \bar{\nu_\mu} + e^- \rightarrow \bar{\nu_\mu} + e^- \\ \nu_\mu + e^- \rightarrow \nu_\mu + e^- \end{aligned} \tag{2.4}$$

With a threshold for this events of 2.2MeV, the neutrino transfers some of its energy and momentum to the target particle and scatter off a very forwarding charged lepton within small angles (< 5). The expression eq. (2.3) for the differential cross-sections is also applied to neutral charge elastic scattering.

Resonance Production

With more Q^2 available, the neutrino enters in the frontiers of inelastic scatterings between the $0.5GeV < E_\mu < 10GeV$ while the production of leptons will look the same, the hadronic sector is going to be more fruitful, pushed into baryonic resonance state involving N^* or Δ. Some process that can be found are (2.5):

$$\begin{gathered}
\nu_\mu n \rightarrow \mu^- \Delta^{++} \rightarrow \mu^- + \pi^+ p \\
\nu_\mu n \rightarrow \mu^- \Delta^{+} \rightarrow \mu^- + \pi^+ n \\
\nu_\mu p \rightarrow \mu^- p \pi^+ \qquad \bar{\nu_\mu} p \rightarrow \mu^+ p \pi^- \\
\nu_\mu p \rightarrow \mu^- p \pi^0 \qquad \bar{\nu_\mu} p \rightarrow \mu^+ p \pi^0 \\
\nu_\mu n \rightarrow \mu^- n \pi^+ \qquad \bar{\nu_\mu} n \rightarrow \mu^+ n \pi^- \\
\nu_\mu p \rightarrow \mu^- p \pi^+ \\
\nu_\mu n \rightarrow \mu^- p \pi^0
\end{gathered} \tag{2.5}$$

The resonances then decay back down to a nucleon, accompanied by a single pion most of the times (which is called **"Resonance Single Pion Production"**) or into multi-pion, other mesonic (K, η, ρ), and photon final states[10] ($\pi^0 \rightarrow 2\gamma$).

Another channel of interaction is when a neutrino coherently scatter off the entire nucleus and produce a very specific forward-scattered single-pion final state for CC $\nu\mu A \rightarrow \mu^- A \pi^+$, $\bar{\nu}\mu A \rightarrow \mu^+ A \pi^-$ and for NC $\nu\mu A \rightarrow \nu\mu A \pi^0$,$\bar{\nu}_\mu A \pi^0$. In the fig. 2.5 we show the historical measurements of ν_μ CC resonant single-pion production.

Neutrinos can also coherently produce single pion final states, where a neutrino scatters off an entire nucleus coherently and produces a very forward-going pion and transfers little or no energy to the nucleus (fig. 2.6). With no nuclear recoil, a distinctly foward-scattered pion and low-Q^2 interactions, coherent production of pions is present in NC and CC interaction, across a broad energy range, which means that is poorly-understood.

[10]Photon production processes are an important background signal in $\nu_\mu \rightarrow \nu_e$ appearance neutrino oscillation experiments, because it can easily look like an electron.

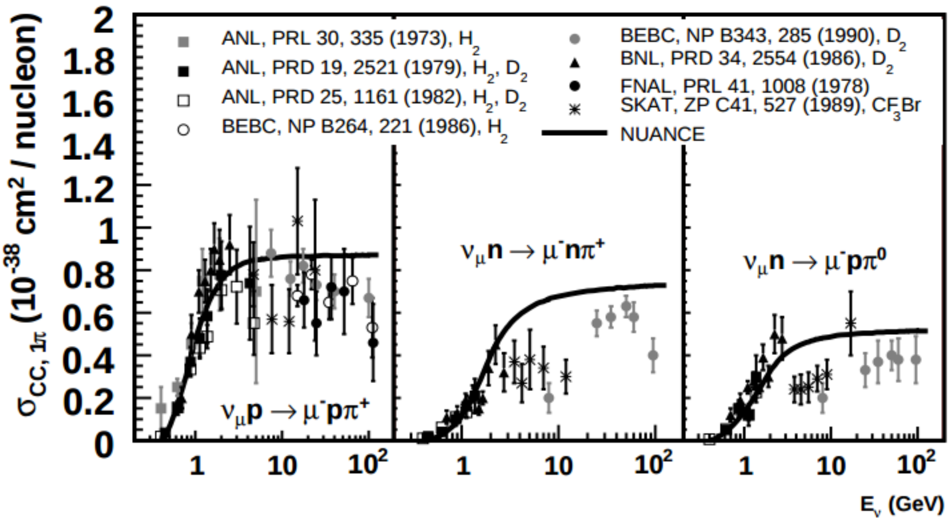

Figure 2.5: Data measurements of ν_μ CC resonant single-pion production reported by experiments with no additional corrections derived of nuclear targets or invariant mass selections. The continuous curve has been generated by NUANCE. [26].

$$\begin{array}{ll} \nu_\mu A \to \nu_\mu A\pi^0 & \bar{\nu}_\mu A \to \bar{\nu}_\mu A\pi^0 \\ \nu_\mu A \to \mu^- A\pi^+ & \bar{\nu}_\mu A \to \mu^+ A\pi^- \end{array} \tag{2.6}$$

Deep Inelastic Scattering

A deep inelastic scattering is generated when via the exchange of a virtual $W^\pm$ or Z^0, the neutrino scatters off a quark in the nucleon producing a lepton and a hadronic system as final states becoming a tool for study QCD. A DIS interaction can be describe in terms of inelastic, 4-momentum transfer Q^2 and the Bjorken scaling variable[13].

$$\begin{array}{ll} \nu_\mu N \to \mu^- X & \bar{\nu} N \to \mu^+ X \\ \nu \mu N \to \nu \mu X & \bar{\nu} N \to \bar{\nu_\mu} X \end{array} \tag{2.7}$$

2.2 Neutrino Cross Sections Measurements

This section try to address the principal challenges that arise in trying to understand the complex interactions in the field of low energy neutrino interactions

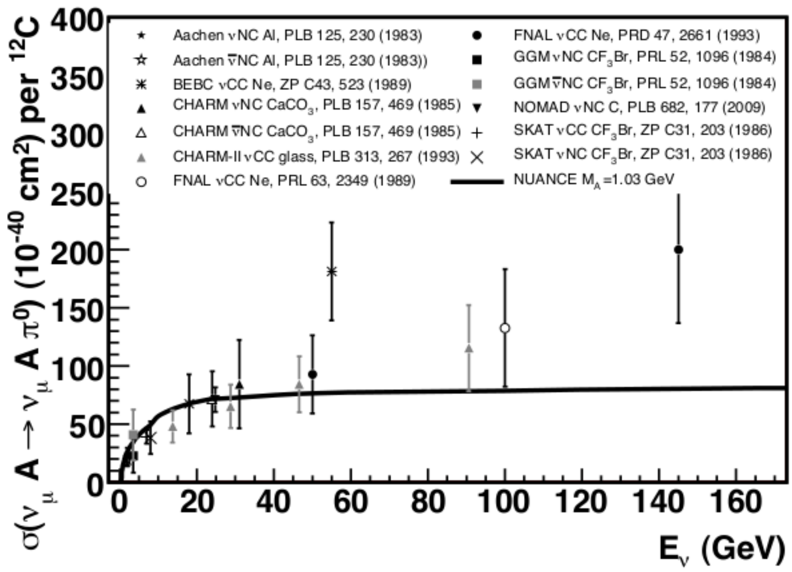

Figure 2.6: Absolute coherent pion production measurements from a variety of nuclear targets and samples for NC and CC data [7, p. 33].

and their principal results. From strong evidence of neutrino oscillations and the existence of neutrinos mass exist from atmospheric neutrinos, solar neutrinos, reactor experiments, and long-line base oscillation experiments, the explanation of

> (...) why the neutrino masses are so small and their mixing are large often rely on physics at the GUT scale. One of the most popular ideas, known as the See-Saw mechanism, coupled with CP violation in neutrinos produces leptogenesis, where a lepton matter/antimatter asymmetry caused by the decay of heavy neutrinos are converted into a baryon asymmetry and explains why today we live in a matter dominated universe.[33]

The neutrino oscillation's hints were discovered in experiments with natural neutrinos and uncontrolled conditions, but a new generation of experiments are taking the advantage of artificial generated neutrinos, mainly in long-baseline experiments around the world. All experiments face similar problems, namely uncertainties in the neutrino energy reconstruction, since the presence of the neutrino is detected indirectly, mainly by product's particles of the interactions of neutrinos with target nucleus in the detectors.

Since there is no cleanly interaction neutrinos with a single quarks, the experiments that look for experimental oscillation measurements rely in detectors where the knowledge of how the neutrinos interact with nucleus is more important than before.

Due to this neutrino cross sections and nuclear effects' uncertainties, there is an estimated of 20% to 50% in oscillations experiments[20, p. 10]. Therefore, with large errors, make a precise determination of oscillation parameters is more difficult and can not be considered.

In the case of MINERνA, the uncertainties in the knowledge of neutrino scattering measurements comes from the level of knowledge of the beam parameters and the cross-sections, as well with to uncertainties of the detector itself.

The knowledge of neutrino cross-sections along this energy region can be summarized from experiments conducted in 1970's and 1980's using bubble chamber and spark chamber detector technology, and then scintillator technology and liquid argon technology. Also of importance is the electroweak parameters ($sin^2\theta_W$) and structure functions in the deep inelastic scattering region. The following experiments are still taking data and will update the figure (2.3): ArgoNeuT, K2K, MiniBooNE, MicroBooNE, MINERνA, MINOS, NOMAD, SciBooNE and T2K (fig. 2.7).

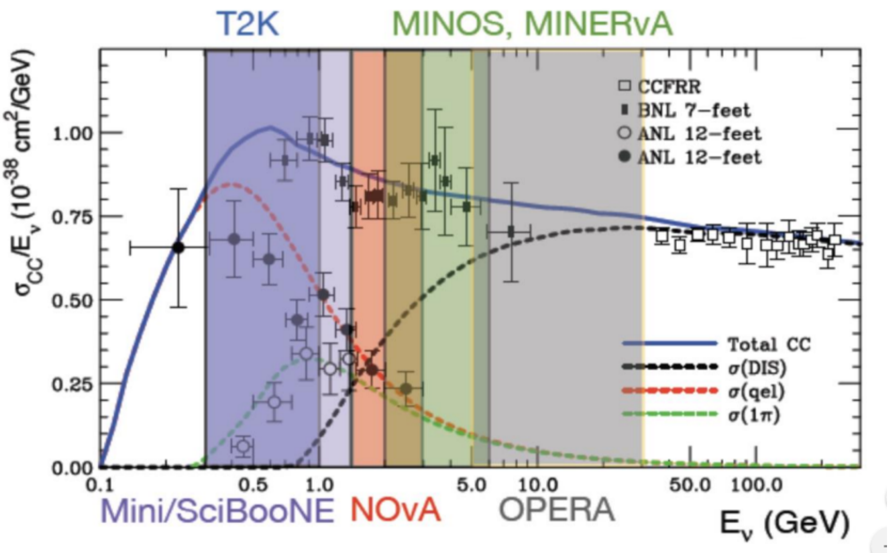

Figure 2.7: Charge Current Neutrino interactions in the intermediate region and the experiments that cover those regions. From M. Martin presented in the NuFact15 [22].

2.3 Neutrino experiments

The new emphasis in neutrino scattering has increased due to the oscillations neutrino experiments, where both charged current (CC) and neutral current (NC) channels have been collected over many decades using a variety of targets,range of energy, analysis techniques and detector technologies.

The detector technologies needed a renewed appreciation for nuclear effects and the importance of improved neutrino flux calculations, performed in the low and medium energy with an emphasis on inclusive, quasi-elastic, and single-pion production processes. The table 2.1 shows a list of modern accelerator-based neutrino experiments, the table 2.2 show the neutrino oscillation experiments and in the table 2.3 the detection technology that is used by some experiments.

Table 2.1: Experiments focus on cross-sections and oscillation of neutrinos and the type of channels of interaction focus on.

Experiment	beam	E_ν GeV	neutrino target(s)	run period	σ_ν publications
ArgoNeuT	$\nu, \vec{\nu}$	3.3	Ar	2009-2010	CC
ICARUS	ν	20.0	Ar	2010 - present	
K2K	ν	1.3	CH, H_2O	2003-2004	QE π
MicroBooNE	ν	0.8	Ar	2014 - present	
MINERνA	$\nu, \vec{\nu}$	3.3, 5.6	He, C, O, Fe, Pb	2009 - present	QE
MiniBooNE	$\nu, \vec{\nu}$	0.8	CH_2	2002-2012	QE π[15,16,17,18,19]
MINOS	$\nu, \vec{\nu}$	3.3, 6.5	Fe	2005 - present	CC
NOMAD	$\nu, \vec{\nu}$	26.0	C	1995-1998	CC , QE, π
NOvA	$\nu, \vec{\nu}$	2.0	CH_2	2010 - present	
SciBooNE	$\nu, \vec{\nu}$	0.8	CH	2007-2008	CC , π
T2K	$\nu, \vec{\nu}$	0.85	CH, H_2O	201 - present	CC

Table 2.2: Neutrino experiments and their localizations.

Experiments	Range E_ν	Located	Source
K2K	1.5 GeV	Japan	Low neutrino beam
			sent from KEK (started 1999)
			with a near detector at KEK site
MINOS	3 -12 GeV	Fermilab	at a distance of 730km
		(USA)	in the NuMI beamline
			high-energy neutrino beam
CNGS	17GeV	Gran Sasso	730 km away of
		(CERN)	Neutrino source at CERN

Table 2.3: Experiments and their detection technology.

Experiment	Scope	Technology
T2K	Reconstruction of	Water
	neutrino energy spectrum	Cherenkov
MINERνA	Reconstruction of	Calorimetric
	neutrino energy spectrum	detectors
MicroBooNE	Identification and	Water
MiniBooNE	Reconstruction of	Large hydrid
	tau neutrinos	tracking/emulsion detectors

2.3.1 T2K experiment

T2K (Tokai to Kamioka) is a long-baseline neutrino experiment in Japan that search for oscillations from muon neutrinos to electron neutrinos, produce by the intense beam of muon neutrinos with a energy of $\langle E_\nu \rangle \sim 0.6GeV$ J-PARC in the center of Japan, and directed towards the Super-Kamiokande detector 295km away.

The near detector (INGRID) is situated 280 meters from the target in the centre of the neutrino beam, at its objective is to check the direction and intensity by daily basis of the neutrino beam. The far detector on the other hand, is located 100 meters underground in western Japan and is a very large cylinder of ultra-pure water. By detecting the production of muon and electron neutrinos, T2K has seen almost 7 times more electron-neutrino events than if there were no oscillations.

The physics goals of the experiment is to calculate the ν_μ to ν_e oscillation, the value of mixing angle θ_{13}, precision measurements of oscillation parameters in ν_μ disappearance and the search for sterile components in ν_μ disappearace in neutral-current events.

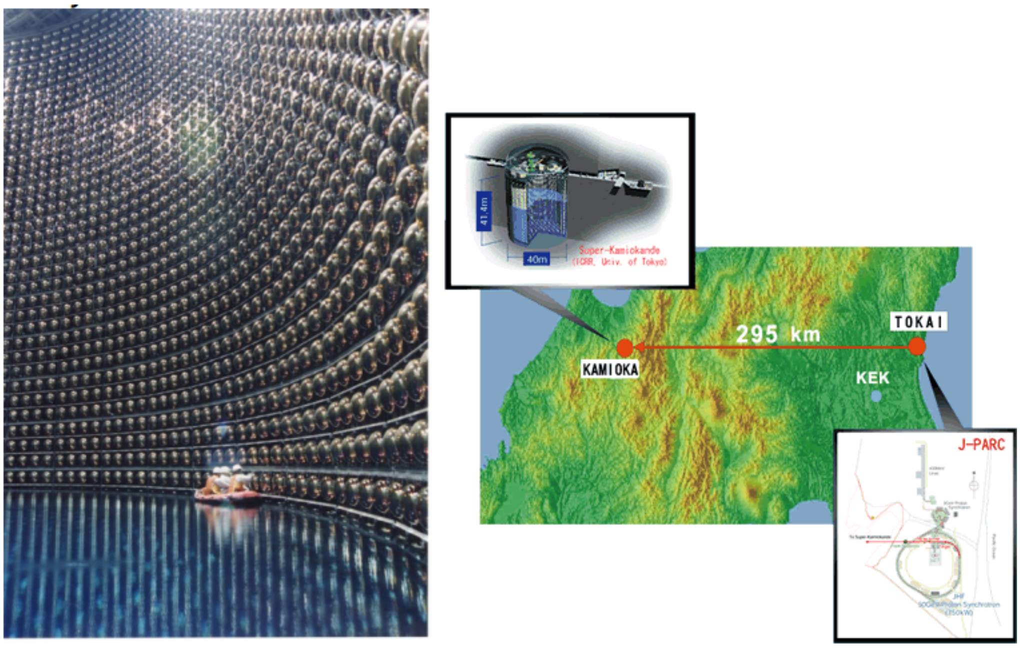

(a) (b)

Figure 2.8: Geographical map of the T2K detection the east coast of Japan. Images from the ofical page of T2K experiment http://t2k-experiment.org/.

2.3.2 MiniBoone

Using the beam from Fermilab's Booster accelerator in the energy region of $E_\nu = 0.5 - 1 GeV$ a 800 tons of mineral oil and 1280 PMTs dectector, MiniBoone was aimed to confirm the excess of electro neutrino events and support the neutrino oscillation interpretation of the LSND (Liquid Scintillator Neutrino Detector) experiment $\nu_\mu \nu_e$ and $\bar{\nu_\mu} \bar{\nu_e}$.

One of the open questions is if there are more neutrinos (”sterile” neutrinos) that would interact only through gravity. The LSND experiment sets hints in this direction, puzzling the neutrino community.

As in same case of MINERvA, MiniBooNE detector receive neutrinos produced in the decays of mesons and muons, looking for few oscillation to occur, since the decay length is only 500 meter away. The experiment results finally rule out a fourth sterile neutrino.

Another currently operating experiment, **MicroBooNE**, is measuring low energy neutrino cross sections and investigating the low energy excess events observed by the MiniBooNE experiment. Also, this experiment is testing the future construction of massive kiloton scale LArTPC detectors for future long-baseline neutrino physics (DUNE).

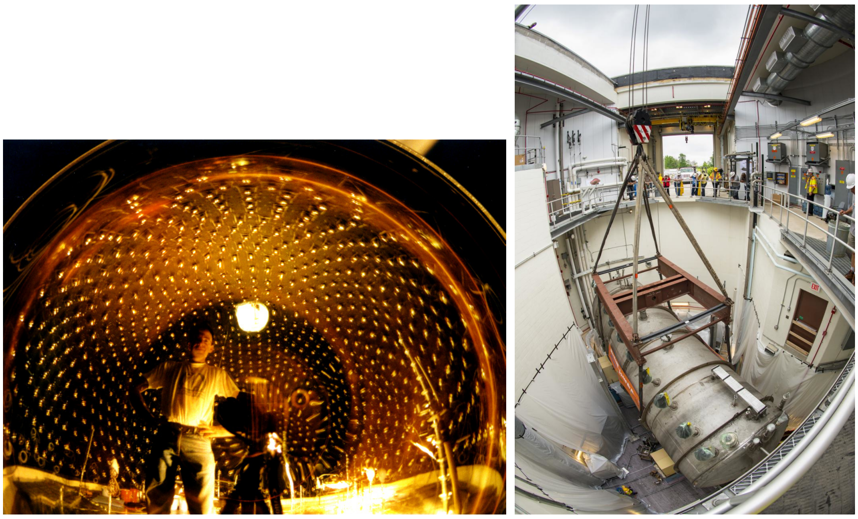

(a) MiniBoonE Phototube Support Structure. (b) MicroBooNE detector at Fermilab

Figure 2.9: MiniBooNE and MicroBooNE experiments

Chapter 3

MINERvA a cross-section neutrino experiment

As mentioned in the former sections (2.1), (2.2) and (2.3) the neutrino oscillation experiments need better models of interaction with the detectors. However, the signal and backgrounds measurements present in the process that are the poorly measured. MINERvA provide data that considerably improve the models neutrino-nucleus scattering and thus reduce the systematic uncertainties in the result from oscillation experiments.

Our experiment (fig. 3.1) is a fine-grained, fully active neutrino detector placed in the NuMI neutrino beam (3.1.1) with a good high-rate studies of neutrino-nucleus interactions and good resolution of final states using ν_μ and $\hat{\nu}_\mu$ incident of 1-20GeV.

In this chapter I will describe the most important components of the MINERvA detector (3.1), why the experiment includes a scale-down replica of the detector (3.2.1) and finally the main components of the MINERvA's Test Beam Experiment are stated in the last section (3.2).

Figure 3.1: Front view of the MINERvA detector at NuMI Hall at Fermilab.

3.1 "Bringing Neutrinos into Sharp Focus"

MINERvA[1] is a neutrino experiment dedicated to explore precision neutrino cross-section measurements in multiple nuclear targets in order to study nuclei and nuclear effects, as mentioned in [33]:

> The experiment provides the opportunity for a broad array of physics studies, using neutrinos as probes to study nuclear processes and nucleon structure as well as exploring the properties of neutrinos themselves. (..) Uncertainties in the cross sections for these processes contribute to the systematic error of oscillation measurements, so improved measurements of the cross section will contribute directly to improved precision in the measurement of neutrino oscillation parameters.

By receiving around 10^{20} proton on target, the number of events for CCQE, Coherent Production of Pions and DIS has improved substantially (we expect 800K events) allowing to study topics that have not been systematically analysed and/or are plagued by sparse data.

A much complete description of MINERvA physics' goals can be found on [2], here we state some of the most relevant:

[1]This MINERvA web page's title describe exactly the objective of the experiment `https://minerva.fnal.gov/`

- Precision measurement of the quasi-elastic neutrino-nucleus cross-section including its E_ν and q^2 dependence and study of the nucleon axial form factor.

- Determinate the cross-section in the resonance-dominated region for both neutral-current (NC) and charged-current (CC) interactions.

- Make precision measurements of coherent single-prion production in carbon, which is a significant background for next-generation of neutrino oscillation experiments probing $\nu_\mu \rightarrow \nu_e$ oscillation.

- Study of nuclear effects on $sin^2\theta_W$ measurements, and the NC/CC ratio for different nuclear targets.

- Improve the measurements of the parton distribution functions with a expected sample of DIS events.

3.1.1 The NuMI Beam at Fermilab

The NuMI beam (Neutrinos at the Main Injector) is a beam of 120GeV protons from the Main Injector that collide into a graphite producing secondary pions and kaons, which are focused with two magnetic horns and directed into a 675m long decay pipe where most of them decay (eq. 3.1) producing neutrinos and muons. Muons are absorbed and monitored, through a total of 240 m of rock downstream. Neutrinos finally reach to the MINERvA and MINOS experiment (fig. 3.2).

$$
\begin{aligned}
\mu^+ \rightarrow \mu^+ + \nu_\mu, \qquad & K^+ \rightarrow \mu^+ + \nu_\mu \\
\mu^- \rightarrow \mu^- + \bar{\nu_\mu}, \qquad & K^- \rightarrow \mu^- + \bar{\nu_\mu} \\
\mu^- \rightarrow e^- + \nu_\mu + \bar{\nu_e}, \qquad & K^+ \rightarrow \pi^0 + e^+ + \nu_e \\
\mu^+ \rightarrow e^+ + \nu_e + \bar{\nu_\mu}, \qquad & K^- \rightarrow \pi^0 + e^- + \bar{\nu_e}
\end{aligned}
\tag{3.1}
$$

The NuMI beam provide around 10^{20} protons per target, by a hadron focusing system it can produce energies of 1-3 GeV (low energy beam), 3-8 GeV or 8-20GeV (more energy, higher pion energy and neutrino energy). Regarding time, the beam is delivered in small package called spills with a duration of $10\mu s$ long, every 1.6667 seconds. The change in the current of the horn allow the experiments to have neutrinos and anti-neutrinos.

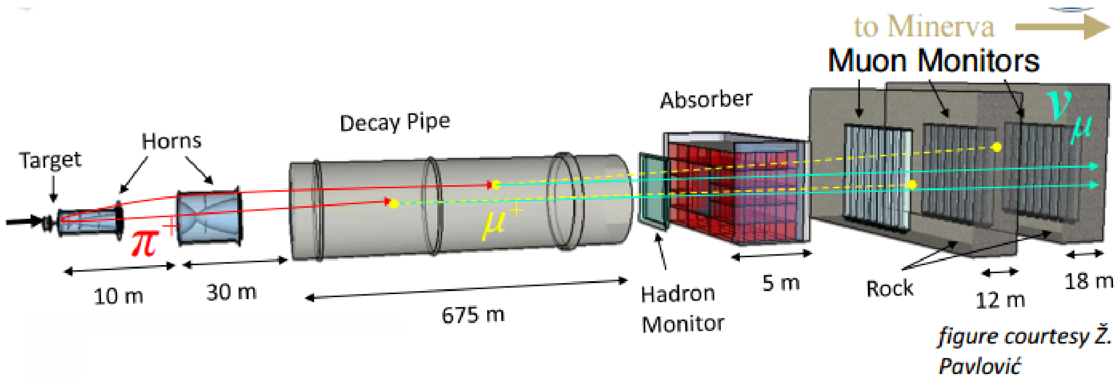

Figure 3.2: Diagram of NuMI and its different elements that produce the neutrino beam used by MINERvA, MINOS and NOvA experiments. fig. by . Pavlovic.

3.1.2 MINERvA Detector

As mention in the sec 2.1, there are many channels for neutrinos to interact with the nuclear targets depending of the energy and the type of charged final state particles, whom enter into the tracking region and are finally detected. Muons or pions have specific energy deposition footprints and it is the light produced in the scintillator strips that are transformed into an electrical and digital signal ready to be calibrated and reconstructed. In this section I will describe the most important parts of the MINERvA detector.

Module Assemblies, Nuclear Targets, ECAL and HCAL regions

The module assemblies and nuclear targets are the core of the MINERvA detector and where the interactions take place composed by 120 hexagonal-shape modules suspended vertically and stacked along the beam direction. There are four types of modules: tracking, electromagnetic calorimeter, hadronic calorimeter and passive nuclear targets.

The tracking modules consist of two scintillator planes, each composed of triangular scintillator strips glued together, in two specific directions: U-axis and

V-axis specially defined for MINERvA detector and transversal to the axis parallel to the beam named the the X-plane.

Respect to the x-y plane, the the U- and V-planes are rotated 60 degrees clockwise and counterclockwise in order to avoid ambiguities with reconstructed multiple-tracks hits associations. A squematic view of the detector can be seen in the fig. 3.3

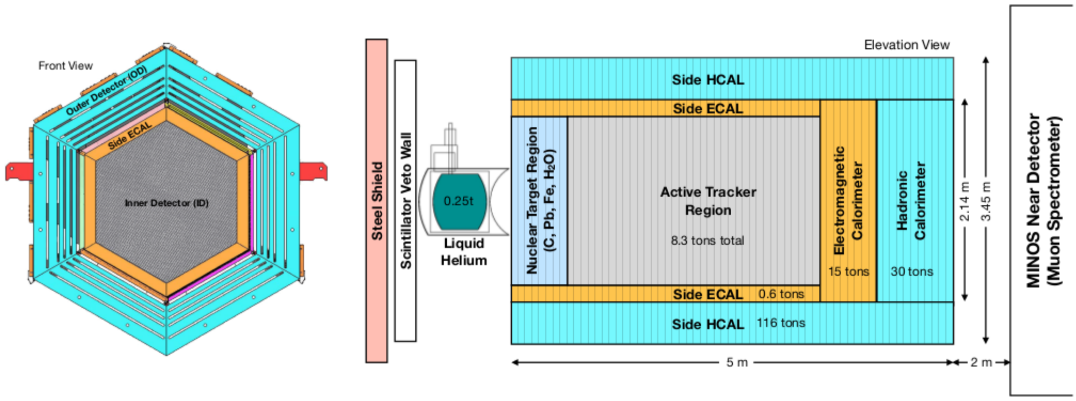

Figure 3.3: Side view of the complete detector showing the nuclear target, the active region and the surrounding calorimeter regions. Image[2]

Nuclear targets

The most upstream part of the detector include five layers of nuclear targets separated by four tracking modules that ensure a good vertex position resolution for events originated in the nuclear targets. In the right side of the fig. 3.3 it can be seen the area for the nuclear targets where neutrinos interact with.

There are 3 types of solid nuclear targets materials: lead (1014 kg, located in targets 1,2,3,4), carbon (166 kg, located in target 3) and iron (976 kg, located in target 1,2,3) that form the targets modules, the fourth one is an hexagonal-shape pure lead plane, while the others contain mixed materials with different regions of the detector. Also MINERvA has two liquid nuclear targets: water (500 kg currently unfilled) and helium (250 kg of cryogenic liquid). In the fig. 3.4, it can be seen the organization of the modules, and how they are mixed.

ECAL/HCAL regions:

The electromagnetic (ECAL) and hadron (HCAL) calorimeters region wrap around the ouside the region trackers in order to contain the energy deposited

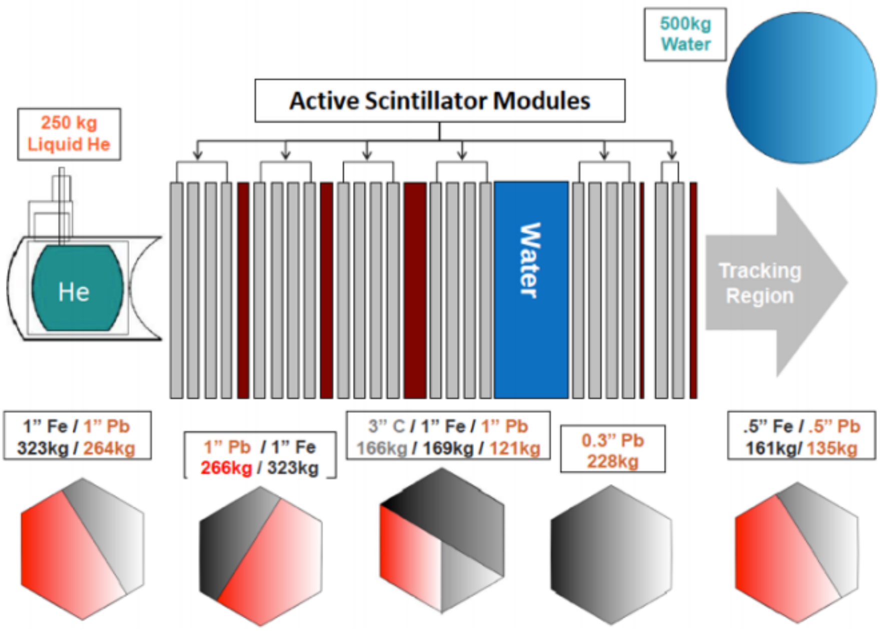

Figure 3.4: Active Scintillator Modules, and the 5 types of nuclear modules. Image from A. Norrick [25]

and stop the electromagnetic (e.g. photons) and hadrons particles (e.g. pions) correspondingly.

Ten tracking modules compose the ECAL region, this modules are 0.2 cm thick lead collar wrapping around the entire scintillator plane and a 0.2 cm lead sheet on the downstream end of the last plane in the module. While HCAL region consists of 20 tracking modules are organized by one module of scintillator and one 2.54 cm thick hexagonal steel plane in the inner detector region. In the fig. 3.3 (right), it can be seen where the ECAL and HCAL regions are.

One advantage of the calorimetric detectors over large Cerenkov detectors, is that all particles all visible in principle, but the pay off is that is needed heavy materials such as steel. This configuration produce as a results an outgoing lepton plus pions and secondary particles, therefore the incoming neutrino energy must be reconstructed from the muon and the energy of associated shower. This technique has the downside that any unaccounted particle, either because a pion was absorbed in the steel planes or within the iron nuclei themselves is expresed as an error on the reconstructed energy scale.

Finally in the most upstream part of the detector, the **Veto Wall** is made of two planes of scintillators which tag the events produced by the charged particles outside the detector like rock muons.

Optical System

As mention before, the key concept in the MINERvA detector is the collection of light pulses due to the interaction of particle products of the neutrinos interactions with the nuclear targets. Light signals from more than 32000 scintillators strips in the detector is converted into electrical signals which have amplitudes proportional to energies deposited and carry timinig information.

The MINERvA Optical Systems is composed by three processes: the collection of the energy deposited in the tracking modules, the transformation of light into an electrical signal, the readout electronics and one subsystem: the Data Acquisition System.

The scintillators (fig.3.5) are strips of extruded plastic with a fixed triangular profile made of polystyrene pellets doped with 1% of 2,5-diphenyloxazole (PPO) and 0.03% (by weight) 1,4-bis(5-phenyloxazol-2-yl) benzene (POPOP) and a white reflective coating based on 15% TiO_2 (by weight). Inside the strips, there is a 1.2mm diameter wavelength shifting (WLS) fibers that collect the light and transmit it into the DAQ system in one end. On the other end has been deposited a 2500 $\dot{A}$ thick reflective coatting of 99.999% pure aluminium by sputtering [2, p. 20].

Finally, the Fujikura-DDK optical conectors transmit the light from one end of the fibers into the Hamamatsu Photonics H8804MOD-2 PMT boxes above the detector (OD) with a spectral response of 300 - 650 nm and a peak wavelength of 420 nm. The light output for a minimum ionizing particle (MIP) is redirected into a low quantum efficiency photosensor within a 5 ns resolution that allow to distinguishing the overlaping of NuMI beam spills, decay times or charged mesons and time-of-flight measurements events. The readout process and the DAQ is discused below.

Data Acquisition System (DAQ):

By DAQ systems we understand a set of interdependent components subsys-

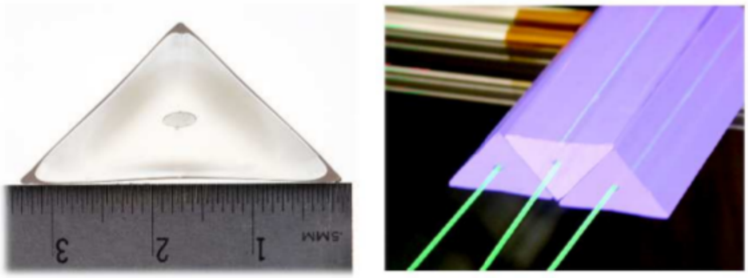

(a) (Left) Cross-section profile of the scintillator strip. (Right) fibers inside the strips.

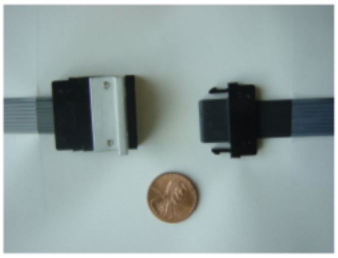

(b) Fujikura-DDK optical conectors

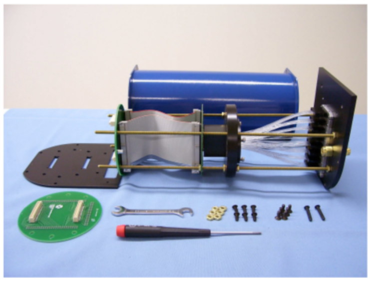

(c) The complete PMT and its parts.

Figure 3.5: Images form [2]

tems that readout the data. MINERvA DAQ systems is formed by the readout electronics and the Data Acquisition, which it main objective is to digitize the electrical pulse signals through the FEB (Front Board Electronics), provide high voltage to the PMTs and communicate with the computer interface readout system (VME).

Some particularities have to be addressed. The systems must be able to differentiate between NuMI spills of 10μs, work closely with the Accelerator Division (AD) trigger systems and be robust enough to maintain a continuously readout data during all the days of the year.

The former requirement is set since the MINERvA detector is trigger-less gate, this means that we rely on AD signals for ”opening and closing the record of data” in our detector and be more efficient in the managment of 32448 channels of data (around 100kB/s) each 10 microseconds[2].

[2]The main detector has 507 PMT, each one controls 64 channels (one channel per scintillator strip).

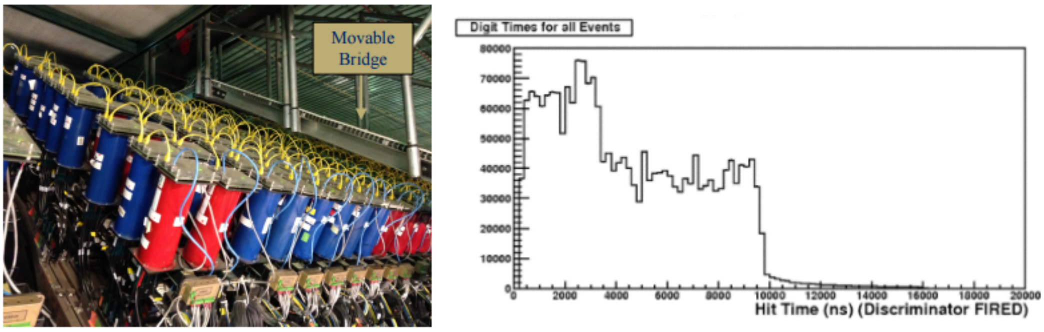

(a) Front Board Electronics in MINERvA detector

(b) Time Profile of events in the NuMI beam

Figure 3.6: Images by C.L. McGivern

Event formation and Calibrations

The event formation refers to the process that allow us to recognize the individual interactions in time and energy. Since the detector is trigger-less the separation of events has to be done offline, one for energy and one for the time that took the event to happen.

The time-to-digital TDC data are first corrected for propagation delays to the center of each scintillator strip. The fig. 3.7 shows a typical readout gate in the MINERvA detector.

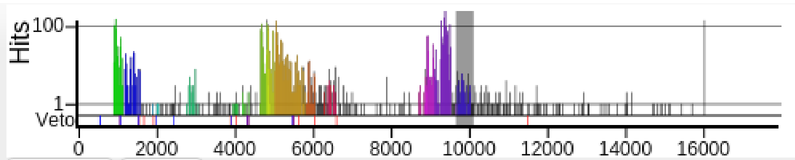

Figure 3.7: Typical time slice of . Screenshoot taken on 3/9/16

Time: an offline peak-finding algorithm create ”time slices” (the peaks with different colours seen in fig. 3.7. If during 80ns after the hit, which fired the discriminator, the energy of hit is 2/3 of the signal over a plane for a normally-incident minimum ionizing particle, then the time slice continue to be recorded until the energy condition is not longer met. A single neutrino interactions are usually contained in a single time slice.

Energy: The raw analog-to-digital converter ADC data must be calibrated to provide an estimate of the energy deposited in each scintillator strip, but considering the correction needed since there are four effects must be taken into account.

(A) Attenuation of photons while they travel along the wavelengtth shifting fiber to the end of the strip, (b) the light signal is attenuated in the clear optical fibers, (c) PMT gains in the amplification of the photoelectrons and (d) the application of the ADC conversion function in the digitalization by the FEB of the electrical signal. The estimation of the energy with all the correction can be found in more detail in [2, p. 35].

Calibrations: Since we are measuring time and energy, we need a reference point from where we set the zero level, but because we are working with a dynamical system, the calibration process is made in order to continuously correct the true zero value for the 32000 channels.

There are two types of calibrations: in situ (dynamic measurement), and ex situ (static measurements). The ex situ calibrations were made in order to characterize the tracking region, for example measuring the attenuation length in the shifting fiber and apply the rightful correction for obtain the true energy.

An in situ calibration is performed during the readout process, in order to dynamically set the zero value or the background voltage of the PMT without interactions.

3.2 Test Beam Detector

The MINERvA's Test Beam experiment is a scale-down detector replica of solid scintillator tracking and sampling calorimeter regions used in the Fermilab Test Beam Facility (FTBF) which recieve particles of know momentum and type. These particles are produced by a beam of 120GeV protons that hit an aluminum target, creating secondary beam of particles ($e^{\pm}$, $\pi^{\pm}$, $p^{\pm}$, $K^{\pm}$). A set of focusing magnets select the momentum of the different particles that arrives to our detector with energies from 1GeV to 16 GeV. In the fig. 3.8 it is shown the location of the facilities.

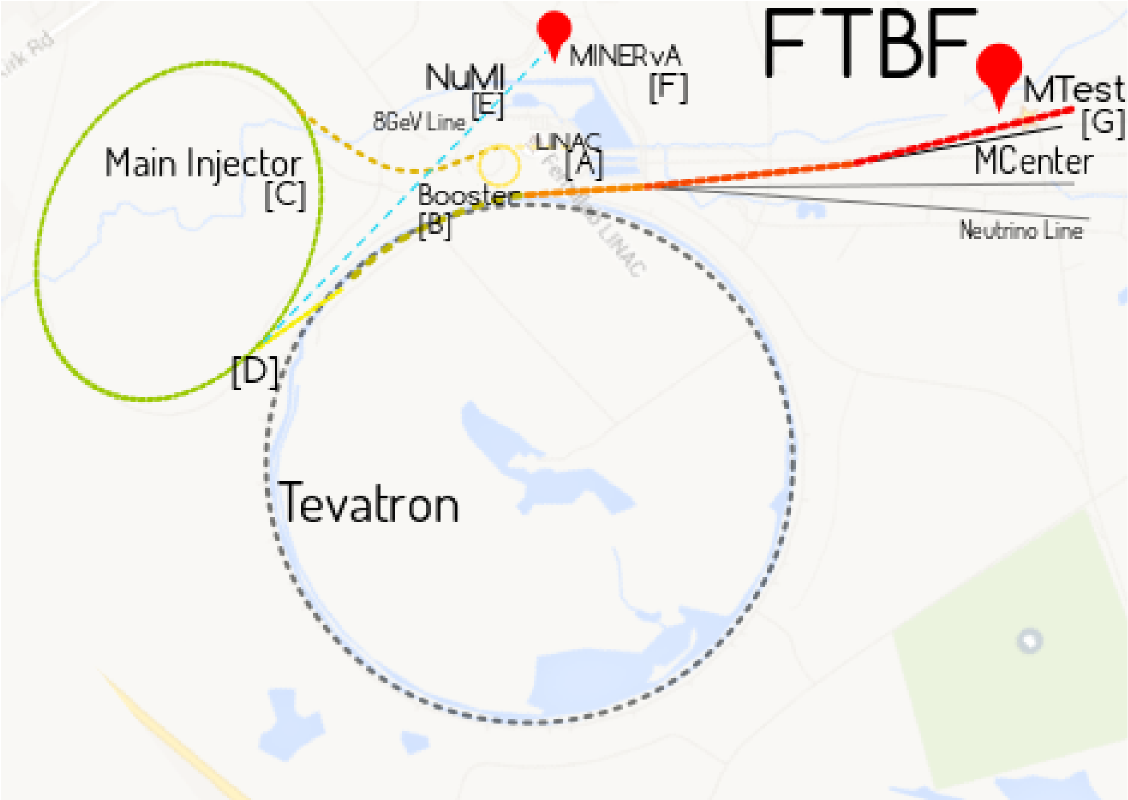

(a) Map of the location of the FTBF at Fermilab.

(b) Buildings of the FTBF with two versatile beamlines (MTest and MCenter) in which the experiments like MINERvA can run a full Detector R&D experiment.

Figure 3.8: Images of the FTBT.

3.2.1 Why is necessary to have a Test Beam program

There is a continuous requirement of improvement the simulations models of the calorimetric response of single state particles in the MINERvA detector. And the validation of theses models has been conducted in a test beam program at the Fermilab Test Beam Facility in 2010 for low energies and 2014-2015 for medium energy[3].

A tertitary test beam with hadron momenta between 0.4 and 2.0 GeV/c was used in the low energy in order to study the response of a small-scale down MINERvA detector with the final particle state from neutrino interactions with the nuclear targets. An auxiliary detection system has been placed in order to identify the momenta, the direction and the identity of the incoming particles. The data acquired was compared with a Monte Carlo simulation of the testbeam geometry and by using the same software and calibration infrastructure of the MINERvA detector the models of calorimetric response are improved. In the fig. 3.9 we can see that by increasing the of positive pions, the Test Beam 1 detector reduces its response below to 60$\%$, a similar insight is shown on the right side for negative pions.

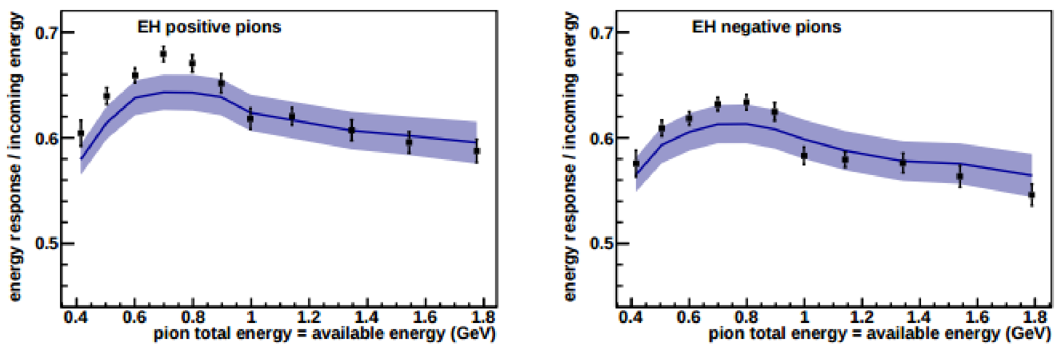

Figure 3.9: Calorimetric response for positive (left) and negative (right) pions for low energies in the Test Beam Program 1 for low energies.

In 2014-2015, a second stage of the MINERvA Test Beam program has been conducted in order to study the models and the calorimetric response in the medium energy using the seconday beam at MTest. My participation at MINERvA has been concentrated in a small analysis regarding the time structure of the income beam at the FTBF. The final results of the Test Beam for medium energy are still been analyzed.

3.2.2 FTBF Beam production

From the Proton Source, 750keV H^- ions are extracted from the LINAC (A in fig. 3.8) that accelerates them up to 400MeV. As the ions are injected into the Booster (B), the electrons are removed leaving protons to circulate into the Booster and be delivered to MicroBooNE (2.3.2) or continue through the Recycler and Main Injector (C) where the protons are accelerated to 120GeV (C) with frequency of 53MHz. At this point (D), the beam can be delivered to the NuMI (E) and experiments like MINERvA (F) or NOvA, or to the FTBT (G).

As can be seen from the fig. 3.2.2 (up), the 120GeV protons hit an aluminum target (G), producing $e^{\pm}$, $\pi^{\pm}$, $p^{\pm}$ and $K^{\pm}$ that are used in the MTest [I] where the experiments place their scale-down detectors, and in particular the MINERvA's Test Beam detector 2 (from now on TB2).

The beam at the FTBF, has a inner structure regarding the time as a variable composed by three scales that allow us to describe the time profile of the beam[4]:

Bucket: this time correspond to the RF rate in which one particle (ideally), is extracted and accelerate in the Radio Frequency Cavity. The duration of a bucket is the 19ns. A collection of 84 buckets (1.6μs) form a **batch**.

Batches: lenght in time of one Main Injector cycle that is form by 7 batches (11.2μs).

Spill: the time of resonant extraction of the beam from the Main Injector over 375000 MI Cycles, to create a 4.2 seconds spill ($21 event) on every rotation the beam make around the machine.

Chapter 4 is dedicated to explain time beam structure, and appendix C review radiofrequency cavity' s theory in more detail.

[4]In the case of NuMI, the beam spills are around 10μs ong every 1.667 seconds DAQ triggers off of $A9s signals

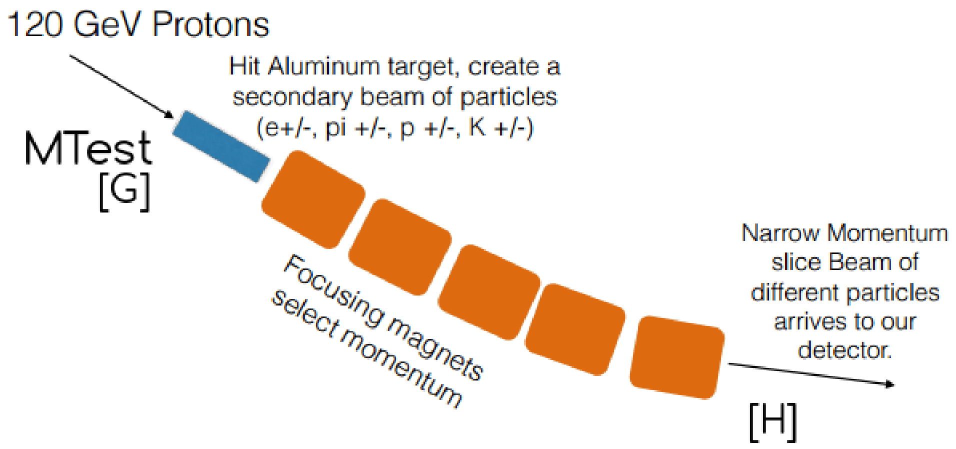

(a) Creation of the secondary beam in the FTBF. Image made by A. Norrick.

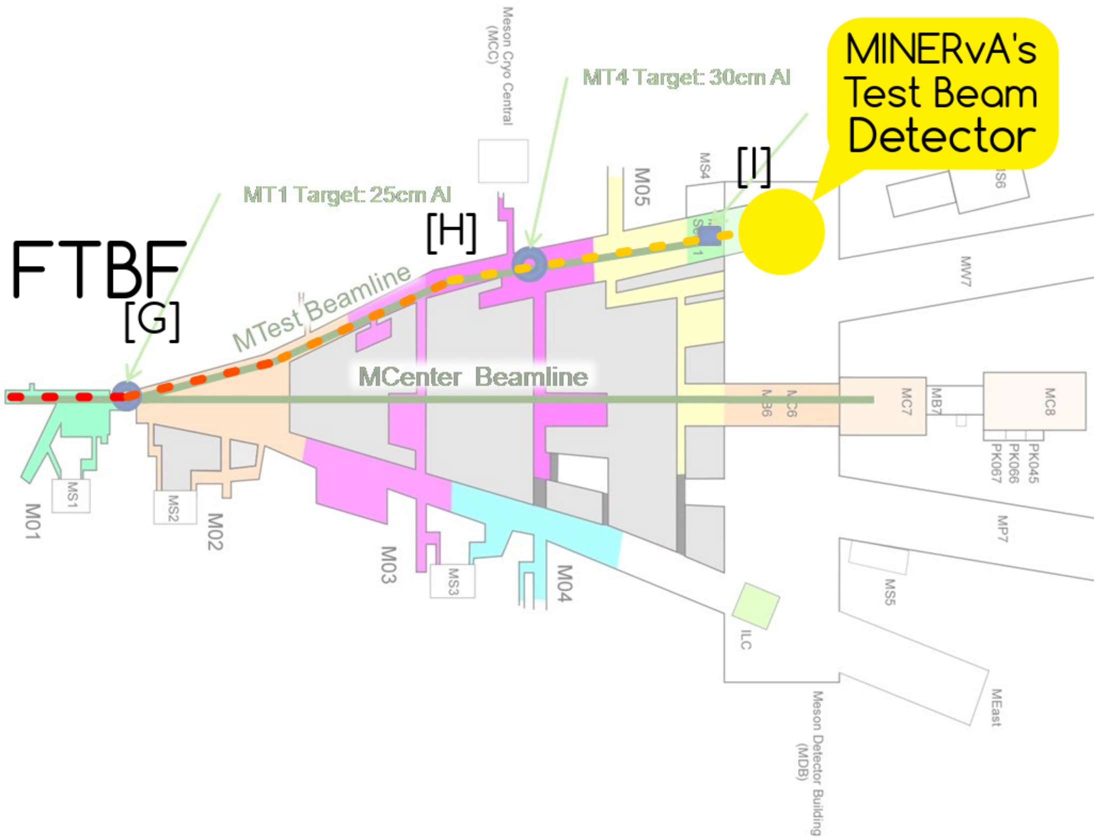

(b) Inside the FTBF

Figure 3.10: Path that follows the beam inside the FTBF before enters into the MINERvA'sTest Beam Detector 2[3].

3.2.3 Test Beam detector's auxiliary systems

The MINERvA's Test Beam 2 detector have two calorimetric regions (ECAL and HCAL) which resembles the ones in the main detector, in order to reproduce the conditions of the final states of neutrino interactions in a controlled enviorment and so forth improve the models of detections of $p^{\pm}$, $e^{\pm}$, $\pi^{\pm}$ and $\mu^{\pm}$ as mentioned in the sec. 3.2.1 within the range of 2GeV through 16GeV both polarities.

During 2015, the TB2 detector has been receiving electrons and hadrons, the premliminary numbers of amount of particles can be looked in the fig. 3.11 and 3.12.

Nominal Energy	True Energy*	# Pions	# Electrons	# AntiProtons
-2	-1.9	38	0	0
-4	-3.9	738	1475	16
-6	-5.52	2878	3040	7
-7	-6.52	0	3935	0
-8	-7.52	3261	3798	11

(a) ECAL/HCAL Negative Beam

Nominal Energy	True Energy*	# Pions	# Electrons	# Protons
+1.77	+1.87	1229	3493	361
+2	2.1	1944	3794	566
+3	3.1	2431	3328	524
+4	4.1	2480	3193	437
+6	6.48	2700	1367	164
+7	7.48	0	6284	0
+8	8.48	2613	4103	240

(b) ECAL/HCAL Positive Beam

Figure 3.11: Energies and Polarities taken in the Run 1. Tables made by R. Fine.

Nominal Energy	True Energy*	# Pions	# Electrons	# Protons
-2	-2	0	> 0	0
-4	-4	14652	> 0	97
-6	-6	14724	0	181
-8	-8	23601	> 0	556
-9	-9	23897	0	935

(a) Tracker/superHCAL Negative Beam

Nominal Energy	True Energy*	# Pions	# Electrons	# Protons
+2	+2	0	5489	0
+4	+4	12435	13782	1753
+6	+6	15487	0	1636
+8	+8	17798	2616	2562
+9	+9	23860	0	810

(b) Tracker/superHCAL Positive Beam

Figure 3.12: Energies and Polarities taken in the Run 2 and 3. Tables made by R. Fine.

The data that has been taken is divided according a two configurations of the calorimetric regions (ECAL/HCAL and Tracker/SuperHCAL) of the TB2 detector and the chronological time in which it was recorded (Run 1, Run 2 and Run 3). The CAL/HCAL configuration is composed by 20 planes of scintillator/PB and 21 planes of Scintillator/Steel, while the Tracker/SuperHCAL configuration: 20 planes of Scintillator, 4 planes of Steel/Scintillator, 11 planes of Double Steel/Scintillator and 6 planes of Steel/Scintillator. The fig. 3.13 shows this.

The TB2's auxiliary detection system has been choosen in order to recognize single particles of known type and momentum in a calibrated detector, the components can be seen in fig. 3.14: four Wire Chambers (L), Veto System (M) the Time of Flight System (ToF J and N) and the Cerenkov detector (K). We will describe the different parts of the systems.

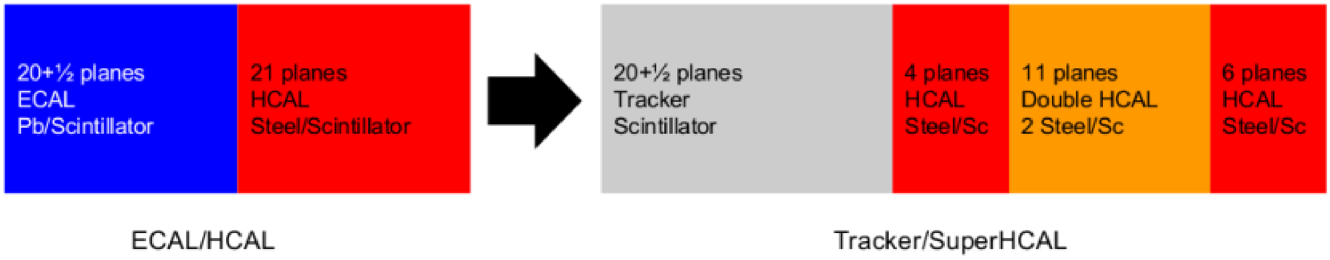

Figure 3.13: The two configuration for the calorimetric regions in the TB2. Image made by A. Bercelli.

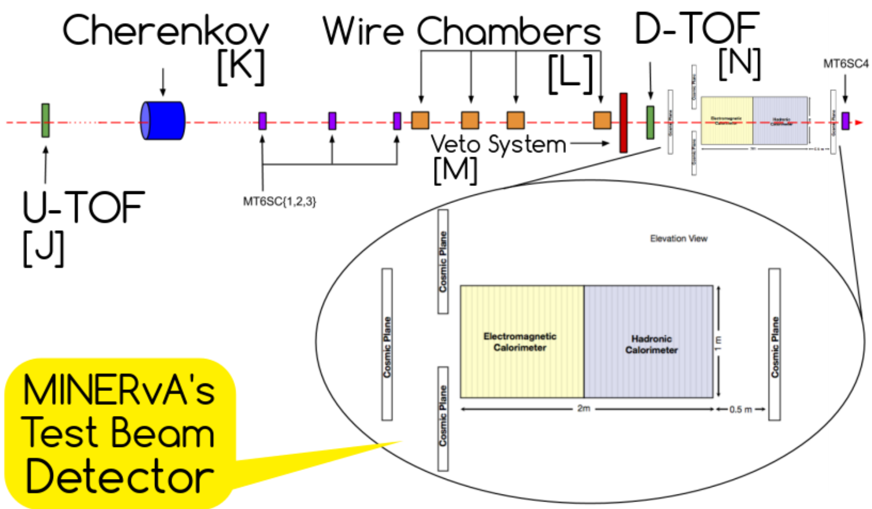

(a) Tracking logic of the TB2 auxiliary detection system. Image made by R. Fine, the annotations are ours.

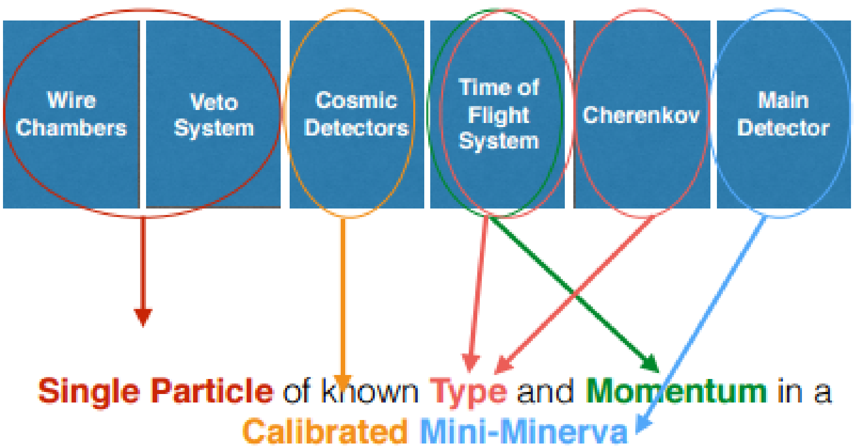

(b) Particle ID logic. Image by Anne Norrick.

Figure 3.14: (Left) Schematic view of the Test Beam Detector and the Auxiliary detection System. (Right) Components of the Test Beam and its functions.

The Time Digital Converter TDC/CAMAC Lecroy 3377

The TDC (Time to Digital Converter) CAMAC Lecroy 3377 (CAMAC 3377 from now on) is a machine that provide a digital representation of time when an event has ocurred. The CAMAC 3377 provides us with a high-resolution time measurements for low measurements dead times. It has 32-channel, each individual input channel has a LIFO (last in, first out, a time of processing the data) type buffer attached to it such up to 16 hits can be recorded on the channel with respect to the common hit.

The CAMAC 3377 is the interface between the auxiliary system (the Veto Wall, ToF, Wire Chambers) with the Data Acquisition System readout information from the ToF and Veto systems, control trigger sent to the MWPC and identify triggers in spill and out of spill.

The multihit capabilities allow us to record multiple events in the same windows of time (that we set). Its pulse width measurements is up 16bit dynamic range with 500psec of last significat beat, which mean that the minimum window of time that we can reach with the CAMAC 3377 is 500ps. The time is meaured with respect to a common reference time mark or ”COMMON HIT”, that can occur before or after the infividiual time signal.

Some other characteristics:

- 32-channel multihit TDC: we can measure up to 32 channels in the same window of time
- Each channel can measure up to 16 measurements on each channel (512 events per window of time)
- 500ps digitizing resolution (LSB): this is the maximum resolution that we can achive
- 32 μs of time full scale: we can construct our windows of measurements in multiples of this value
- 8 trigger outputs programmable

Table 3.1: Modes of operation of the CAMAC 3377 TDC. The ? means that there is no information

Mode	Off set resolution	Time range	Full scale time range
Single word	500ps - 4 ns	255 ns - 4μs	0 - 32μs
Double word	500ps	8ns - 32.7μs	32.7 μs
Mode	**Off set resolution**	**Steps**	**Full scale time range**
Standard	no info	8ns	8 ns - 32 μs
Common Start mode	no info	50 ns	up to 32 μs
Common stop mode	no info	no info	no info

- The number of edges measurements recorded per channel is 1 to 16
- Multi event buffer allows up 31 small events and 4 full events can be recorded before readout
- The readout can occur in background, while the fron end is recording data hits.
- The readout is by event
- Modes of operation shown in the table 3.1

The double word format preserves the full 16 bit data for wide dynamic range. At the end of acquisition the data is unloaded from the MTD133s and stored in a multievent FIFO buffer. Dead time is 1.8μs plus 100 ns per recorded hit (200 ns per hit when in double word mode).

Veto System

The Veto System is a set of 12 scintillator paddels that surrounds the central region and looks for particles entering the detector outside of the direct beamline. A 300 ns resolution has been set up since this is the value the maximum resolution that the MINERvA detector have to recognize two different events.

As will be explain in the sec. 4.3, in theory the AD deliver zero or one particles of know energy per MI bucket, but in practice this is no the case. Sometimes send more of one particle in single MI bucket, or more than one particle in adjacent buckets/batchs. Since the detector needs to know that the input is one particle of know energy, the Veto System allows to tag all other events.

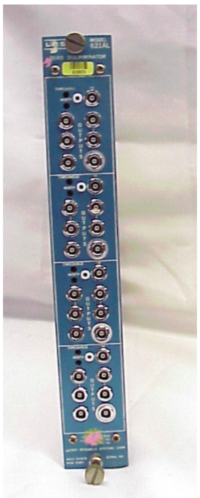

(a)

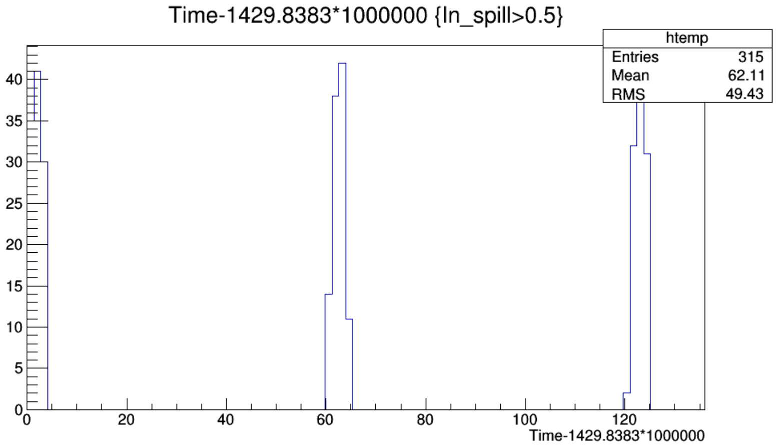

(b) Main Injector Spill seen by the CAMAC 3377 during a normal data taking.

Figure 3.15: (a) TDC-CAMAC Lecroy 3377 used in NuTeV and CDF.

Figure 3.16: Veto system and its six paddles. Photo by A. Norrick

The Wire Chambers and Veto System are responsible for detection of single particle events and discard multi-particle events. The Wire Tracker 4 (MWPC4) centered on the central value of the beam position in X and in Y allow us to know if a particle is on the axis beam, but for other angles the mentioned array of scintillators counters, all the space for approximately 1/2m around the beam axis send a signal if some particle hits them.

Time of Flight (ToF)

The Test Beam experiment is able to measure the time that it takes for a particle of known momentum to travel between two known locations. From this, it can be calculate the mass of the particle and consequently its identity. The system is formed by two stations with PMTs that record the time that a particle passed through them. The stations are 104.5 m apart, the dowstream station have two paddles while the upstream; four PMTs as shown in the fig. 3.17.

If a particle is sending through the detector, the ToF system will receive the trigger signal which opens the gate for all the six different PMTs independently in both stations. The channels will continue counting until the stop signal is received. And, the security condition is placed in order to stop recording other signal.

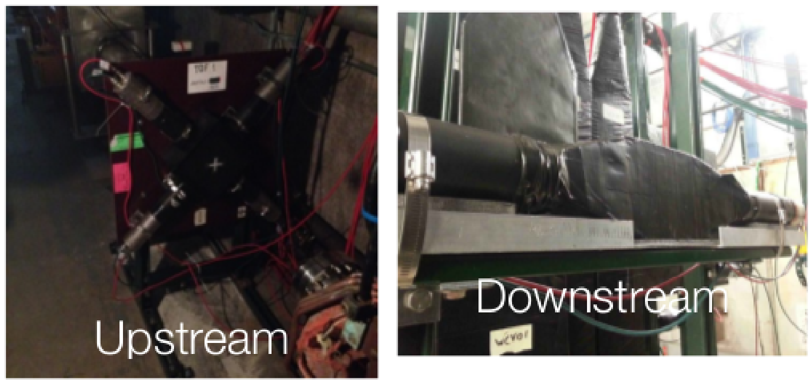

Figure 3.17: Time of Flight Upstream and Downstream detectors. Photos by A. Norrick

The rise time of the two downstream PMTs is 3.0ns, with a jitter of about 0.4ns, while the upstream PMTs has a rising time of 1.3ns and a dead time of about 0.3ns[5][5].

Cerenkov detector

The Cerenkov dectectors (2) are gas chambers with PMTs attached to them, that when a particle emits a characteristic cone of light. Particles moving slower than certain thresholds speed are invisible in water Cerenkov, but fast charged particles may create electromagnetic wave while traveling along a medium, this is called Cerenkov radiation if the particle velocity is greater than the velocity of the light in that medium. The radiation generated is spread in the shape of a cone, along the direction of the particle.

[5]In sec. C.3 we outline very briefly the physics of the ToF.

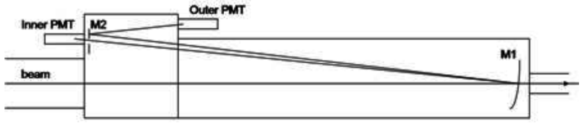

Figure 3.18: A diagram of the Cerenkov detector used at MTest (Fermilab). Copyright Fermilab.

The following equations 3.3, show the relationship between the angle in the cone with the velocity of the particle and the index refraction. While in the other equations it can be seen that by changing the pressure and assuming an isothermal behavior, a simple spring model of electrons in a diaelectric medium describe the phenomena, a threshold pressure and a relation between pressure and the refraction index is found.

$$cos(\theta_c) = \frac{1}{\beta n} \tag{3.2}$$

$$\frac{P_1}{P_2} = \frac{\rho_1}{\rho_2} = \frac{n_1 - 1}{n_2 - 1} \qquad P_T = \frac{\frac{1}{\sqrt{1-\frac{m^2}{E^2}}} - 1}{\delta} \tag{3.3}$$

where $\delta = n_{1atm} - 1 = 0.000297$ and P_T is in atm.

The Cerenkov detectors at MTest can be used as threshold counters (particle ID) in order to tag the electrons in the beam. There are two Cerenkov counters at MTest, one upstream is ’80 long and one downstream, ’50 long. They have two PMT attached that collect the light form the cone and amplifies the signal, while subtracting the noise with help of other equipment.

The highest momentum at which a particle can be identified is determined by the velocity resolution of the counter combined with the characteristics of the beam. While the lowest momentum that can be tagged for a given particle is set by the particular gas used and the pressure. In the table 3.2 it can be seen the value on GeV for two different gases and particles.

Table 3.2: Lowest momenta value for detection in Cerenkov detectors at MTest (Fermilab)

	electron	muon	pion	kaon	proton
Nitrogen	0.02	4.0	5.0	1.8	35
C4F8O	0.01	1.8	2.4	8.0	15

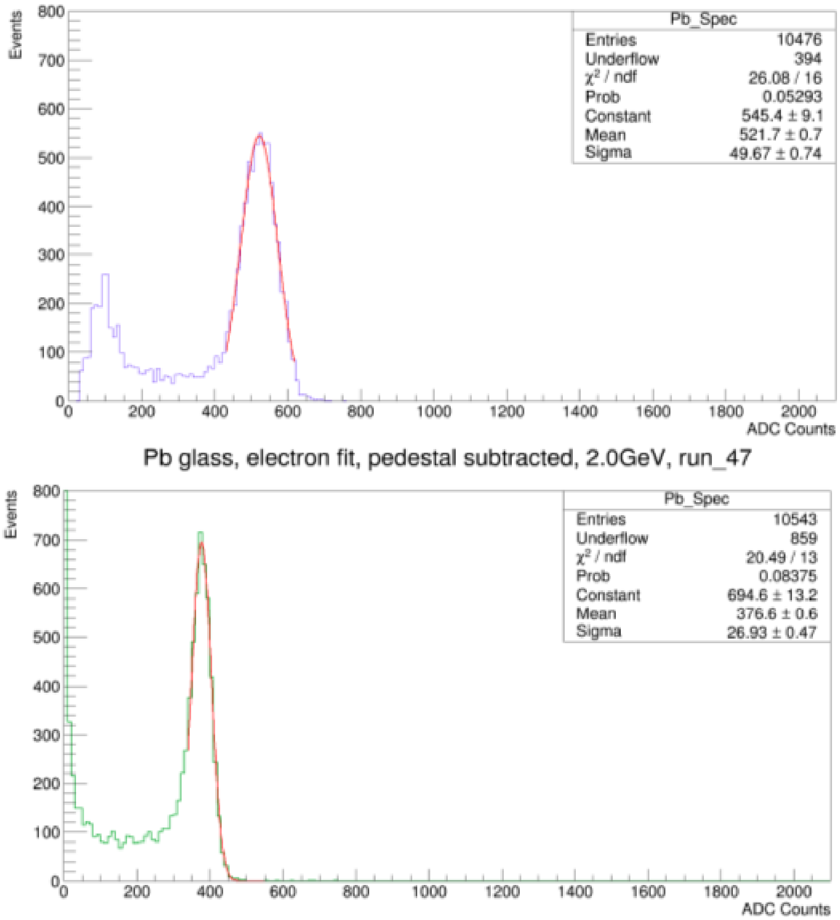

Figure 3.19: Spectra of de Cerenkov detectors at MTest for the MINERvA Experiment. Work done by M- Ramirez

Wire Tracking Chambers

When a charged particle passes through the material (the two planes at 90 degree angle) a signal is generated with the xy position for each hit. The ability of track in space the particles and with the help of 4 wire chambers in the detection system, allow us to track particles as they go into the detector.

3.2.4 How an event is recorded: trigger logic and DAQ for MINERvA Test Beam 2

In all the measurements in physics, time is an important parameter that allow not only to study the dynamic relationships but also structure the way the data is taking. In this last section I will describe how the detector (and all their subsytems) are triggered, this mean the physical signal that tells the detector this is an event that I am interested in recorder for further analysis. In specific, the FEBs are the ones that open and close the data readout and increase the voltage in the PMT and integrate the charge into a digital signal.

Triggers in the Main Detector

The Main Detector is triggers-less, this means that we rely on other systems for opening and closing the process of taking data. In our case is the Accelerator Division through the $39 signal that start this. Every 1.67s (or 1.33s) the MINERvA detector receives 10μs neutrinos spill.

From the beginning of the signal, the time that takes for setting the correct high voltage into the PMT is $20\mu s$, and it ends just before the beginning of the spill mentioned before. The FEB integration is closed after 5.5 μs after the neutrino pulse and from this point the Data Acquisition begins.

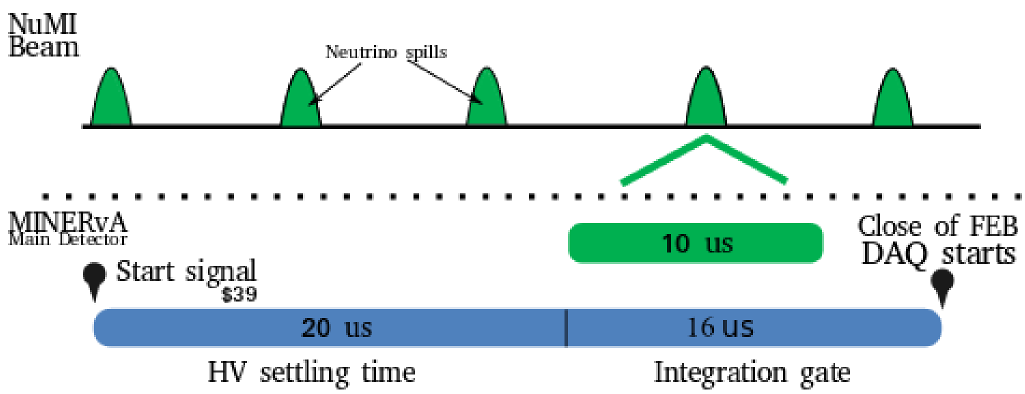

Figure 3.20: Underground trigger timing with the MINERvA Main Detector.

When a burst of neutrinos reach the MINERvA Main Detector, the FEB are open hoping to read an interesting event. This does not happen in the Test Beam detector.

FEB Gates at the Test Beam

In the case of the Test Beam, the timing trigger is different since the time structure of the beam is different from NuMI and we, in theory, receive individual particles instead of a neutrino pulse. Here, the FEB gate is open as often as possible and hope that a particle hits the detector when the FEB gate is open.

Each minute, we receive a slow-spill of 4.2s, having also a signal from Accelerator Division telling us that beam is coming to the test beam detector. But, the trigger (the signal that difference data from no-data) is constructed with an Auxiliary System. By using the electronics from the Main Detector, the HV settling time and the integration gate is the same, the differences are that FEB integration gate have an overlapping with the HV settling time of $1\mu s$, an $9\mu s$ of window time in which **if a particle is detected the Data Acquisition will start**[6]

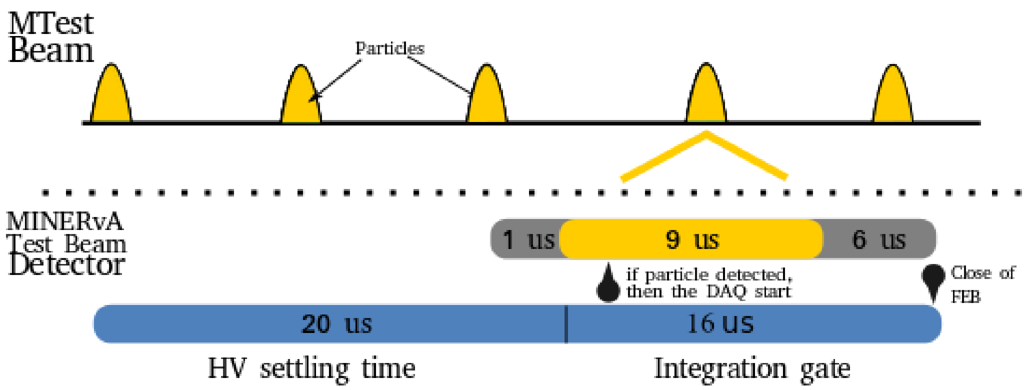

Figure 3.21: Underground Trigger timing within the Test Beam Detector.

Since, the Test Beam detector is always "open", some no desire events will be detected and needed to be tagged in order to remove it from the final data. This is done through conditions set up with the auxiliary system. There are two types of triggers: beam and cosmic trigger. The last one because, from time to time, cosmic particles will reach the detector. This events are used for internal calibrations. The readout is done by the CAMAC and correspond to the variable **out-spill** in the ROOT file.

Regarding the beam trigger, its main objective is to set the signal that a particle during the main injector spill is aimed at the detector. Constructed by a logic between the auxiliary detection system (Veto, Cerenkov and CRIM).

If we have a cosmic particle out of spill or a particle from the beam, with the confirmation that it is not a electron (in this case the trigger output is restricted

[6]Remember that in the Main Detector, a minimum energy during a specific window of time has to be reach in order to consider that event as a neutrino interaction event.

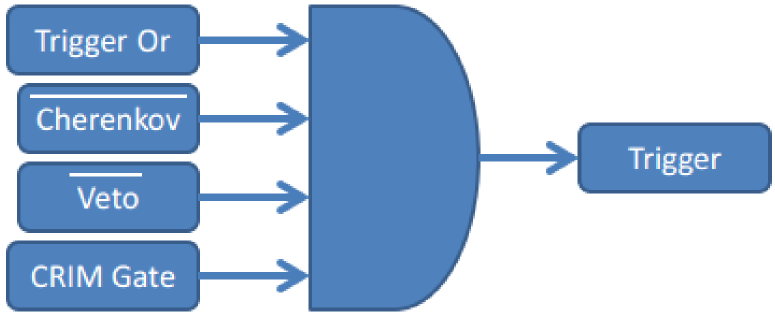

(a) Events and logic that **do fire** the Test Beam DAQ to begin the readout of the data. Image by G. Savage.

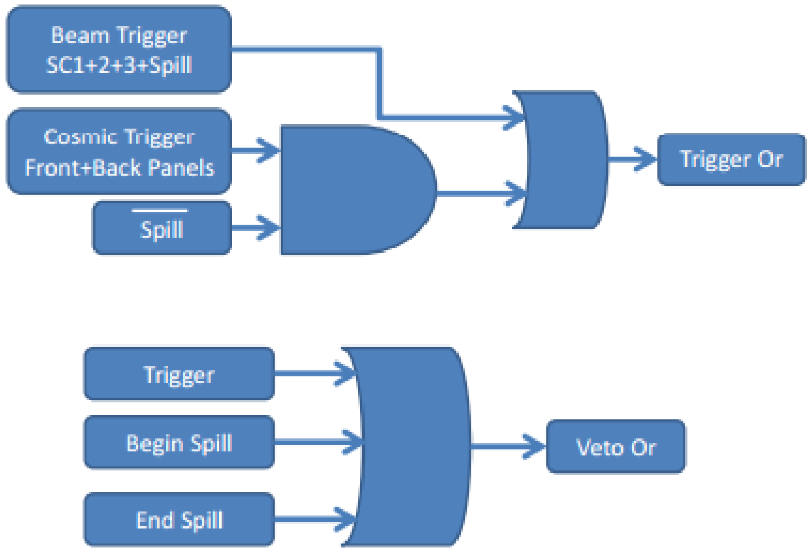

(b) Events and logic that **do not fire** the Test Beam DAQ to begin the read-out of the data. Image by G. Savage.

Figure 3.22: Logic of the triggers in the Auxiliary Test Beam detectors.

by the Cerenkov and spill signal) and that did not hit the Veto System, then that particle will tagged as data. Therefore the Veto inhibit the DAQ to readout triggers for these conditions: Trigger (allow CAMAC readout to complete), the begin and end of the spill. The CAMAC DAQ is responsible for mapping of out-spill/in-spill triggers in MINERvA DAQ.

Chapter 4

Time structure of the FBTF Beam

As mentioned in sec.3.2.1, the MINERνA experiment is composed of two detectors places in different parts at Fermilab, with different physics's goals[1]. We have describe the production of the NuMI beam that is used for neutrino cross-section scattering in the main detector, and in the sec. 3.2 we did the same for the FTBF Beam, that is used in the MINERνA experiment.

This chapter is meant to give an overview of the concepts involve in the production of a beam of particles that is use in the experiments at Fermilab, and specially at MINERνA experiment. We start with general concepts that are needed to understand how the beam is produced (sec. 4.1), then we describe the Fermilab's Accelerator Complex (sec. 4.1.1) which produce the beams used in the experiments. One of the most important elements in modern accelerators is the Radio Frequency Cavities (RF) which accelerates the particles; an introduction modes in the RF, the Q factor of the cavity and the Phase Focusing hability of the RF systems are described (sec. 4.2), in order to explain in the last section (sec. 4.3) why the beam has a defined structure[2].

The approach followed in this thesis regarding the details of the production and delivery of the beam is focus on the periods of cycles of production of the beam that we receive at the FTBF. Topics of physics of beamlines, monitoring, control, production and instrumentation are away from the scope of this work.

[1]The principal detector is placed at the NuMI Hall 3.1.1 while a small replica is placed at the Fermilab Test Beam Facilities. More information can be found in the sec.3.2

[2]As a remainder the aim of this thesis is to show that the MINERνA's Test Beam Experiment is able to resolve two of three scales in the beam structure

4.1 General Concepts in Accelerator Physics

Beam of particles

A **beam of particles** are a concentrated group of charged particles, that are accelerated by increasing their kinetic energy in particle accelerators. While **beam intensity** is defined as the number of particles in the beam that we can measure as the number of particles. Usually the **beam direction** is defined along two direction in order to describe the particle motion: the longitudinal dimension (the direction in which the beam travels) and the transverse dimension that it is form by the horizontal and vertical axes and form the transverse plane.

An accelerator is a machine that accelerates particles over a trajectory, and are use with the help of other machines in order to deliver a specific type of beam. Roughly speaking there are two types of accelerator: fixed-target accelerators and colliders. The former, produce a beam that is smashed into a fixed targed which produce secondary particles that are used by the experiments. In the later, two beams are guided and then collided, the particles that results from this are studied.

One of the most well know collider laboratory is the CERN's Large Hadron Collider (LHC), while the most powerful neutrino beam in the world is produce by NuMI's Fermilab. As mentioned in sec. 3.1.1, the NuMI beam is produced when 120GeV protons collide into a carbon target.

The two principal elements of an accelerator are: radiofrequency cavities, which produce the acceleration of the particles, and magnets. Whom change the direction of the beam with the help of the force exerted into a charge particle within an electric and magnetic field. Magnets, bend the direction of the particles' trajectory, dipoles change the trajectory of an entire beam while quadrupoles magnets, focus or defocus the beam. Usually, the magnets are arrange in a lattice of different types.

Momentum and energy of particles

Since the particles travels with velocities near the light's velocity, $\beta = \frac{v}{c}$, the energy total energy is $E_{Total} = \gamma mc^2$. A proton extracted from the Main Injector at 120.00 GeV, have a energy at rest ($E_{rest} = mc^2$) of 938.26 MeV so forth it will have a velocity of 99.997$\%$c.

$$\gamma = \frac{120.00GeV}{938.26MeV} \qquad \beta = \sqrt{1 - (\frac{120.00GeV}{938.26MeV})^2} = 0.99997 \tag{4.1}$$

Dynamics of accelerators

The only way to interact with electric charges is through the electromagnetic fields. If a particle has a velocity $\vec{v}$ the force exerted on a particle of charge q is:

$$\vec{F} = q(\vec{E} + \vec{v} \times \vec{B}) \tag{4.2}$$

From this equation, we can see that the force due to a static magnetic field is perpedicular to the particle's velocity. By the Work-Energy Theorem, this force won't increse the kinetic energy of the particle.

Lets assume that a particle is moving along a curve through an electromagnetic region with where the fields have single components $\vec{E} \to E_\theta$ and $\vec{B} \to B_z$. The Newton-Lorentz force in a curvilinear coordinate system reads:

$$\frac{d\vec{p}}{dt} = e\vec{E} + e\vec{v} \times \vec{B} \tag{4.3}$$

$$\frac{d(mv_\theta)}{dt} \cdot \vec{u}_\theta - m\frac{v_\theta^2}{\rho} \cdot \vec{u}_r = eE_\theta \cdot \vec{u}_\theta + ev_\theta B_z \cdot \vec{u}_r, \tag{4.4}$$

where ρ is the local radius of the trajectory. It can be see electric field provides energy and momentum to the particle where magnetic fields bends the particle trajectory.

$$\begin{aligned}\frac{p_\theta}{dt} &= eE_\theta \\ p_\theta/e &= B_z\rho\end{aligned} \tag{4.5}$$

4.1.1 Fermilab's accelerator complex

In the fig. 4.1 it can be seen the machines that compose the Fermilab Accelerator Complex composed by: the Ion Source, the LINAC (A), the Booster (B), the Main Injector (C) and the different outputs for low-energy neutrino experiment, muon experiment, high-energy neutrino experiments and the Test Beam Facility.

750keV H-minus ions are extracted from the source into the Linac. The Linac accelerates the ions to 400MeV, and then extracts them to the Booster Accelerator. As the ions are injected into the Booster, the electrons are stripped off leaving 400MeV protons to circulate in the Booster.

The **LINAC** is formed by RF cavities placed in-line with one another in order to provide a large amount of energy gain per unit length. The beam only pass onces because is linear and since the beam is composed by similar particles, they tend to electrostaticaly repel one another, which generate a spread in the beam size and has to be corrected with the help of quadrupoles.

The **Booster** is a 1500-foot-circumference rings that accelerates the beam up to the energy of 8GeV, which provides a low-energy neutrino beam for the Main-Injector and to low-energy neutrino experiments like MiniBooNE. The Booster captures the protons into 84 bunches (1 batch) and accelerates them to 8GeV. Each of these bunches is 19nsec long. Typically, 8 - 30 of these bunches are extracted to the Main Injector (MI) for Test Beam operation (a process known as Partial-Batching) At the injection total energy of E = 8.938 GeV, the Main Injector has a circumference in time of 11.13 µs, which is exactly 7 booster batches long.

The **Main Injector**, situated directly beneath the Recycler in the same tunnel, ramps up to proton beam from the Recycler from 8GeV to 120 GeV. Being a circular accelerator know as ”synchrotron”, that is compose by a magnet system and a RF system. Both are ”synchronized” as the kinetic energy of the beam increases. The **Recycler**, is a stage area for proton beams after exits the Booster.

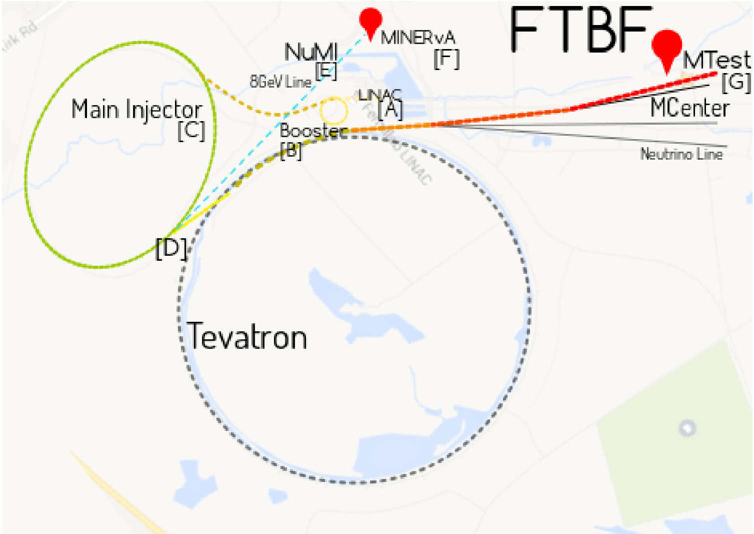

(a)

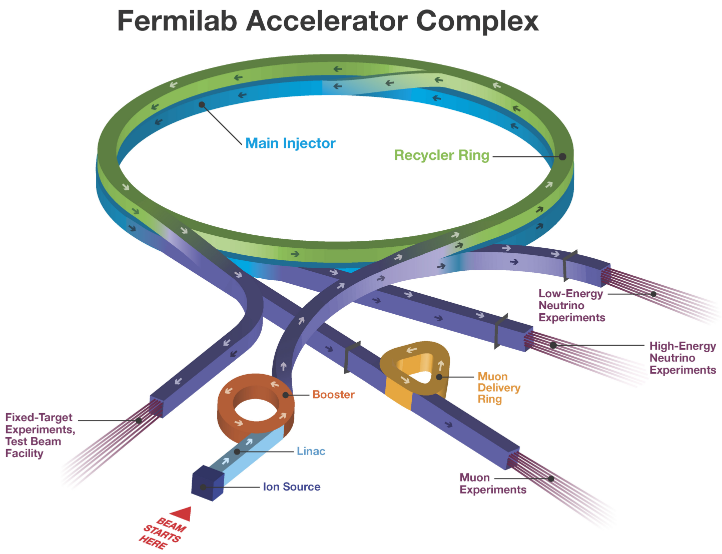

(b) Fermilab Accelerator Complex and th principal outputs from the Main Injector, to the different experiments.

Figure 4.1: Fermilab Accelerator Complex.

Here is where the beam is combined into batches of protons to form a more intense beam. Once it is done the proton enters the Main Injector, on top of the Recycler.

The Main Injector accelerates the beam to 120GeV at a frequency of 53 MHz, at which point a process called Resonance Extraction is started and a fraction of the beam is resonantly extracted in a slow spill for each Main Injector rotation.

The **machine cycle** is the cycle, in which a defined sequence of task are performed in regular intervals, and it is shared by all the machines that compose the accelerator complex. The entire machine cycles at a fixed rate of 15MHz, this means that all of the equipment performs a given task fifteen times a second. This is called a ”beam cycle”[12].

4.2 Radio Frequency Systems (RF Systems)

A RF cavity is a electromagnetically resonant structure that generates a strong longitudinal electric field that accelerates beam and does not affect the orientation of the longitudinal or transverse dimensions. Usually working around of 3 kHz to 300 GHz, modern particle accelerators use them in closed geometries that produce standing waves and increase the kinetic energy as the beam passes[3].

This section is devoted to explain the basic operation of the RF cavities, since them play an important role in the inner structure respect of time of the beam. In the appendix C we review the electromagnetic theory of the RF systems, while in sec. 4.3 we connect how the RF systems impact in the time structure of a beam in synchrotrons.

4.2.1 RF Cavities

EM in vacuum or matter accept monochromatic plane waves that propagate along the space with a well define velocity. In both cases, when the surface is reached, the EM wave will have a reflected, transmitted and incident wave.

EMW in conductors consider the existence of free charges and currents, that we don’t control ρ_f and $\mathbf{J} = \sigma\mathbf{E}$ will impose the following boundaries conditions:

[3]If we where using DC voltage, electric breakdown at the HV terminal is one of the main problems to overcome when a particle is accelerated, instead for modern accelerator it used AC generator of RF waves. Only for the Main Injector, the required voltage is 120E9 while the dielectric strength of the air is 3E6. In order to avoid the arcing between electrodes the separation between them would need to be of 40 kilometers in a ”static” the Main Injector. [12]

$$
\begin{aligned}
\bar{E}_1^{\parallel} &= \bar{E}_2^{\parallel} & \bar{B}_1^{\perp} &= \bar{B}_2^{\perp} \\
\epsilon_1 \bar{E}_1^{\perp} - \epsilon_2 \bar{E}_2^{\perp} &= \sigma_f & \frac{1}{\mu_1}\bar{B}_1^{\parallel} - \frac{1}{\mu_1}\bar{B}_2^{\parallel} &= \bar{K}_f \times \hat{n}
\end{aligned}
\tag{4.6}
$$

Which in the case of a perfect conductor the incident wave will be totally reflected with a -180 phase shift.

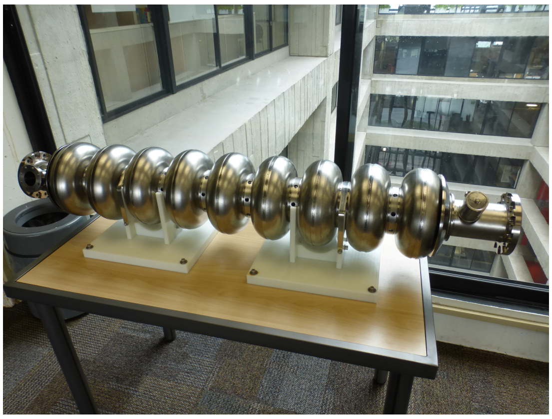

Figure 4.2: A niobium-based 1.3 GHz nine-cell superconducting radio frequency to be used at the main LINAC of the International Linear Collider. Photo from FNAL.

The generation and transmission of electromagnetic radiation involves metallic structures with dimensions comparable to wavelengths (meters) that we are working with. Hollow metallic cylinders that produce the propagation or excitation of electromagnetic waves are called **wave guide**. From the Maxwell's equations, and considering a axial symmetry a general solution can be found.

$$
[\nabla_t^2 + (\mu\epsilon\frac{\omega^2}{c^2} - k^2)]\begin{Bmatrix}\mathbf{E}\\ \mathbf{B}\end{Bmatrix} = 0 \tag{4.7}
$$

The explict solution is composed from a tranversal electric and magnetic fields with the boundary conditions imposed to the normal component to the surface of the electric field and the parallel component for the magnetic field since the wave guide surface is a perfect conductor.

$$
\mathbf{B}_t = \frac{1}{(\mu\epsilon\frac{\omega^2}{c^2} - k^2)}[\nabla_t(\frac{\partial B_z}{\partial z}) + i\epsilon\mu\frac{\omega}{c}\hat{k} \times \nabla_t E_z] \tag{4.8}
$$

$$
\mathbf{E}_t = \frac{1}{(\mu\epsilon\frac{\omega^2}{c^2} - k^2)}[\nabla_t(\frac{\partial E_z}{\partial z}) - i\epsilon\mu\frac{\omega}{c}\hat{k} \times \nabla_t B_z] \tag{4.9}
$$

As can be seen, in order to fully calculate the fields, it is only needed the E_z and/or B_z. The two boundary conditions can not generally be satisfied simultaneously, therefore we have two distinct categories of EMW that can exist in the wave guide: a **tranverse magnetic** mode (TM) and a **transverse electric** mode (TE).

$$\begin{array}{cc} \multicolumn{2}{c}{\text{Transverse Magnetic (TM)}} \\ B_z = 0\text{, everywhere. Boundary condition:} & E_z|_S = 0 \\ \multicolumn{2}{c}{\text{Transverse Electric (TE)}} \\ E_z = 0\text{, everywhere. Boundary condition:} & \frac{\partial B_z}{\partial n}|_S = 0 \end{array} \tag{4.10}$$

The logic choice in order to accelerate charge particles is to use the TM mode, since the B_z is zero everywhere, avoiding the change in the trajectory of the particle (eq. 4.5).

Furthermore, the boundary conditions constrains to a spectrum values that γ_λ can take. Each λ is called *modes of the guide*, and the frequency of the electromagnetic planes (ω) is determined according to the values:

$$k_\lambda^2 = \mu\epsilon(\frac{\omega^2}{c^2} - \gamma_\lambda^2), \tag{4.11}$$

ω_λ is defined as the cutoff frequency, since :

$$\omega_\lambda = c\frac{\gamma_\lambda}{\sqrt{\mu\epsilon}} \tag{4.12}$$

and the wave number can be written as:

$$k_\lambda = \frac{1}{c}\sqrt{\mu\epsilon}\sqrt{\omega^2 - \omega_\lambda^2} \tag{4.13}$$

it can be seen that, for $\omega > \omega_\lambda$ the wave number is real and the wave propagates through the wave guide. When it is not positive, k_λ is imaginary, and it is attenuated while it propagates, which is not the desired case for RF Cavities.

At this point we know that RF wave guides generate an electric field which in the axis of the guide is parallel to the axis, but a cavity has ends, so forth an additional condition is impossed to eq. C.16. The cavity's walls are taken to have infinite conductivity, while the cavity is filled with a lossless diaelectric with constants μ, ϵ.

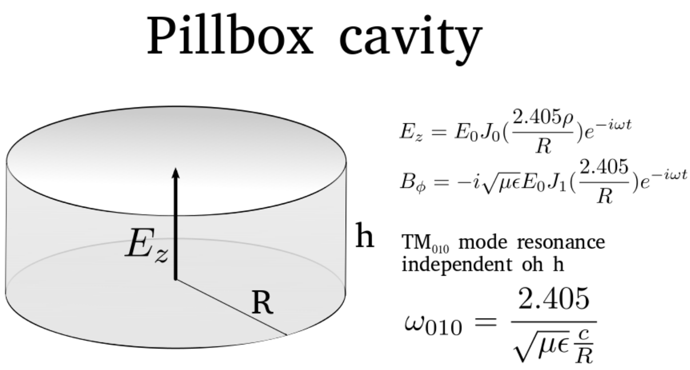

Figure 4.3: A pillbox cavity. The lower mode frequency does not depend from the height of the cavity.

The reflections on the ends of the cavity add additional boundary conditions, which means that the waves will be reflected. The general solution for TM waves are:

TM waves

$$\begin{aligned} E_t &= -\frac{p\pi}{d\gamma^2}\sin(\frac{p\pi z}{d})\nabla_t E_z \\ B_t &= -\frac{i\epsilon\mu}{c\gamma^2}\cos(\frac{p\pi z}{d})\hat{k}\times\nabla_t E_z \end{aligned} \tag{4.14}$$

For a pillbox (a cavity cylinder) the TM mode the transverses equation have solution that includes Bessel functions and an angular dependence in ϕ. For $\psi = E_z$ and with the boundary conditions $E_z = 0$ at $\rho = R$, the solution for the lowest resonance frequency in TM mode (m=0,n=1,p=0):

$$\begin{aligned} E_z &= E_0 J_0(\frac{2.405\rho}{R})e^{-i\omega t} \\ E_t &= E_0 J_0(\frac{2.405\rho}{R})e^{-i\omega t} \\ B_\phi &= -i\sqrt{\mu\epsilon}E_0 J_1(\frac{2.405}{R})e^{-i\omega t} \end{aligned} \tag{4.15}$$

The resonance frequencies depend on three indexes one from the periodicity of the cavity and two from Bessel's solutions.

$$\omega_{mnp} = \frac{c}{\sqrt{\epsilon\mu}}\sqrt{\frac{x_{mn}^2}{R^2} + \frac{p^2\pi^2}{d^2}} \tag{4.16}$$

As can be seen in the the eq. 5.15 the electric field points longitudinally, the magnetic field has a minimal transverse effect on the beam, while the energy is stored and moves back-and-forth between the electric and magnetic fields with a phase difference of 90 degrees.

4.2.2 Power Losses in Cavity

Resonant cavities have definite field configuration for each resonance discrete frequency of oscillation. Fields will not built up unless the exciting frequency matches the resonance frequency, but in reality there is a narrow band of frequencies around the eigenfrequencies where excitation occurs. The **quality factor** or "Q" measure the energy efficiency of an oscillator or the sharpness of response of the cavity to external excitation:

$$Q = \omega_0 \frac{\text{Stored energy}}{\text{Power loss}} \tag{4.17}$$

Assuming ohmic losses, the stored energy decay exponentially according to $e^{-\omega_0 t/Q}$, where for larger values of Q, the decay is slower than small values of Q (fig. C.3). Accepting that there is no single frequency but a superposition of frequency around $\omega = \omega_0$, there will be a range of frequencies that will generate standing TM waves in the cavity. For this range of frequencies, the energy distribution in the cavity can be calculated:

$$|E(\omega)|^2 \propto \frac{1}{(\omega - \omega_0)^2 + (\omega_0/2Q)^2} \tag{4.18}$$

which has a Lorentz line shape shown in the fig. C.3 with a full width at half-maximun equal to ω_0/Q. The energy of oscillation in the cavity will follow the resonant curve in the neighborhood of the particular resonant frequency. $\Delta\omega$ is the frequency separation between half-power points, so Q can be defined also as:

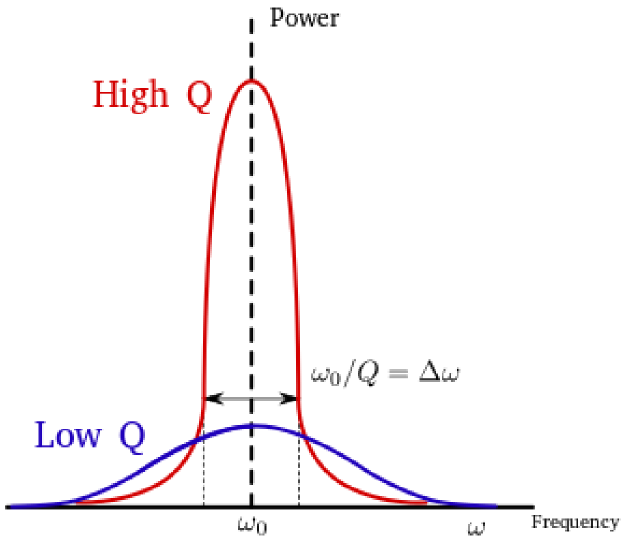

Figure 4.4: The resonance curve's full width is equal to the central frequency ω_0 dived by Q.

$$Q = \frac{\omega_0}{\Delta\omega} \tag{4.19}$$

This definition makes explicit that Q is related to the frequency width of the cavity response. Since RF cavities with high-Q have a narrow frequency response (a lower frequency width). This feature of RF cavities are useful for linear accelerators, where the cavity frequency does not change. The Fermilab's accelerator complex (sec. 4.1.1) is composed by two synchrotrons (the Booster and the Main Injector) that require the RF increase with the beam energy that is achieve by attaching small coaxial RF transmission lines to the RF cavities that are loaded with ferromagnetic material. This ferrite tunner change the inductance of the entire system, altering the resonant frequency of the RF cavity while it is needed in the synchrotron.

4.3 Time structure of the Beam

4.3.1 Synchronicity condition

Since the RF cavities are connected with other machines along the beamline, the RF oscillations must match in time with the arrival of beam in the cavity, and take advantage of the right force direction, during half of the oscillation. The particle arrival time with respect to the RF cycle is know as the **RF phase**. By doing this, the particle will always see an accelerating voltage at each RF gap.

To achieve this, the distance between cavities in a linear accelerator and the RF frequency have to be chosen to prevent the beam to arrive in the cavities on the other half of the oscillation. For this to occur, the following relationship must be hold:

$$\omega_0 L = \frac{n\nu}{2}, \tag{4.20}$$

where ω_0 is the RF frequency, the distance between cavities L, the particle velocity ν, and interger n. This equation is know as the "**synchronicity condition**".

In the case of synchrotrons like the Main Injector, the RF cavities are placed along the circumference of the machine and the frequency of revolution along it, must be an interger of the RF frequency. The interger multiple of the revolution frequency, h is call the "harmonic number".

$$\omega_{0_{RF}} = \omega_{REV} \tag{4.21}$$

Considering a particle with speed $v = \beta c$ circulating along the machine with period of revolution:

$$T_{rev} = \frac{2\pi R}{\beta c} \qquad \omega_{REV} = \frac{\beta c}{2\pi R} \tag{4.22}$$

We can see that it depends on the radius and the velocity that at the end we want to reach β, there is a maximum numbers of "spots" that can be accelerated on a synchrotron[4].The segments of the circumference centered on these points are called **buckets**.

[4] In the case of the LHC, there are approximate 35640 buckets but not all of them all filled with particles with only 2808 of them occupied.

4.3.2 synchrotron Oscillation, Buckets and Bunchs

A particle that is exactly synchronised with the RF frequency is called synchronous particle, but there are always slightly deviations in the particles momentum in the beam and particles with different velocities will not met the synchronicity condition 4.20.

That is why the beam will have a non-zero energy and phase spread, because each particle will arrive at a slightly different time, feeling a different electric field strength.

Lets consider the case of three particles arriving on different times into a RF cavity. The early-arriving particle (A) will feel a weaker electric field than synchronous (B) particle, moving it toward the synchronous phase. For later-arriving particles (C) will see a higher electric field that help them to adjust its velocity into phase synchronous particles speeding up.

All particles will oscillate longitudinally around the synchronous particles under the influence of the RF electric field, this longitudinally-focusing process is called phase focusing. However there are limits to the phase focusing ability of the RF, a particle outside the range of synchronous phase will not be pushed to maintain stable oscillations. A **bucket** is defined as the stable RF space that can be phase focused. For all the particles in the bucket, the beam has a net acceleration, phase focusing adjust the beam momentum for stability: this longitunial motion is called ”synchrotron oscillation”.

In the case for synchrotrons the number of RF buckets in a machine is limited, because the number of RF buckets will depend of the time it takes a particle to make one orbit. The phase focusing process causes beam to be collected into discrete packets known as **bunches**. Since the bucket area is the only stable place for beam to exist, it is often said that the bunches fill the buckets.

For high energy particles in synchrotrons, they will have longer orbits and a lower revolution frequencies (delaying its arrival at the RF cavity). Reciprocally, low energy particles will have a shorter orbit, reaching the RF cavity sooner [5]. Particles in the same time than synchronous particles but with higher energy will

[5]Since the angular frequency is defined as $\omega = v/r$, where r is the radius and v the velocity of the particle.

see a decelerating electric field, reducing its energy and velocity until is enough to surpass the correct revolution frequency, this particles will be accelerated by the RF cavity reaching the same situation than the first turn. As can be seen, synchrotron oscillation is inherent to the RF cavity. A beam is called unbuched beam (DC beam) if it does not comes in bunches.

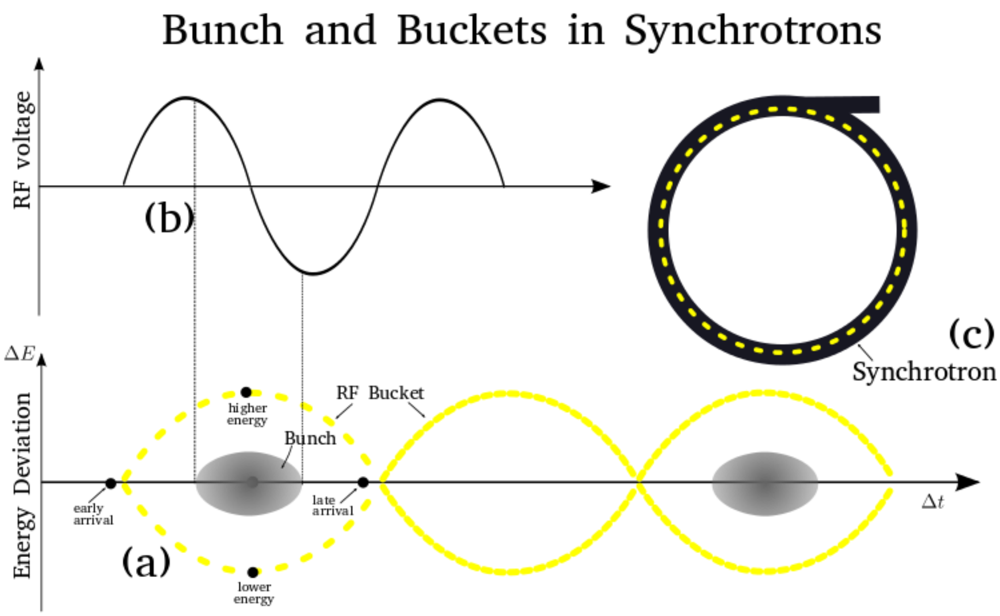

Figure 4.5: Graphic description of a Bucket and a Bunch, the RF voltage that the particles see while they are in a bunch and how the buckets arrange themself on a synchrotron's ring.

4.3.3 Time Structure of the Beam at MCenter

The beam at the FTBF, has a inner structure regarding the time as a variable composed by three scales that allow us to describe the time profile of the beam

Table 4.1: Time structure of the Beam according to Accelerator Division.

Scale	Composition	Related with	Duration
RF Bucket	”one” particle	RF's frequency	19ns (52.8MHz)
Batch	84 RF buckets	Booster length	1.6μs
MI cycle	7 Batches	1 cycle of the Main Injector	11.2μs
Spill duration	375000 MI cycles	Resonant extraction	4.2s

We will explain in detail why it is structure in this way, and the role of the different machines mentioned in the sec. 4.1.1 in the production, composition and the duration of this scales.

It is necessary to mention that, the protons that compose the beam initiate its journey in the Proton Source at Fermilab, where a pre-accelerator process accelerates the protons from 0 to 750KeV through a RFQ cavity. After this, the ions are injected into the LINAC.

4.3.4 The Booster and the formation of Buckets and Batchs

The linear accelerator (LINAC) accelerate H^{-}-ions from 750KeV to 400 MeV across a set of cavities that operate at a resonant frequency of 804.96 MHz. By using magnets, the LINAC is able to provide the 400MeV protons to the Booster. There are two RF frequency used in the LINAC: 201.24 MHz and 804.96 MHz. The later value is the RF frequency that goes into the Booster during the injection of protons that has to last the exact value of the revolution period of Booster $(2.2\mu s)$.

After injection is complete, the Booster's RF accelerates the beam from 400MeV to 8GeV, but with different RF frequency comparing to the LINAC. The process of re-bunching the beam according to the new RF frequency is called *paraphasing*. The Booster is a synchrotron made of 19 RF stations, that change the frequency from 37.8 MHz to 52.8 MHz as the beam revolution as the beam period is reduced from $2.2\mu s$ (injection) to $1.6\mu s$ (extraction)[6]. So the buckets, will have a length in time of $1/52.8MHz = 18.9ns$. The harmonic number for the Booster is 84, the value of buckets that circulate along the Booster. A **booster batch** is composed of this 84 buckets that goes into th extraction process.

The extraction is done by injecting the protons into the MI-8 beamline that delivers the proton beam to the Main Injector, the BNB beamline, the Recycler or the Booster dump.

[6]High energy particle in synchrotrons will have higher values of revolution period, and low energy particles; will have lower values of revolution periods

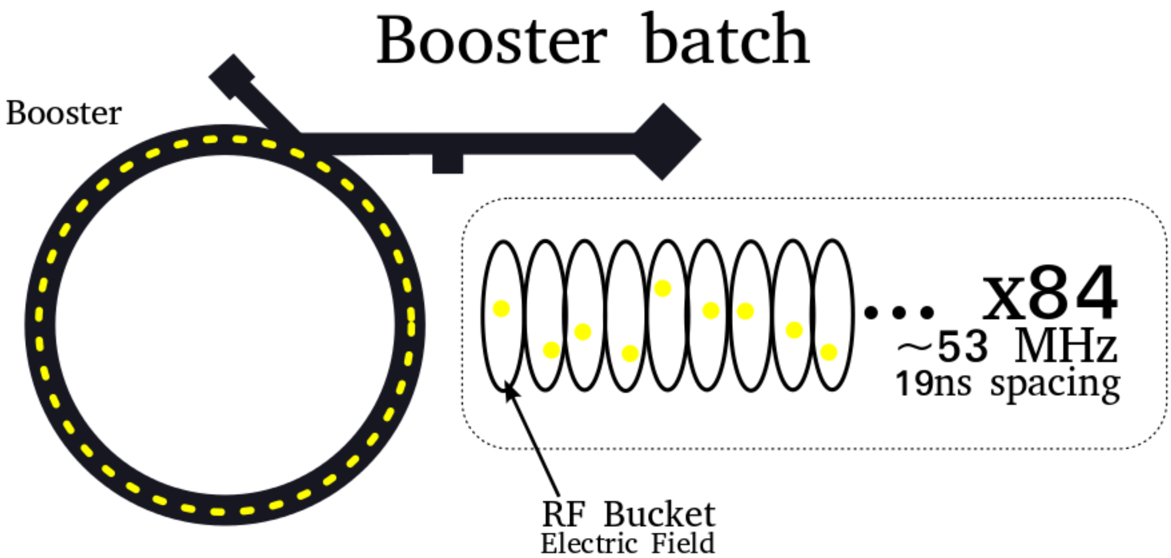

Figure 4.6: How is the booster bacth formed and the value of it.

4.3.5 Main Injector: formation of MI Cycle, Resonance Extraction and Spill frequency

After the Booster, the beam proton is injected to the Main Injector where it ramps up the kinetic energy from 8GeV to 120 GeV. Made of 20 RF cavities, during the acceleration the frequency sweep from 52.8 MHz to 53.1 MHz, allowing the transfer from bucket-to-bucket from the Booster. While the protons are circulating the time beam structure remains the same, and the buckets slightly shrink in time to $1/53.1MHz = 18.8ns$.

As the same with the Booster, due to the length of the circumference of Main Injector (3319.4 m), 7 booster batches are injected during a time of 11.2μs. This is the value of the MI Cycle, the time that takes a particle to go around all the machine.

After reaching the 120GeV energy, the extraction process is done in order to deliver beam to the different beamline that provide beam to experiments like NuMI, or which is the case for this thesis, to the Test Beam (MTest) Facility where the data has been taken.

The extraction of the beam that is use in the MTest is made using the process call **resonance extraction or spill duration** that allow us to have a long low-intensity pulse, in other words the beam is shaved off on every rotation the beam makes around the machine, which in our case is 375000 MI cycle giving the length in time of 4.2s each 60s. Typically, only the first batch will have particles in it and the process is repeated around each minute. This interval of time is called **Spill frequency**

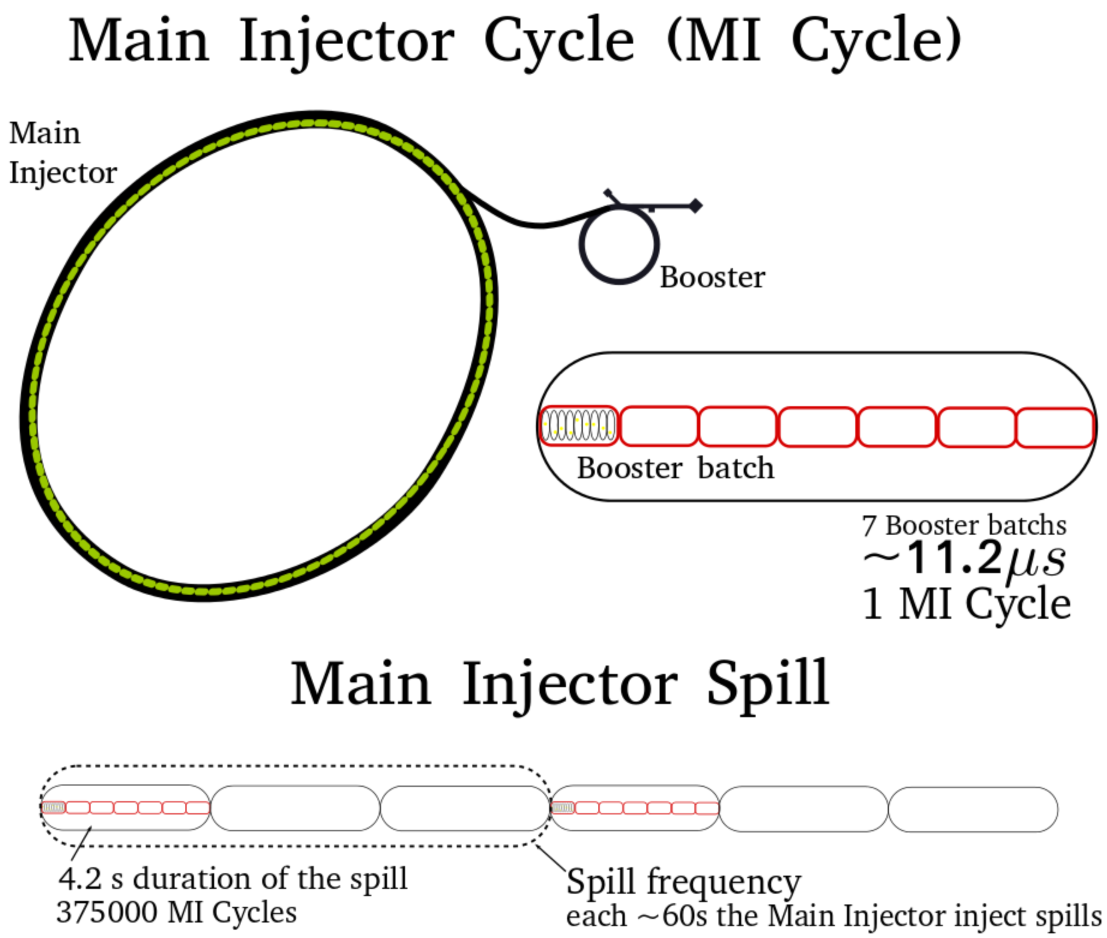

Figure 4.7: Diagram showing the MI's cycle formation, spill duration and spill frequency.

Chapter 5

Tools for Data Analysis

In the chapter (1) we describe the weak interactions interactions and how the neutrino's mass change the experimental neutrino physics research, shifting the focus into neutrino mass oscillations and the interaction of neutrinos with matter experiments (1.2.1, 2.2).

And since MINERvA (3) started in 2009, its construction was made in order to have fully functional detector of neutrino interactions in the low and medium energy (with publications like B.6). The success of this kind of analysis rely on the ability to remove the systematic errors and be able to reduce them in order to get the true constructed energy of the incoming neutrino by improving the models.

That is why exists the MINERvA Test Beam experiment (3.2.1) which is currently studying the calorimetric detector response in the medium energy. In this experiment is important to know the energy and type of the incoming particles by knowing as best as we can the characteristics of the beam. Chapter 4 explain why the structure of the beam has three scales (bucket, batch and spill) and how the length in time of those structure are set up. The appendix C backs up this analysis with a more theoretical description of the Radio Frequency cavities, the key elements in the acceleration of the beam.

In this chapter, we outline the results of the analysis of the time structure of the Test Beam program for medium energies. In the first section we describe some general concepts about Statistical Analysis 5.1 which is mostly descriptive statistics and the use of the statistical package 5.1.1 ROOT. In the sec 5.2 we describe the data taken in the experiment, in 5.3 the developed tool (named TbTaTool) and in sec. 5.3.3 the implementation of these tools into the data.

Finally the results are shown in 6.1 and 6.2, while the conclusions in 7 and further work are describe in **??**.

5.1 General concepts of Statistical Analysis

Statistics is the science of drawing conclusion from data, data are measurements of some quality or quantity of the world, a value that can be obtain when we apply a tool to an observable variable, for example: a ruler marked off in inches is a measurement tool for measurement the variable length of an object. The object can be related with this measurement, and formally it can be defined as logic set of rules and steps that tell us how to apply the measurement scale to an observable variable.

The data is composed of only *approximate measurement* from the *true measurement*. If we increment the sensitivity in our instruments, we can improve on many decimal places but there is a limit to even the most powerful instruments.

A **systematic errors** of measurements, result from weakness in the measurement procedure that produce distortion making the measurement always too large or too small, while the **random errors** are produced by random stochastic variations in the measurement. Two familiar concepts, accuracy and precision, are deeply related with the type of errors.

Accuracy of a measurement refers to how close the measurement made is to the true measurement, depending of the sensitivity of the measuring instrument and the presence of errors in the process of measurement, particularly systematic errors. **Precision** of a measurement deals with how identical measurements are able to reproduce similar values.

The tools of statistics are divided by two big divisions: descriptive statistics and inferential statistics. While descriptive statistics ordered the data from the measurements in order to gain insights about it, **inferential statistics**, infer properties of a population from a random sample. Histograms are great tools for data visualization, compose by bars with their areas' being the fraction of data in each class interval. Finally apart from the usual measurements of central tendency, it is important to remember the definition of the **standardd deviation**, which measure the average distance from the data to their mean (or the RMS of the deviations of the data from their mean).

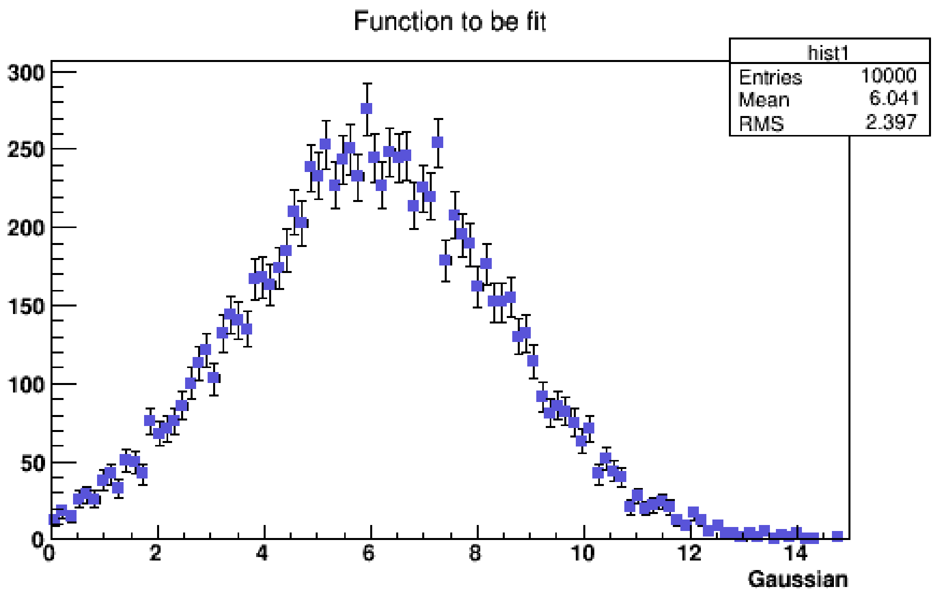

Figure 5.1: A standardd histogram with box plots generate in ROOT.

A way to resume all the statistical information from a set of measurements is throught the five-number summary or **box plot**, which is floating-rectangle graph constructed horizontaly with the measurement scale along the X axis, or respectively in the Y axis. The graph displayed $\bar{x} \pm s$ and the range. The rectangle's ends display the first (25%) and thrid quartile (75%) along the measurement scale. The horizontal line through the box is the mean.

In the fig. 5.4, we show a histogram formed by different measurements and box plots (blue boxes) for each of them.

5.1.1 ROOT: Data Analysis Framework

"ROOT is a cross -plataform C++ framework for pentabyte data storage for statistical analysis and visualization"[4], developed in order to manage large amounts of data in a efficient way. For example, the expected data amount produce by

LHC is (1PB = 10E6 Gb) per year[1]. ROOT is cross-plataform since implementation of ROOT in C++ or python allow the user to take advantages of the inner characteristics of these language programs.

The hierchacy of the programs follows the model of trees and branches. A ROOT file contains all the data saved in different chains. A chain is a collection of Trees, a Tree can have many branches and each branch has many leafs (this is call a n-tuple). Each leafs are variables that we read through each event. Since these events produced by the experiment are statistical independent, they all have the same data structure. That is why ROOT has a hierarchical object-oriented database with plentyful of package for statistical analysis and high-performance data processing.

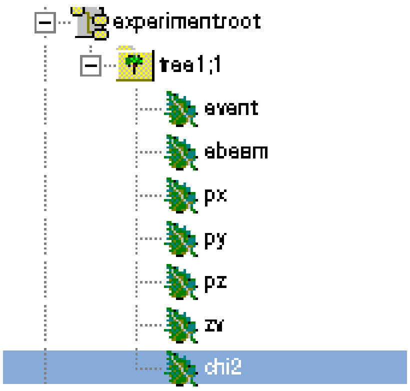

(a) A tree named tree1, and all the variables that where recorded

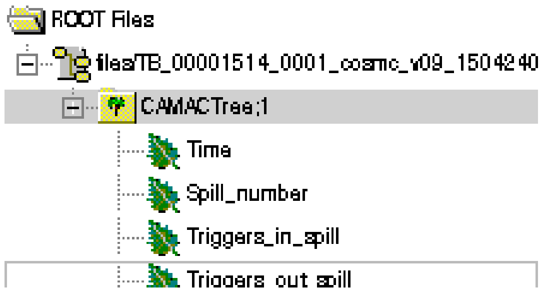

(b) Data recorded from the data readout auxiliary system, a n-tuple.

```
*    Row   *      event *      ebeam *         px *         py *         pz *
zv *       chi2 *
*********************************************************************************
****************
*        0 *          0 * 150.14041 * 14.333598 * -4.021043 * 143.54425 * 22.2641
10 * 0.9405828 *
*        1 *          1 * 149.78578 * 0.0509290 * -1.373310 * 148.60041 * 0.61407
61 * 1.0205643 *
*        2 *          2 * 150.16188 * 4.0079331 * 3.8898270 * 145.68779 * 16.5689
65 * 0.8934459 *
```

(c) How the data is recorded for each event. The rows correspond to the values and the columns to the variables. ROOT reads the information acording to branches, not as events. A Ntuple is storage in terms of events (horizontal).

Figure 5.2: Structure of the data in a ROOT file.

Having the same data structure with many events, the analysis are done run-

[1] In case of MINERvA, the NuMI low-energy data size is around $\sim$ 3 GeV with about half of those data are beam spill data and half are calibration data [29].

ning macros (a collection of well defined steps) which automates the analysis performed for all the events. Actions like fitting a histogram, plot histograms and made correlations graphics, include bar errors and present the data in more comprehensive visual format is done with few lines of code in ROOT. However, the curve of learning is higher since the C++ and specific sintax requirements are used by ROOT.

In the next section we will explain some concepts of statistical analysis while, showing some commands in ROOT that allows us to work with them.

Fitting a histogram

Fitting a histogram allow us to get an approximation of the parameters that characterize the curve like the mean or the standard deviation. This can be achieve in ROOT's graphic mode or through algorithms that includes them.

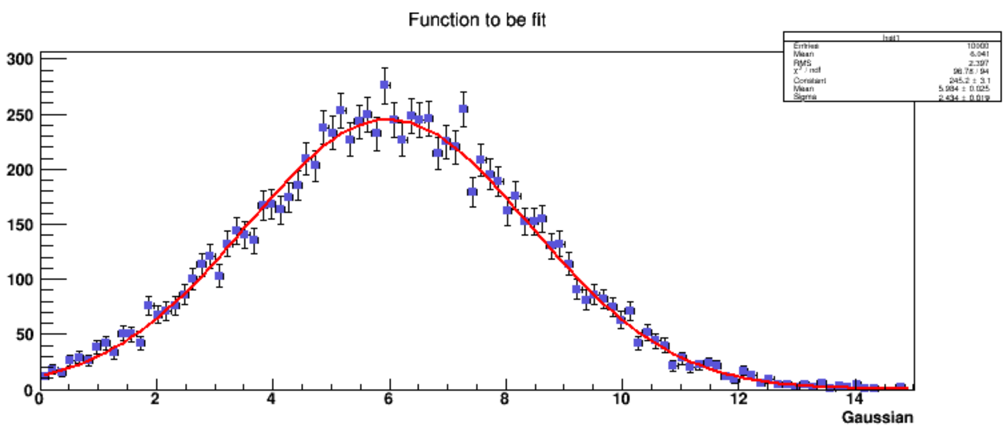

Figure 5.3: Fitting a histogram made with three lines of code.

```
[root] TF1 func("mydoublegauss","gaus(0)+gaus(3)")
[root] func.SetParameters(5.,5.,1.,1.,10.,1.)
[root]  hist1.Fit("gaus")
[root] hist2.Fit(    mydoublegaus     )
```

Running a Macro

A macro is a set of well defined steps that are going to be apply to each event of the variables that we are using to analyse.

```
void AnalyzeSpill::Loop()
{
 if (fChain == 0) return;
     Long64_t nentries = fChain->GetEntries();
     Long64_t nbytes = 0, nb = 0;
   "LINE1" // == Begin of the Loop ==
     for (Long64_t jentry=0; jentry<nentries;jentry++) {
        Long64_t ientry = LoadTree(jentry);
        if (ientry < 0) break;
        nb = fChain->GetEntry(jentry);   nbytes += nb;
    "LINE2" // == The Loop over all the events goes here ==
        // == The cuts are apply here  ==
        if (In_spill > 0.5  ){
          Time_spill= (Double_t) Time -1429838450;
          }
        else if (Spill_number == 1 ){
          "LINE3"
          // == Assign values to the variables
          Time_spill_1= (Double_t) Time -1429838450;
          tree_spill->Fill();
          }
}
f_spill.Write();
```

In **LINE 1** we are initiation the ”loop”, the set of steps that will be repetead for all the events that pass the cuts or condtions. From the **LINE 2** the coditions are placed using the if conditional *if(condition) steps* . Finally in **LINE 3** we calculate the variables with the filtered sample. In our case we were subtraction a fixed value to the timestamp and then filling the result into the root file.

Simple Analysis

Lets assume that we have a set of data with three variables: energy of the beam (ebeam), final momenta in the x,y and z direction (px, py and pz). In this example, a particle is traveling in a positive direction before it is deflected by a material at a distance zv.

We can create a histogram of one of the variables (a), or plot two variables at once (b), create a scatterplot observing the correlations between two variables or apply conditions (c -cuts) to the variables in order to get insights (d) (fig. 5.4)[2].

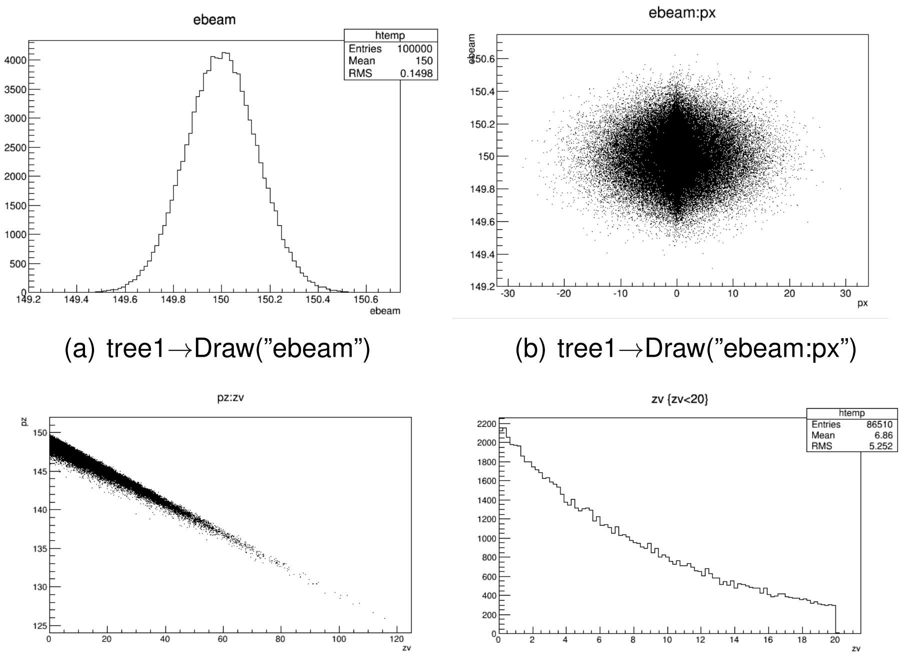

(a) tree1→Draw(”ebeam”)

(b) tree1→Draw(”ebeam:px”)

(c) tree1→Draw(”px:py”)

(d) tree1→Draw(”zv”,”zv<20”);

Figure 5.4: Structure of the data in a ROOT file. The comments below the plots are the ROOT commands.

[2] Due to the process of learning ROOT during the development of these tools, a full manual has been written and can be accessed here `https://www.dropbox.com/s/k64vh4k52smlqmm/manual_root.pdf?dl=0`.

5.2 Description of the Spill scale in the beam at MTest

In the former section, I have described how to fit, running a Macro and make a simple Analysis with just one line. However in order to gain insights about the time structure of the beam thought the TB data, the code is more complicated.

Since we are measuring a physical variable with an instrument, it is important to know how the process of measurement is done and what are we actually measuring. This will help us to know not only the sources of systematic errors but also to consider the necesarry filters or cuts in order to eliminate the background or data that it is not important to the analysis. In this thesis it has been important to know how the detector and auxiliary systems have been designed, the readout process of taking data, the resolutions timing and the characteristics from the input. I will explain more on these points.

The auxiliary system of the Test Beam (sec. 3.2.3) has been desing in order to maxime the number of particles of know momentum and type that will be detected. This impose some specific constrains to the readout system and DAQ, with the most important one that the system must discard events that have not pass the "trigger criteria". As mentioned in the sec. 3.2.4, the triggers conditions avoid of taking data for other events than the particles that we requested to the AD. **So we only see events during the spill**, anything else is background and can not be analyze.

As mentioned in the sec. 3.2.2 and 4.3, there is a specific structure in time which depend of the RF frequency and the harmony number of the Main Injector synchrotron. **Particles come in "packages"** (buckets, batchs or spills) and outside these we do not have any particle in theory. The trigger criteria does not allow us to see **out side the spill**, all our results can not prove that the hole structure advertised from the AD is correct, it only can say that the structure during the delivery of particles can be or not correct.

As it has been stated in the previous sections sec. 3.2.1, it is of real importance the characterization of the secondary beam that we recieve as an input for the Test Beam MINERνA's detector. One of this variables is the timestamp in which we receive the particles ($\pi^{\pm}$, $e^{\pm}$ or $\mu^{\pm}$) without knowing their identity. This thesis has accomplished the study for one scale: the spill scale. In other words, we will describe the time structure of the beam for the first scale. As we recall, the spill is the length in time that the Main Injector (4.1.1) deliver particles into the MTest at fermilab, the oficial time: **4.2s** is the results of the slow extraction process from the main ring sec. 4.3.5.

5.2.1 Description of the data

During the data takeout, the TB detector has been modified in two mode: ECAL/HCAL and Tracker/SuperHCAL and data has been taken during three different periods of time during the year of 2015.

Each mode represent a different configuration of numbers of planes for the ECAL and HCAL regions mentioned before in the sec. 3.2.2. The followig table resume them:

Table 5.1: Configurations of the Test Beam detector and the type of particles that contain them.

Run	Energy	Type	Configuration	Date
Run 1	1.55,1.77,2,3,4,6,8 GeV	$\pi^{\pm}$,$e^{\pm}$	ECAL/HCAL	6-21 April
Run 2	4,6,8,9,10,16 GeV	$\pi^{\pm}$	Tracker/SuperHCAL	23-30 April
Run 3	2,3,4,5,8 GeV	$e^{\pm}$	Tracker/SuperHCAL	during June

However, the "Runs" category has more impact in the PID analysis and not in the timing data which do not differentiate between different Runs or identity of particles. In this thesis we will present the results vs energy and polarities.

It can lead to some confusion but, Run3 or Run2 are refering to the time and configuration of the detector in which the data was taken. However, the data process has been ordered using some similar words: run, subrun and gate. In the fig. 5.5 it can be seen a diagram of how the data have been taken. A **gate** is the internal variable of the CAMAC TDC 3377 which roughly speaking correspond to one event that has pass the trigger criteria. A **subrun** is the collection of gates (d), usually fixed in 1000. And a **run** (a,b and c) is a collection 74 subruns. Each run contain data from an specific value of energy and polarity of an expected type of particle and it is customary that one subrun will have 6 spills in the case of electrons which corresponds to the variable $Spill\_number$.

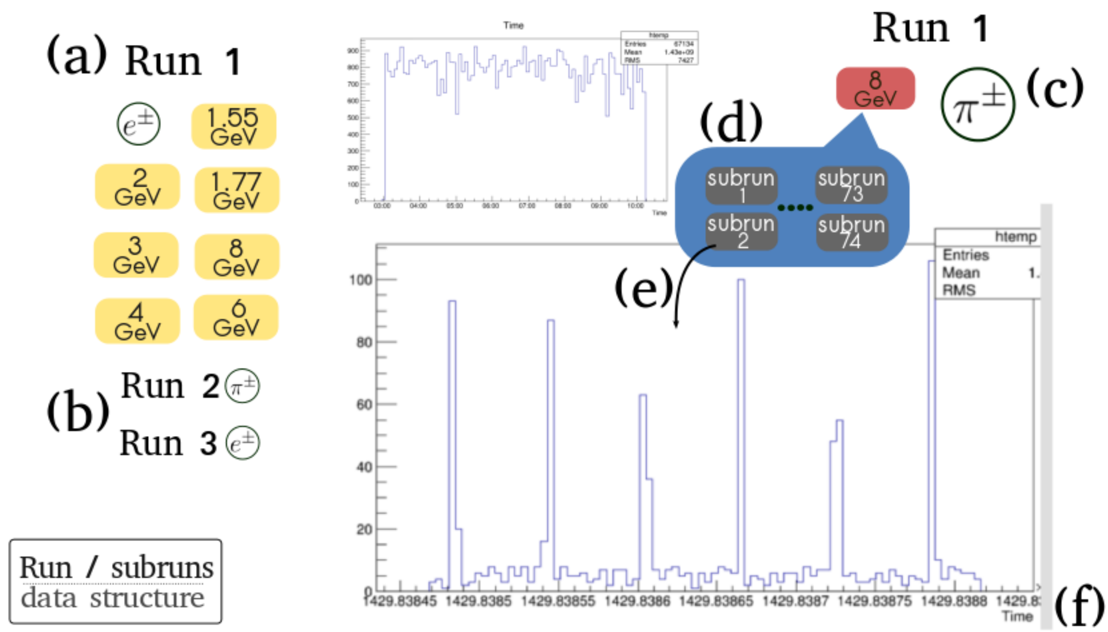

Figure 5.5: Diagram of how the data is ordered in the ROOT file. The variable shown is *Time* of readout. (a) and (c) are the energies that Run 1 contains for electrons and pions in both polarities (all the energies are presented in tab. 5.1). (b) Run 2 and Run 3 contain onlu electrons and pions. (d) Each Run has a number of subruns. (e) Each subrun constains the the data for 1000 gates or events. (f) One of the variables is the $Time$ variable as shown in this figure.

As can be seen, the Run 2 and Run 3 corresponds to only pions or electrons. If those runs have only electrons or pions, a mix of them or if there muons, is a task for the PID analysis made by A. Zegarra. We only use the Run2 and Run3 category as the data that contains only pions and electrons, respectively.

5.3 Development and Features of the Time Analysis Tool (TbTaTool)

The analysis has been made with the data from Run2 (only pions) and Run3 (only electrons) for the following time variable: $Time$, the timestamp[3] in which an event

[3]The timestamp is the time in which and event was recorded. The CAMAC TDC 3377 uses the unixtime which is defined as the numbers of seconds that has passed since 1/1/1970.

comes into the detector readout by the CAMAC 3377, regarding their type.

The variable that we used in order to eliminate the background were: $In\_spill >$ *0.5* which assure us that we where looking particles inside the spill. This signal is provided by the Acceleration Division. With this variable and restiction, we are able to study:

1. The **time profile** of a variable and its reliance with a category-variable.

2. The study of any **time structural** difference in the variable and its dependency with a category-variable by constructing ”time slices”.

3. **Values of any function** of the time and its reliance with a category-variable.

Some words about the general terms that I am using here. By category-variable I am refering to any variable that in the process of measurement help us to characterize the data that we are taking. For example: energy, spill number, polarity, machine that took the data, etc. The use of this variables allow us to look deep into how different parts of the machine are reading out the data, and in terms of the analysis, in the case of category-variable = energy or polarity it allow us to see any difference regarding those variables in the time structure.

And with *”any function of time”* we are talking about any variable that is constructed with some calculation regarding time. For example, in our case we calculate the Spill duration (the time that takes the resonance extraction) and the Spill frequency (4.3.5). In the fig. 5.12 it is shown how is calculated the $Spill\ \ duration$ and the $Spill\ \ frequency$.

However, the TbTaTool need two parameters: the numbers of spills and a zero point in time. The numbers of spills are important since the gates are ordered into spills. For pions and electrons the number was not fixed, by choosing the value of this parameter we are rejecting a percentage of particles to be analyse.

In the case of the reference point, it is needed in order to study the time structural difference, this means the point in which we set as our zero point for each subrun. The following section describe how the values were set up.

5.3.1 Election of a reference point in time

We define the time profile as the "slices of time" of the beam that corresponds to different $Spill\_number$, calculated considering the time of the first event of this slice. But the calculation is made using a point of reference during each subrun. Since the data only have an internal category-variable that order them, but not a point in time where we can start making slices of time profile, it is needed an external reference point.

If we use an internal point of reference, the time profile will be bias for a couple of seconds (2-3) as can be seen in the following figure 5.6.

(a) Diagram of the three points of reference that can be used in the calculation of the *time profile*.

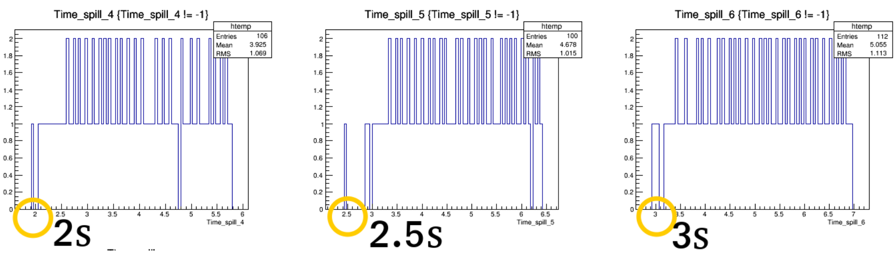

(b) Time profile for one subrun considering the beginning of the ROOT file as the the reference point (2 in the above figure).

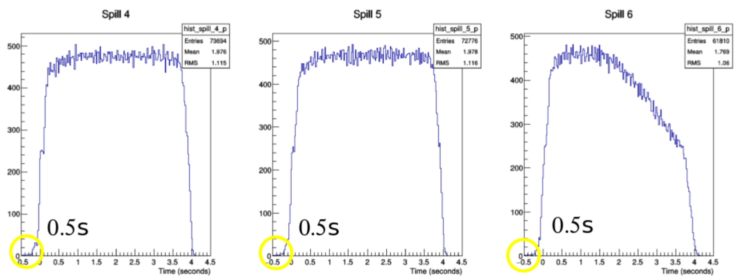

(c) Same as (b) but now considering (3) as the point of reference.

Figure 5.6: Bias in the time profile by using an internal reference point measure in seconds. As can be seen, the (b) elecction allow us to reduce the lost of events between the zero point and the first event.

On the other hand we have the $\$39$ signal, which is the timestamp that is associate with the time after the start of the super cycle, which is start-of-spill.

The code E.4 match each subrun with the closest start-of-spill signal and in order to use it.

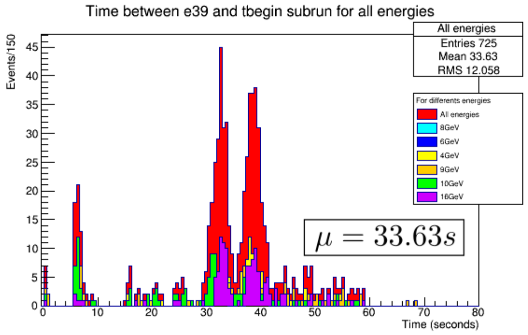

(a) Interval between the $\$39$ and the kick-off the subrun

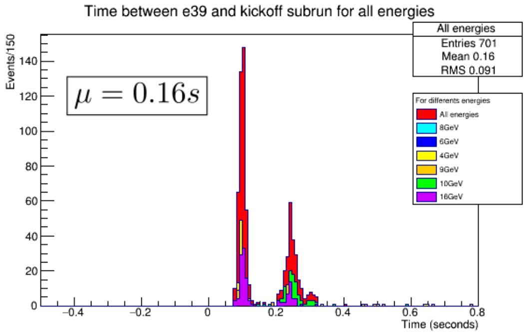

(b) Interval between the $\$39$ signal and the beginning of the root file for Pions.

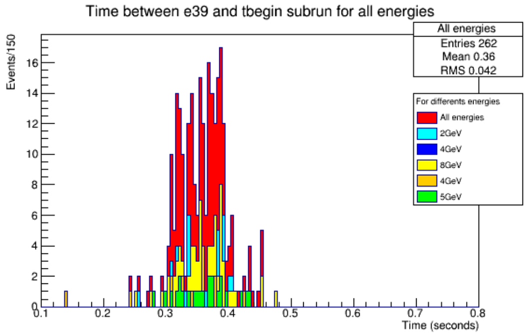

(c) Same as (a) but for data sets containing electrons during June.

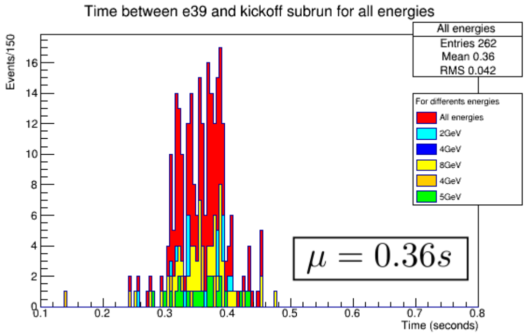

(d) Same as (b) but for same electron data sets.

Figure 5.7: Distribution of the values of the interval between the first event recorded (kickoff od the spill) and two reference points: the $\$39$ signal and the beginning of the subrun.

The interval between the first event and the **beginning of the subrun** is around 33.63 seconds, half of the *MI spill duration* (fig. 5.7 (a)). In the case of the time interval between the **beginning of the spill -** $\$39$ shows that the mean difference is around 0.16s (fig. 5.7 (b)). Less than a second and 210 times smaller. That is why the tool use $\$39$ as the reference point in the calculations of the time profile. In the fig. 5.6 (b) and (c), it can be seen than by changing the reference point we reduce the gap from 2-3 sto 0.5s.

The meaning of 0.5s will be explain in the Conclusions, since it is deeply related with the MI's Spill Frequency. In sec. E.3.1 and D.1.8 can be found part of code and the documentation of the subroutine that make the match between the first event of a subrun and the closest $\$39$ signal from AD.

All the values of time were given in unixtime. The conversion into human-readable time and vice versa, was made through a small python code (E.3.2). In the fig. 5.8 it is shown part of the excel file with the timestamps in central US time of the signal $\$39$.

Time	G:E39SCT	Time	G:E30SCT
21-MAR-2015_12:00:22.487	1,300027	21-MAR-2015_12:00:21.187	0,000001
21-MAR-2015_12:01:22.993	1,300028	21-MAR-2015_12:01:21.692	0,000002
21-MAR-2015_12:02:23.522	1,300031	21-MAR-2015_12:02:22.222	0,000001
21-MAR-2015_12:03:24.059	1,300035	21-MAR-2015_12:03:22.759	0,000001
21-MAR-2015_12:04:24.602	1,300033	21-MAR-2015_12:04:23.302	0,000001

Figure 5.8: File that contains dates from the signal $\$39$ as a reference point.

5.3.2 Number of spills

I have mentioned that category-variables allow us to classify the data while we are taking them or to know how data is been recording respect the different parts/systems of the machine. One of this variables in our data is the $Spill\_number$. The numbers of spills for each subrun is not a fixed number, instead it depends if the number of events (1000) were achieved. The importance of knowing the number of spills for both runs rely on the need to know as an input in know how many spills will TbTaTool cut the spill in order to construct the time profile.

For Run 2, the mean value of spills is 6.287, while Run 3 has $9,86$ as the number of spills during a subrun. The numbers of spills for Run 2 and Run 3 are shown in fig. 5.9. In (a) the distribution of spills for Pions and in (b) for Electrons. The plots are classify in positive and negative polarities, and the stability of spill number during the data taking.

There are cases in which we have more than 15 spills per subrun. The TbTaTool has fixed numbers for the number of spills. For Run 2, 6, while for Run 3: 10. This election do not affect greatly the statistics with which we calculate the other features. In Table 5.2 can be observed the total numbers of events for both situations.

If we consider all the spills, or if we choose 6 (as in the case of Run2) or 10 (Run 3). The last line is the percentage of electrons over pions.

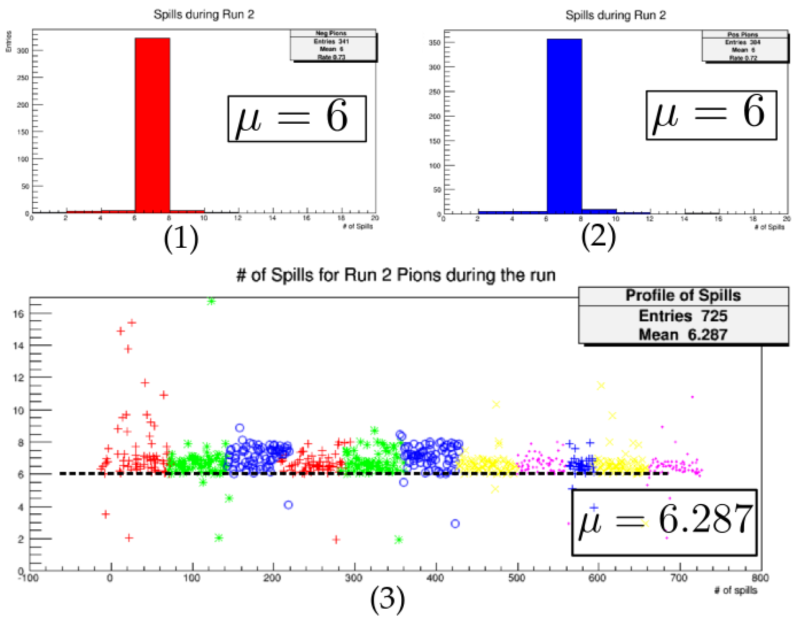

(a) Run 2 only $\pi^{\pm}$. (1) and (2) are the distribution of the numbers of spill versus the polarity. They have the same mean value. (3) Shows the stability of the numbers of spills during all the data taking.

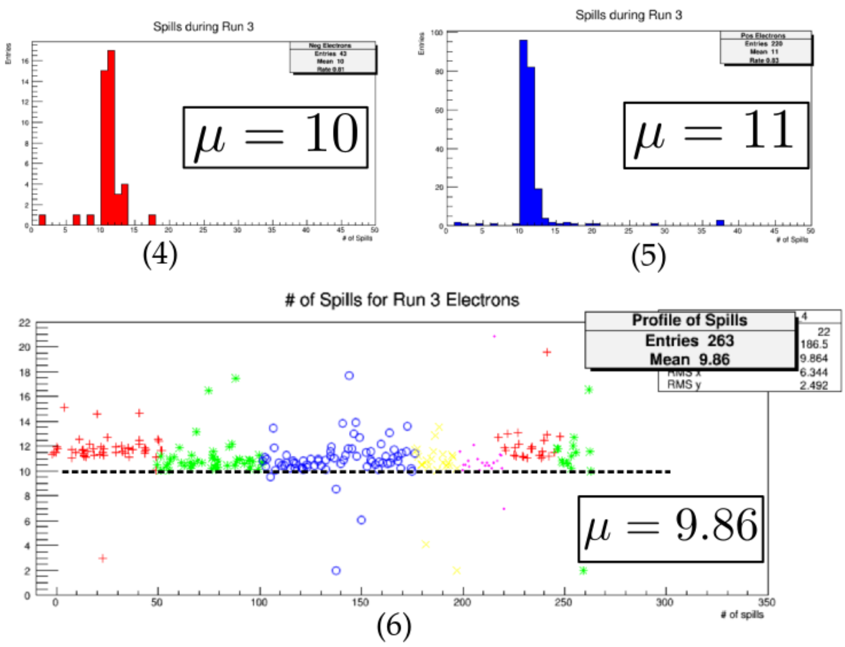

(b) Run 3 only $e^{\pm}$. For (4), (5) and (6) same meaning as in (a). The mean number of spills in this case is 10.

Figure 5.9: Number of spills for Run 2 and Run 3.

Table 5.2: Number of events for Run2 and Run 3 considering all the spills, equal to 10, 6 or 2 spills per subrun.

Run	All spills	≤ 10 spills	≤ 6 spills	≤ 2 spills
Run 2	122285	122285	116782	39111
$\pi^{\pm}$	100%	100%	95.50%	33.49%
Run 3	206432	195383	119648	40702
$e^{\pm}$	100%	94.65%	57.96%	19.72%
$\%$	59.24%	62.59%	97.60%	96.06%

In the case of Run 2 by using only 6 spills per subrun we have 95.50% of all the events. For electrons, Run 3, 6 is not a good election. And by using 10 spills we are analysing the 94% of all the events.

5.3.3 Implementation of the tool for the Test Beam data

The fig. 5.12 is a diagram of how the TbTaTool developed calculate the time profile and any function in time. This part of the tool pile up or stack the different spills for a subrun, and loop over all the subruns according with the condition imposed (for different energies, polarities or type of particle).

In each iteration within a subrun, the value of one *Spill Frequency* (or a multiple of it) is removed to the timestamp of the event, in order to set all the first events around the time zero. The value of the Spill Frequency was provided by the Main Injector according to the fig. 5.10. Before 15/5/5, 60.5246 ± 0.0968 and after; 60.2415 ± 0.1929.

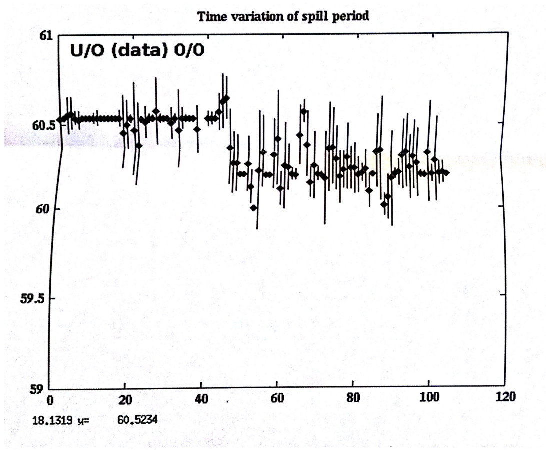

Figure 5.10: MI's Spill frequency during May 2015. Infor provided by A.D.

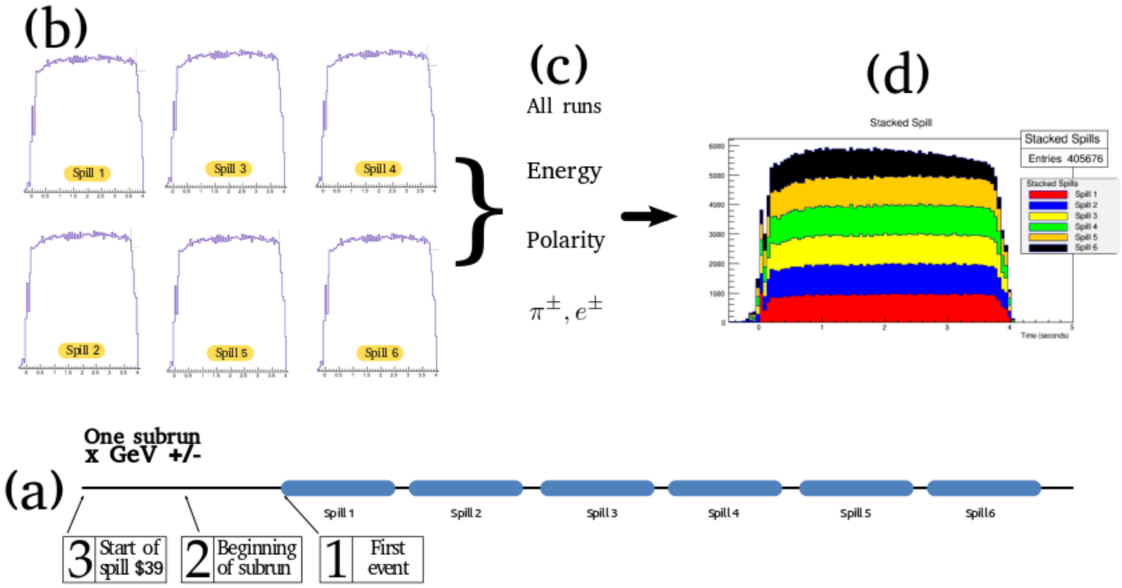

Figure 5.11: How the TbTaTool produced the time profile. In (a) we show a diagram of how the spills come in time and are arranged by the variable $Spill_number$. As it is shown, the point (2) and (3) were used as a reference point. The TAT "cut" the spills (b) independently from one another and then, stack them in one plot (d). The plot can be produced for different energies, polarities or type of particles (c).

Spill Duration is calculated within one spill, the code take the first and last event for that spill, subtract them and recorded in a root file. The same steps are done for all the subruns and energies. **Spill Frequency** is calculated, by taking the first event from two adjacents spills, and calculating the interval of time between those two points. A simple version can be found in E.2 and in the github repository [4].

[4] `https://github.com/gsalazarq/TbTaTool/tree/master/TbTaTool`

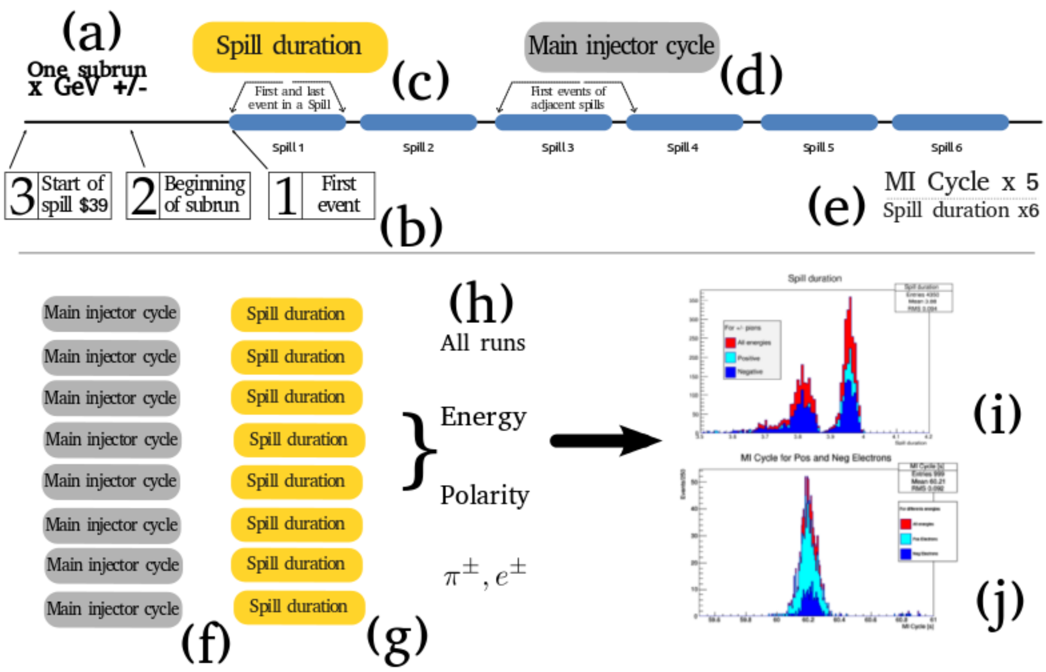

Figure 5.12: From (a) to (e) apply to one subrun. (b) the different points of reference in order to get the time profile. (c) and (d) explain how the spill duration and the spill frequency are calculated. When the calculation for one subrun is done, the next is calculated until the last sunrun. (f) and (g) describe how all of them are stacked and plot (i) and (j) according to different variables (h).

Chapter 6

Results

6.1 Time profile of the MTest Beam

We present the time profile (slices of time) of the beam for the data sets containg pions (Run2) and electrons (Run3)[1].

Time profile of the MTest Beam for Run2

The following plot 6.1 and 6.2 shows the time profile of the Pions in the interval of a Spill for all the energies and polarities. In the bottom part of the plot the length of the spill duration is showed. As we can see, the spills correctly are in the window of time of 4.2s except for the events that are before the zero point.

[1]In this chapter we use $\pm$ for different energies since we have data for electrons and positrons, as well with positive pions and negative pions. The signs describe the charge of the beam delivered.

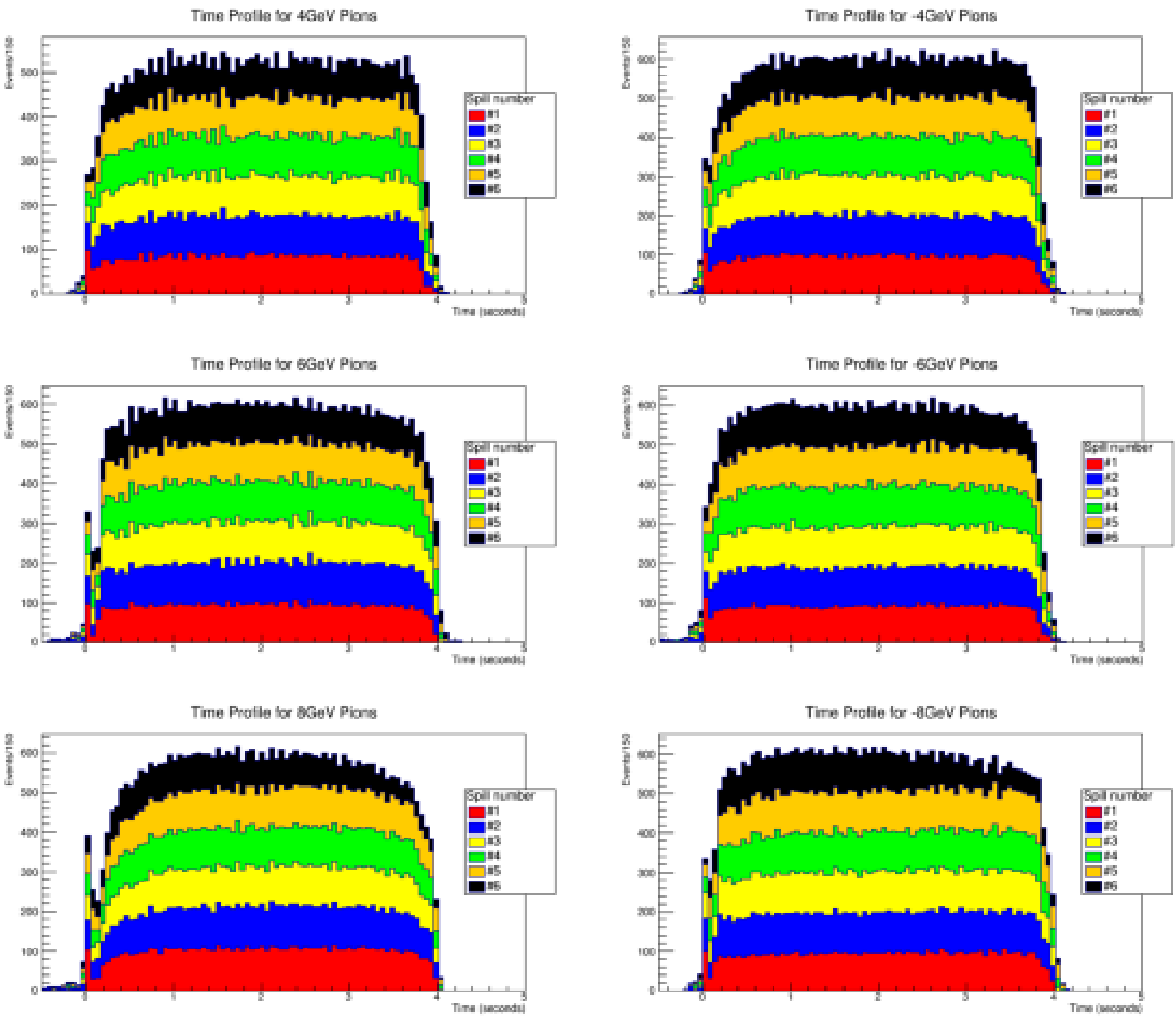

Figure 6.1: Time profile for Run2 ±4, ±6 and ±8 GeV (pions).

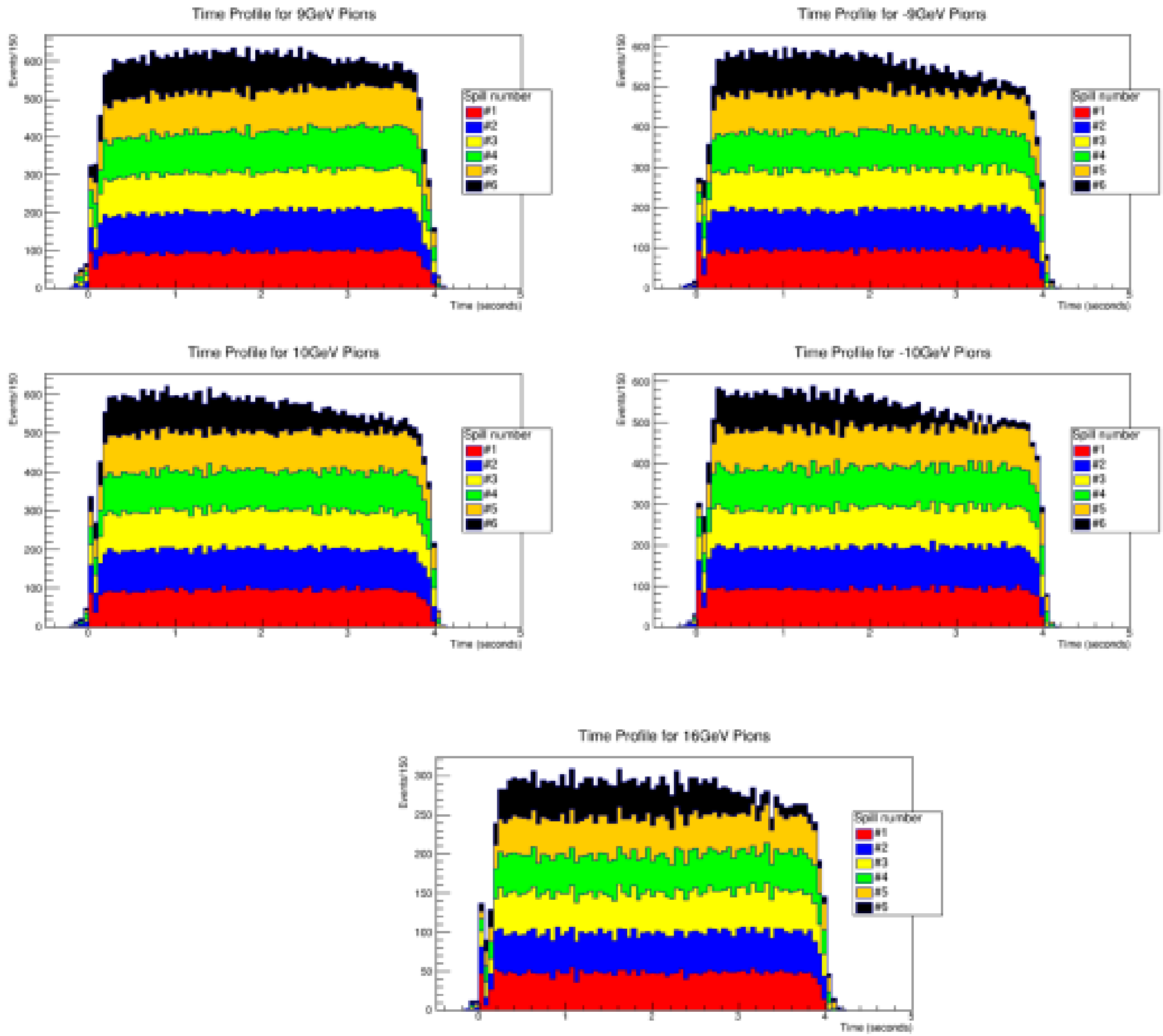

Figure 6.2: Time profile for Run2 ±9, ±10 and 16GeV (pions).

Time profile of the MTest Beam for Run3

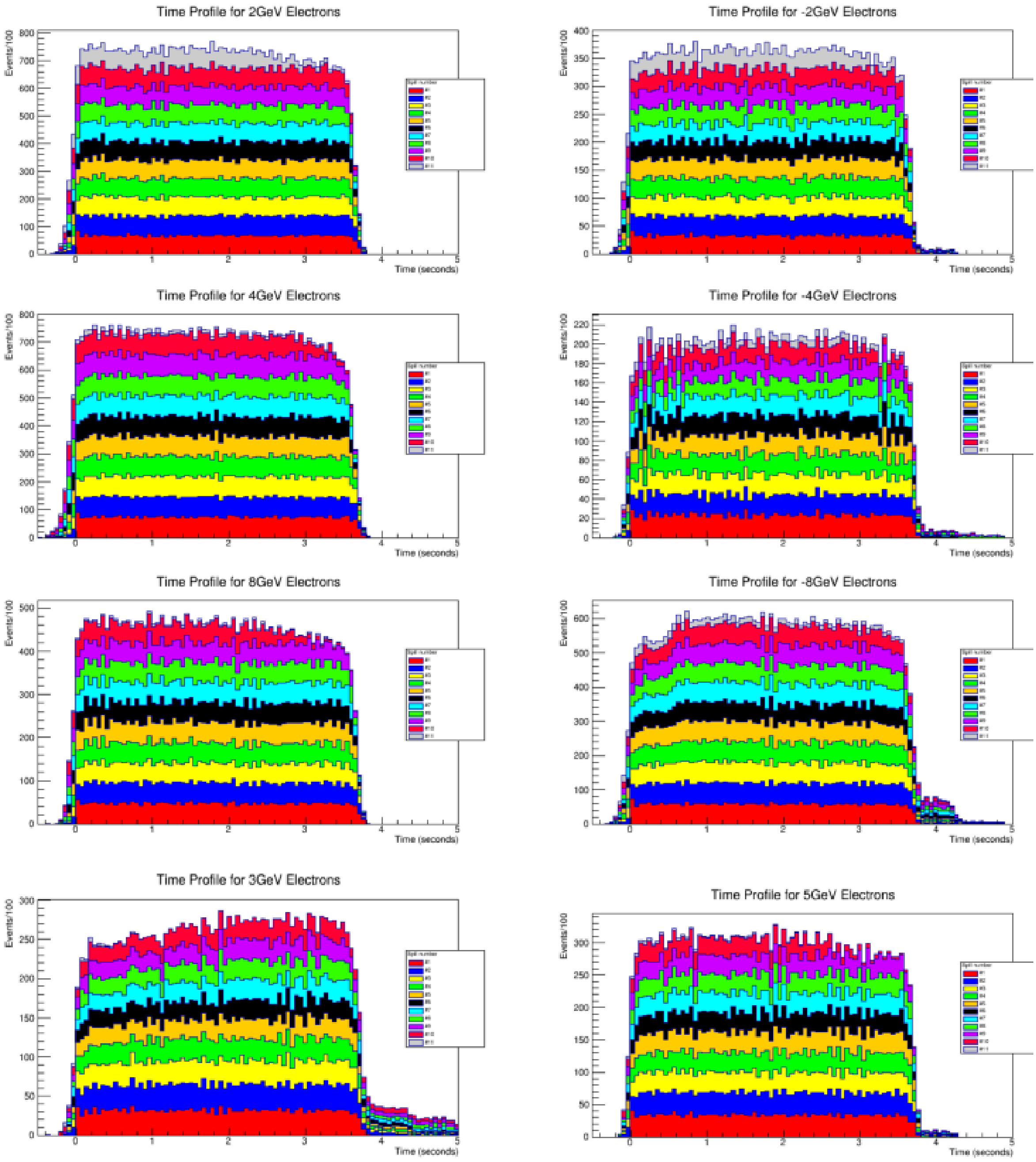

Figure 6.3: Time profile for Run3 ±2, ±4, ±8, 3 and 5GeV (electrons)

6.2 Main Injector's Spill Frequency for Run2 and Run3

The resonance extraction is made each minute according with AD, in order to get the exact value the Spill Frequency has been calculated for Run2 and Run3 6.4.

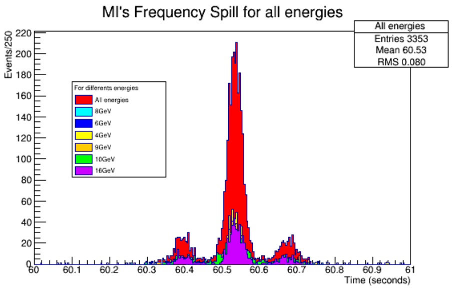

(a) Resonance extraction for data set containing only pions for all the energies

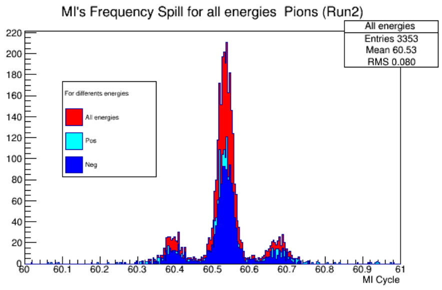

(b) Same as (a) but only for positive and negative energies.

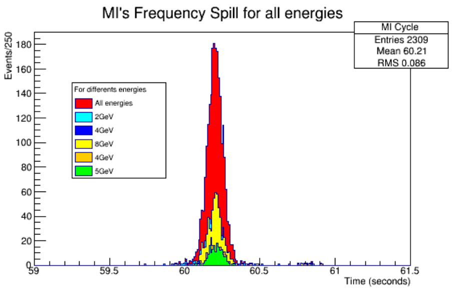

(c) Resonance extraction for data set containing only electrons for all the energies

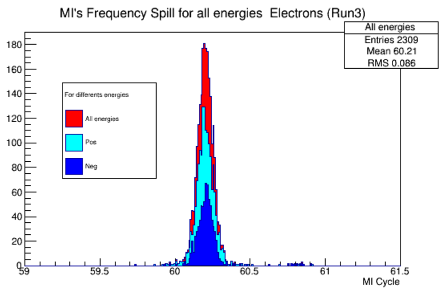

(d) Same as (c) but only for positive and negative energies.

Figure 6.4: Spill frequency for Pions (a,b) and Electrons (c,d). Pions have energies of 4, 6, 8, -8, 9, -9, 10 and 16 GeV, and electrons 2, -2, 4, -4, 8, -8, 3 and 5 GeV

For Pions, the rate of spills arraving to the detector is correctly calculate in 60.53 while the value provided correspond to before May 5. But there are clearly two bumps on both sides of the principal spike in 6.4 (a b). This situation is not present in the Run 3 electrons, where there are not bumps and the average value is 60.21.

6.3 Main Injector's Spill duration at MTest for Pions and Electrons

We can see here the distribution of the spill duration fig. (A.13) for both Run2 and Run3 according to the different energies (left) and polarity (right). In the first case (a) and (b) the average value is 3.85s (all energies) and 3.81s (both polarities). However, in the case of Run3, both histograms show the same value 3.63s.

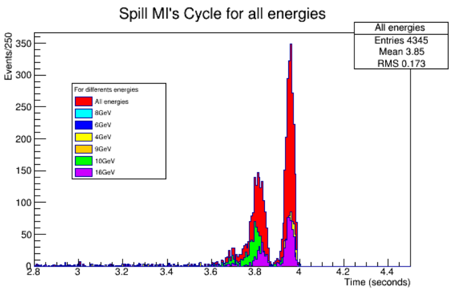

(a) Spill duration for data set containing only pions for all energies.

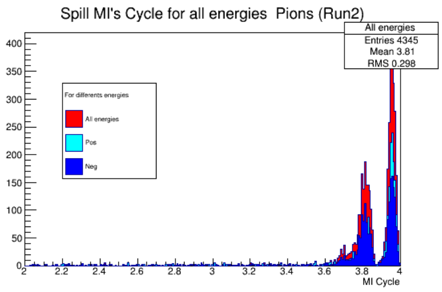

(b) Same as (a) but considering only their polarity.

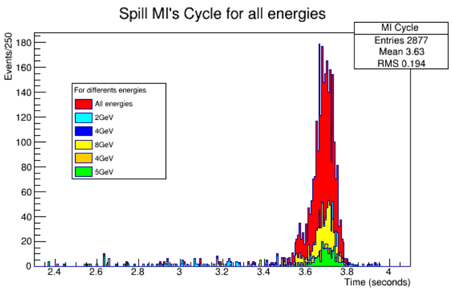

(c) Spill duration for data set containing only pions for all energies.

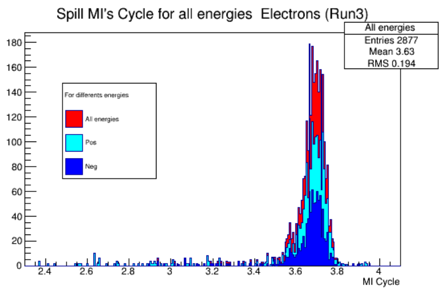

(d) Same as (c) but considering only their polarity.

Figure 6.5: Spill duration for all Runs (a,b) and Electrons (c,d). Pions have energies of 4, 6, 8, -8, 9, -9, 10 and 16 GeV, and electrons 2, -2, 4, -4, 8, -8, 3 and 5 GeV

In the tables of the fig. 6.6, we show all the values for the different variables calculated:

- Delta time between the kickoff of the spill and the e39 signal.
- Delta time between the beginning of the subrun of the spill and the e39 signal.
- the MI's Spill duration

- the MI's Spill frequency

Pions (Run2)

Data set		Delta Time = tbegin		Delta time = kickoff		MI's Spill Frequency	with kickoff		MI's Spill Duration	with kickoff	
Energy	entries	mean	rms_run	mean	rms_run	entries	mean	rms_run	entries	mean	rms_run
Nominal value		--	--	--	--	--	**60.524**	--	--	4.2000	--
Total	725	33.630	12.058	0.160	0.091	3353	60.533	0.0801	4345	3.8078	0.2981
8	75	33.898	10.471	0.155	0.127	304	60.531	0.1188	445	3.7774	0.3511
6	71	33.675	16.106	0.135	0.096	334	60.536	0.0811	426	3.8808	0.1933
4	74	28.345	14.540	0.203	0.069	340	60.535	0.0823	444	3.8046	0.1522
-8	68	35.495	10.618	0.146	0.073	314	60.532	0.0694	408	3.8188	0.3306
-6	69	34.794	15.128	0.234	0.102	320	60.530	0.0909	414	3.7879	0.1703
-4	74	29.250	12.185	0.219	0.084	361	60.530	0.0862	444	3.7990	0.1335
9	68	35.101	10.682	0.167	0.071	330	60.532	0.0895	408	3.7886	0.3425
10	65	33.865	9.131	0.128	0.063	306	60.528	0.0595	390	3.7982	0.3717
16	32	37.962	9.973	0.108	0.044	154	60.535	0.0692	192	3.7980	0.3783
-9	65	36.185	7.017	0.116	0.047	298	60.536	0.0570	390	3.8130	0.3568
-10	63	34.566	7.328	0.108	0.038	292	60.535	0.0408	384	3.8152	0.3990
Mean	724	33.921	11.198	0.156	0.074	3353	60.533	0.0767	4345	3.8074	0.2890
\Delta	**-0.14%**	**0.86%**	**-7.68%**	**-2.40%**	**-23.10**	**0.000%**	**0.000%**	**-4.304**	**0.000%**	**-0.010**	**-3.142%**
VS nominal value		--	--	--	--	--	**-0.01%**			**9.34%**	

(a) Results for Run2

Electrons (Run3)

Data set		Delta Time = tbegin		Delta time = kickoff		MI's Spill Frequency	with kickoff		MI's Spill Duration	with kickoff	
Energy	entries	mean	rms_run	mean	rms_run	entries	mean	rms_run	entries	mean	rms_run
Nominal value		--	--	--	--	--	**60.241**	--	--	**4.2000**	--
Total	150	0.100	0.800	0.360	0.042	2309	60.206	0.0857	2877	3.6300	0.1940
2	51	0.366	0.042	0.366	0.042	481	60.200	0.0592	561	3.6701	0.0577
4	50	0.353	0.040	0.353	0.040	442	60.192	0.0701	550	3.6323	0.1786
8	32	0.357	0.036	0.357	0.036	275	60.199	0.0604	350	3.5665	0.3040
-8	43	0.360	0.041	0.360	0.041	373	60.215	0.1178	471	3.6468	0.1413
3	22	0.335	0.056	0.335	0.056	196	60.233	0.1374	241	3.6754	0.1016
5	23	0.358	0.041	0.358	0.041	182	60.210	0.0661	253	3.5441	0.3610
-2	25	0.362	0.037	0.362	0.037	242	60.204	0.0641	275	3.6624	0.0724
-4	15	0.344	0.030	0.344	0.030	118	60.216	0.1021	176	3.6356	0.1709
Mean	411	0.267	0.102	0.290	0.033	4618	67.735	0.069	5754	4.0829	0.143769
\Delta	**63.50%**	**62.52%**	**-684.75**	**-23.95%**	**-27.14**	**50.000%**	**11.115**	**-23.61**	**90.250%**	**10.112**	**59.898%**
VS nominal value		--	--	--	--	--	**0.06%**			**13.57**	

(b) Results for Run3

Figure 6.6: Errors against the oficial values of the MI's frequency spill and MI's spill duration.

Chapter 7

Conclusions

There were three question that sowed the foundational idea of this thesis and the development of a MINERvA Test Beam Time Analysis Tool (TbTaTool). As mentioned in 3.2.1, a more comprehensive knowledge of the incoming particles into the Test Beam detector is a requirement for improving the models detection of final particle states of neutrino interactions.

- When a specific type of particle is coming in the beam timing?
- How frequently do we have (in the Test Beam detector) a π, e in one bucket/batch/spill?
- How can we use TB2 data to say something about the beam? Do we have any restriction?

Saying that, our approach has been based in the development of a tool in ROOT, python and C++ that it can help us to monitor the process of taking data considering the constrains of how the detection systems was set up and of course, the physics of the measurement itself.

Some words need to be say in order to contextualize and give a clear view on these questions. This thesis is about study the timing of events in the detector, assuming that or with a further checking process, the identity of the income particles. In order to **successfully answer** this, **the TbTaTool allowed us to study any time-variable defined by the user independently of the code**. This means that it can be defined *a priori* in the taking data design process or *a posteriori* inside the code as a function of time.

For example, since the time structure of the beam (chap. 4) has been defined by others, we do not control it and the system of detection has to be defined matching our physics needs and external constrains. That is why we are presenting results that **were inside the spill** (results secs. 6.1, 6.2 and 6.3) because we want events with particles incoming the detector. Grab timing information by studying the background of particles "when we are not receiving particles" is not possible in the current set up of the experiment. Knowing this, one success of this work is that the TbTaTool can be applied to any case inside the spill or outside the spill, any special difference is solved in how the input ROOT files are produced. Needless to say, the TbTaTool does allows us to answer when a particle is coming in the beam timing. Specially for the spill scale, successfully fulfilling the first of three scales that define the time structure of the beam.

Furthermore, since the readout time is concentrated in the CAMAC TDC 377 (sec. 3.2.3), the conversion from analog signal to a digital one, resolution in timing of the different instruments (ToF, Veto, Cerenkov and Wire Chamber) impose some limits in the analysis if we need to go further from nanoseconds, more work need to be done in this area, but we are confident to be able to go into the batch scale.

The **third question** express our curiosity of knowing if the TB2 data itself was enough to study the time profile of the beam. We have a mixed answer. We do study the spill and batch scale, but still we need a reference point in time. That is why in the sec. 5.3.1 we needed to choose the closests e39 point to the kick-off of th subrun in order to set our zero poin of reference.

The histograms showed in the 5.7 show that the election of the kickoff of the spill above the beginning of the run is a correct election, since the gap between boths is reduce to 0.16s, and not the 33.63 if we used the former. In fig. 5.6 we pointed that there is a 0.5s of gap in the profile histograms. A related event is that in fig. 6.1, 6.2 and 6.3 there are events before the zero point.

The reason is that, in order to stack the slices of time, we subtract a fixed value of MI's frequency spill according to the average value provided by Accelerator

Division as can be seen in the fig. 5.10 and as can be seen in the distribution of values (fig. 6.4), the spill numbers it is not fixed, that is why when the calculation is done an excess of deficit is always present. Further work needs to be done, including a subroutine which match the value of the MI's Spill frequency according to the date in which the data was taken.

Also, as a footnote, we chose to fix the spill number (6 for Run2 and 11 for Run3) without excluding events that can affect the statistics, showing in tab. 5.2 that with this election we have calculated up to 95% of the events (95.50% for Run2 and 97.60% for Run3).

The **implementation of the tool for the Time Profile** (6.1), the MI's Spill Duration (6.3) and the MI's Spill Frequency (6.2)demostrate that the tool is working and giving us the distribution of value for this variables. In the tables 6.6 we show those values. For the MI's Frequency spill Run 2, we have a difference of -0.01% with the nominal value by AD, while for Run3, is 0.06%. In the case of the MI's Spill duration, for Run2 we have a difference of 9.34% and Run 3 of 13.57%.

Finally we state that the development of the TbTaTool is important because it has allow us **to use the TbTaTool in other context and experiments**, not necessarily in the fields of particle physics. I will go deeper in this conclusion.

Science needs experiments which use instruments to make the measurements and since we need to repeat a set of well defined steps in order to measure a physical property from the object we are studying, computers are used: they offer predictability in the measurements. This process is called Data acquisition, a process that measure real world physical conditions and converting them into digital signals that can be manipulated by a computer. Data acquisition usually are abbreviated by the acronyms DAS or DAQ[1].

LabVIEW is one of the most well know system-design platform and development environment for DAQ, that interface the sensors with the computer. In the field of particle physics, DAQs use ROOT in the real-time visualization of the measurement process. TbTaTool can be extended to this goal and be implemenented

[1] In the chap. B I have described all the task that been a Detector Expert for the MINERvA experiment involves. This training is basically a training deeply related with the DAQ systems of the experiment.

in other experiments since the code is independent of the production of the data. We are confident to build a real-time visualization tool experiment-independent.

Appendix A

Auxiliary plots

A.1 Spill frequency for only Pions (Run 2)

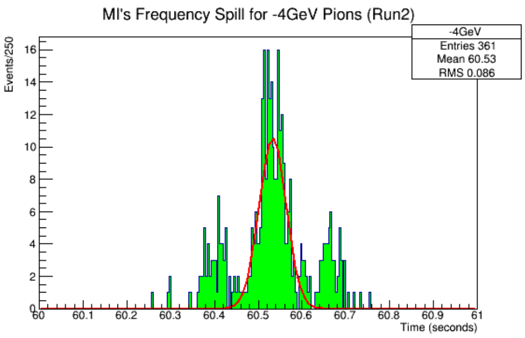

(a) -4GeV

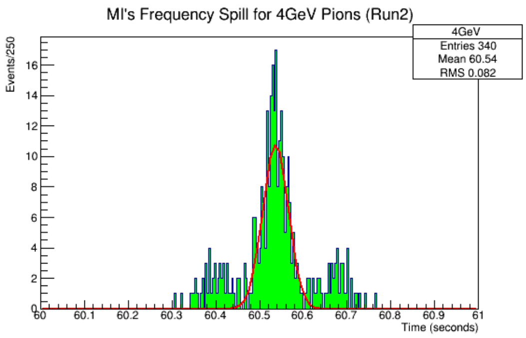

(b) 4GeV

Figure A.1: Spill frequency for 4GeV Pions

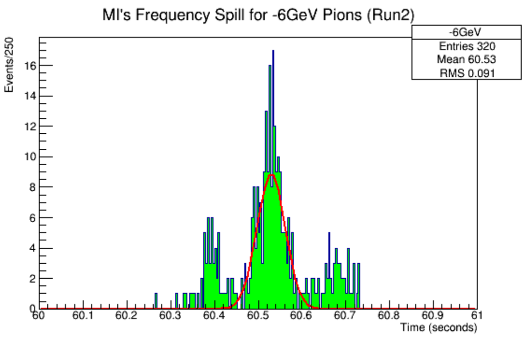

(a) -6GeV

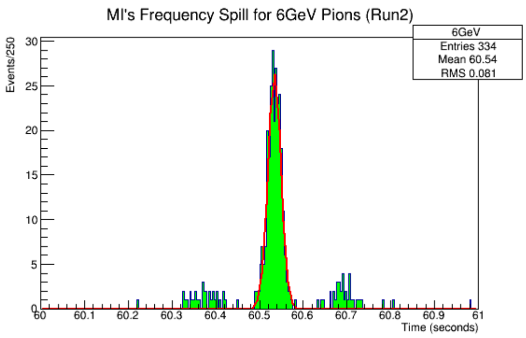

(b) 6GeV

Figure A.2: Spill frequency for 6GeV Pions

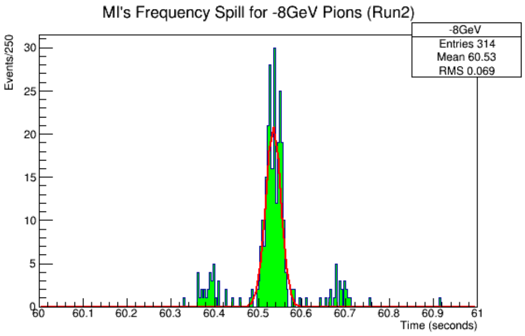

(a) -8GeV

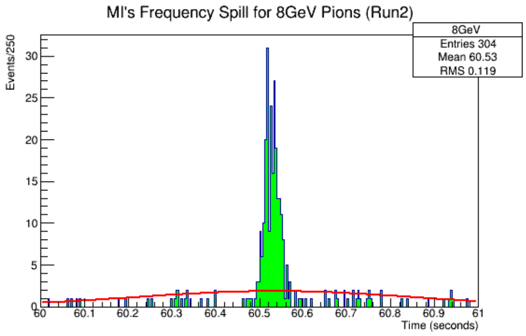

(b) 8GeV

Figure A.3: Spill frequency for 8GeV Pions

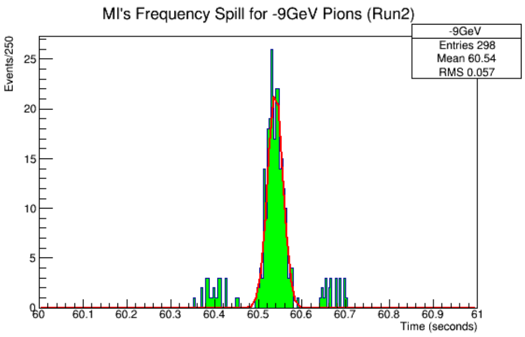

(a) -9GeV

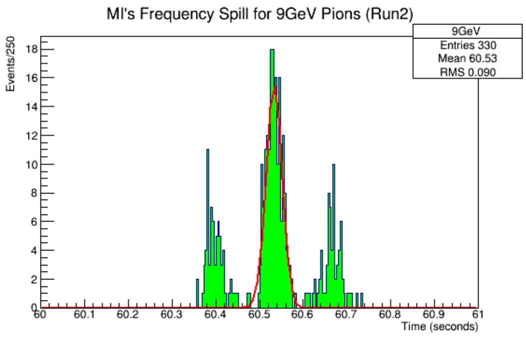

(b) 9GeV

Figure A.4: Spill frequency for 9GeV Pions

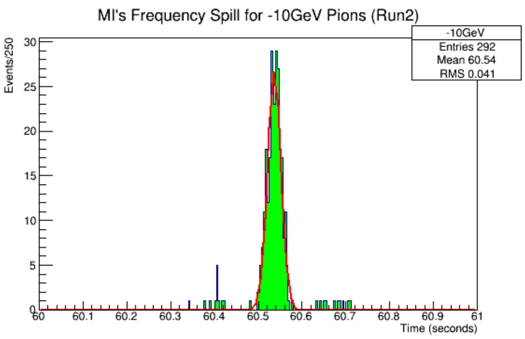

(a) -10GeV

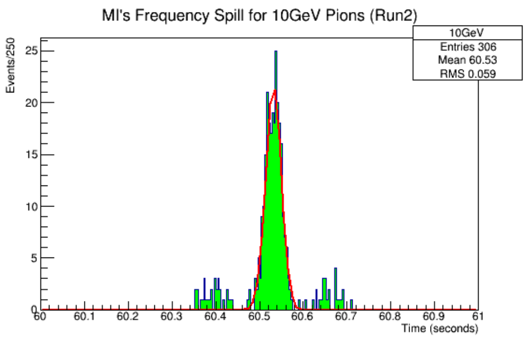

(b) 10GeV

Figure A.5: Spill frequency for 10GeV Pions

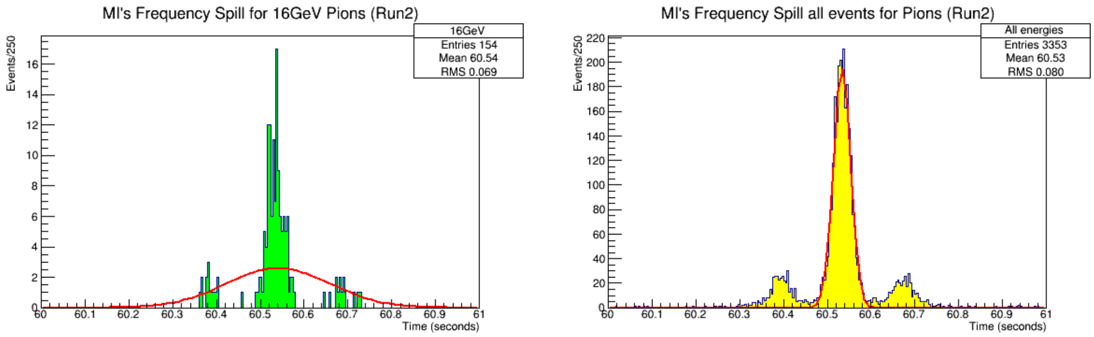

(a) 16GeV (b) All energies

Figure A.6: Spill frequency for 10GeV Pions and all the events

A.2 Spill frequency for Electrons (Run 3)

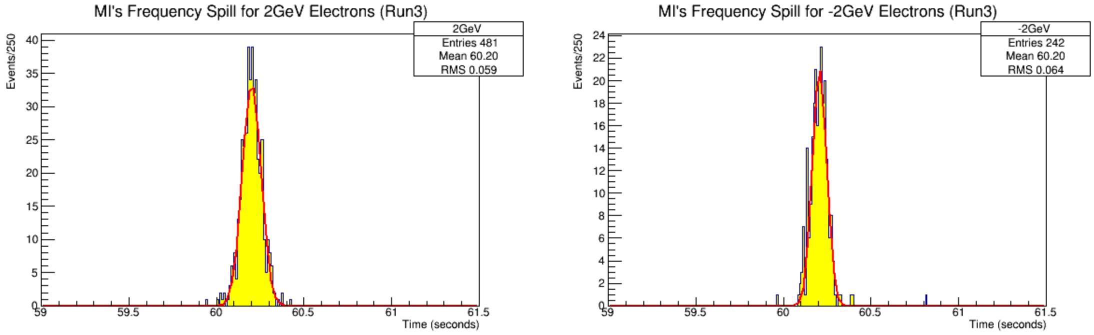

(a) 2GeV (b) -2GeV

Figure A.7: Spill frequency for 2GeV electrons

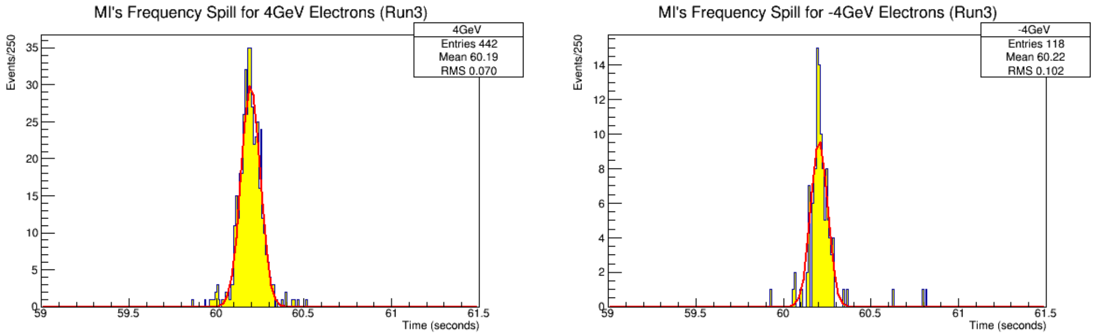

(a) 4GeV (b) -4GeV

Figure A.8: Spill frequency for 4GeV electrons

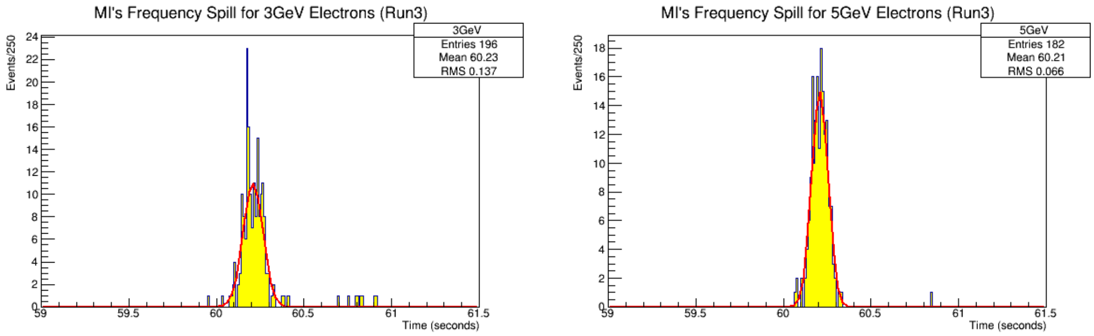

(a) 3GeV (b) 5GeV

Figure A.9: Spill frequency for 3GeV and 5GeV electrons

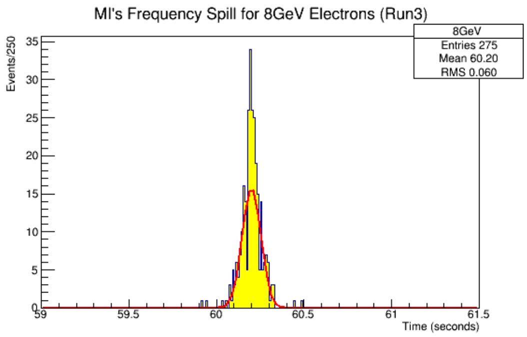

(a) 8GeV

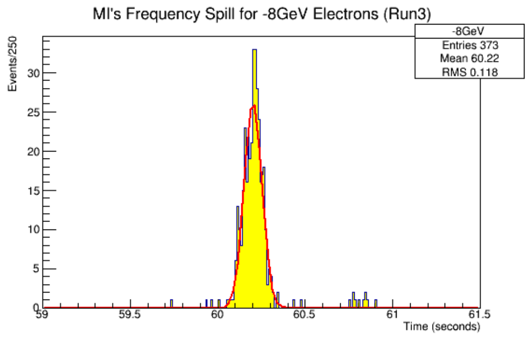

(b) -8GeV

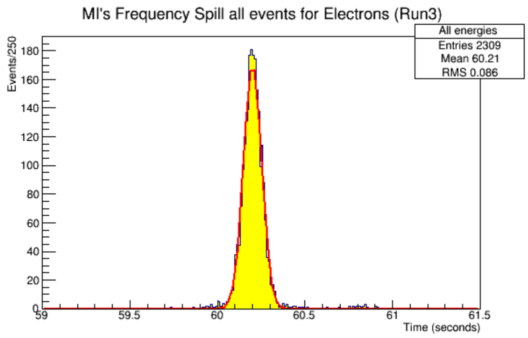

(c) All energies

Figure A.10: Spill frequency for ($\pm$)8GeV and all energies electrons.

A.3 Spill duration for only Pions (Run 2)

Spill duration plots for data set containing electrons (Run 3). Some fits do not work, showing that more statistics are needed for improving this part of the tool.

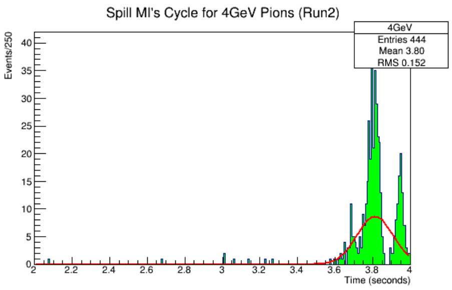

(a) 4GeV

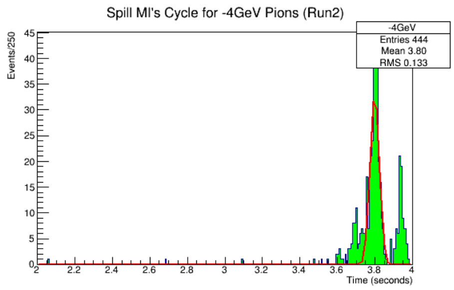

(b) -4GeV

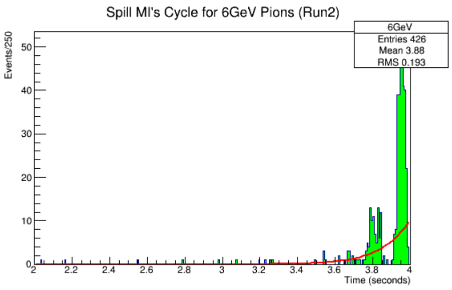

(c) 6GeV

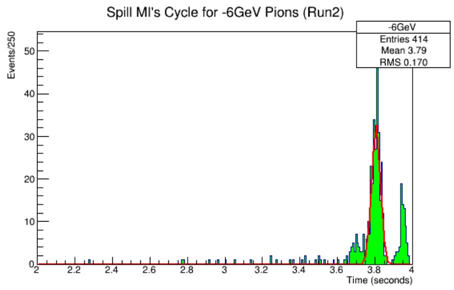

(d) -6GeV

Figure A.11: Spill duration for data set containing only pions (Run2).

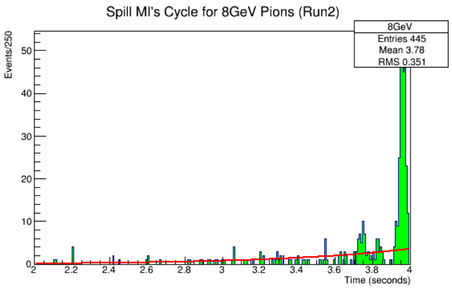

(a) 8GeV

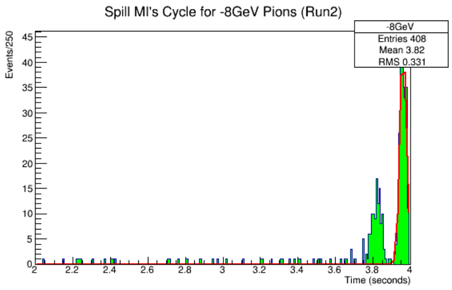

(b) -8GeV

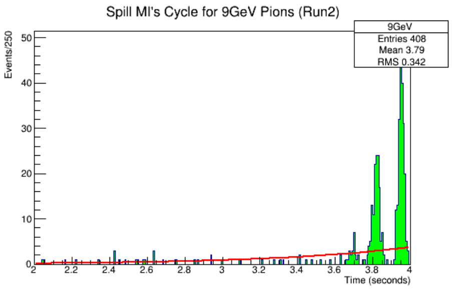

(c) 9GeV

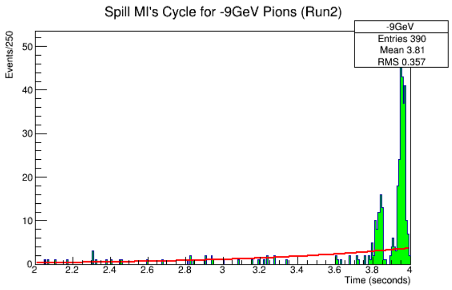

(d) -9GeV

Figure A.12: Spill duration for data set containing only pions (Run2).

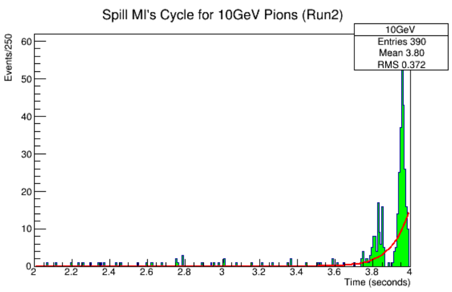

(a) 10GeV

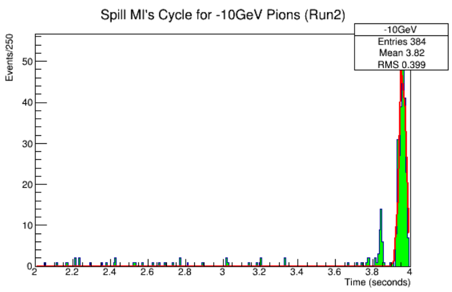

(b) -10GeV

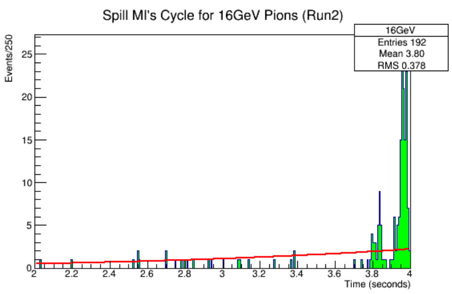

(c) 16GeV

Figure A.13: Spill duration for data set containing only pions (Run2).

A.4 Spill duration for only Electrons (Run 3)

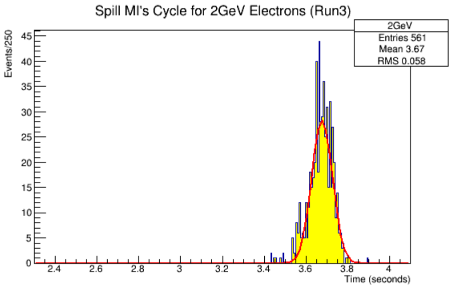

(a) 2GeV

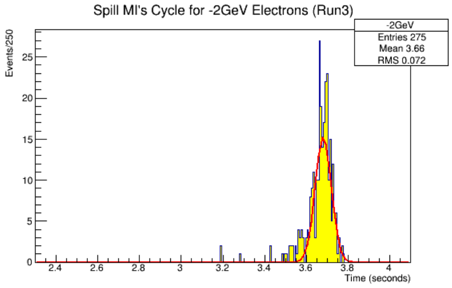

(b) -2GeV

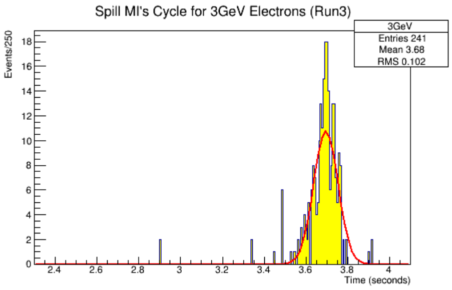

(c) 3GeV

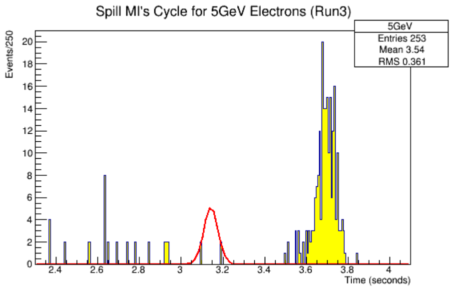

(d) 5GeV

Figure A.14: Spill duration for electrons (Run3).

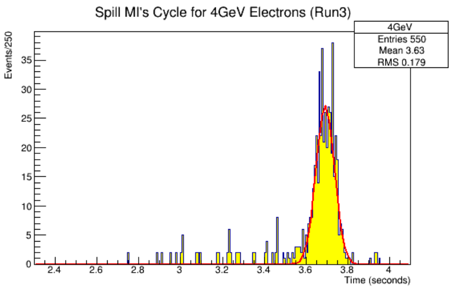

(a) 4GeV

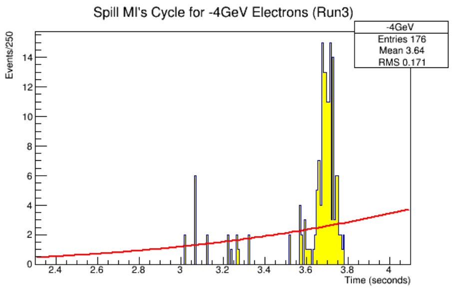

(b) -4GeV

Figure A.15: Spill duration for electrons (Run3).

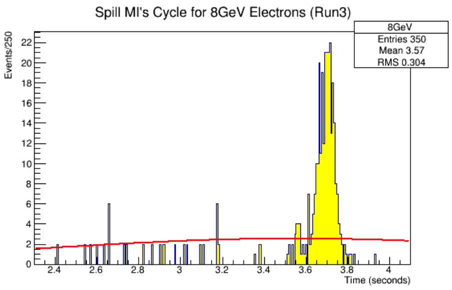

(a) 8GeV

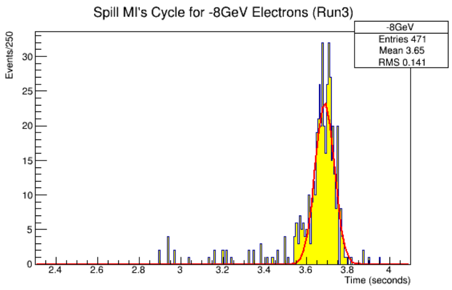

(b) -8GeV

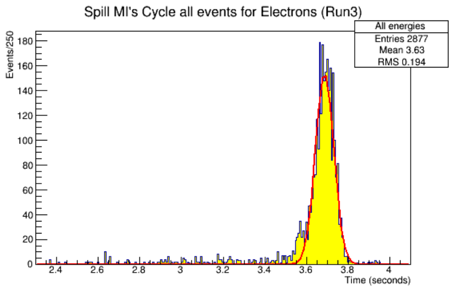

(c) All energies both polarities.

Figure A.16: Spill duration for electrons (Run3).

Appendix B

Participation in the MINERνA experiment during 2015

The MINERνA experiment is collaboration-joint between many institutions and persons. The participation in the experiment is done in many different ways: by doing and analysis of neutrino cross-section usually as a part of a PhD program, by been involved in different teams that the Main Detector needs in order to check the quality of the data, calibration, reconstruction and/or DAQ; and by doing shifts, which means take periods of time of 8 hours in which the person is in charge of keeping the data readout system online and fix any problem that may happen.

In this section I will outline the activites and additional work that I performed during my participation during in the MINERνA experiment.

B.1 Shifts

"Shifts" are the short name that describe a obligatory tasks that all the members of the collaboration have to do in order maintain the Main Detector continuously taking data. These shifts are 8 hours long at least three days on a week, according with a timetable that include all the active members of the experiment.

But not only a shifter (the person how is in charge of the shift) has to maintain the data-taking runs but also "ensure that the DAQ is running whenever possible while the beam is on, monitor the electronics for failures and problems, and stop runs and reset the electronics in the case of a failure, log any electronics or software errors, perform basic data quality checking and calibration analysis, develop tools to do this when necessary and understand how to handle common errors in the data taking and monitoring procedures". Internal documents of the Collaboration.

In this section I will briefly resume elements of this process of taking shift. which include log all the events in the MINERvA logbook as a complement of the **??** and 3.1.2. First, it is mandatory to have control of the MINERvA Run Control fig. B.1 (a) and that all the voltage values in (b) for the Near MINOS DAQ are in the accepted values.

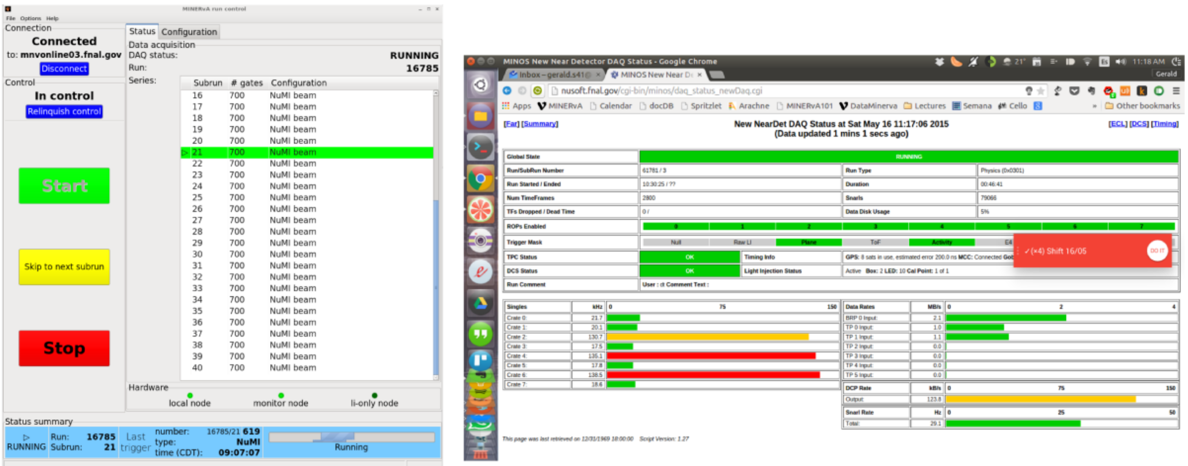

(a) (b)

Figure B.1: (a) Left. Run Control of the MINERvA Main Detector. (b) Right. Near MINOS DAQ, not all information is useful for MINERvA, just the two bottom columns.)

Then, it is important to check if the Main Detector is receiving beam from the NuMI Beam, in fig. B.2 (a) and (c) can be seen plots that characterize the quality of the beam, the interval between the last spill of particles (usually 1.3s) and the amount of protons on target that the experiments are receiving.

From time to time it is needed to check the quality of the data that we are taking. That is why the fig. B.2 (b) is an automatic generated checklist where the shifter accept or deny that that particular run contain data of good quality.

There are other mandatory tasks, like: fill out the start shift form, phone MCR that you are on shift, fill out the *Rock Muon Check List*, check the *MINOS DCS*

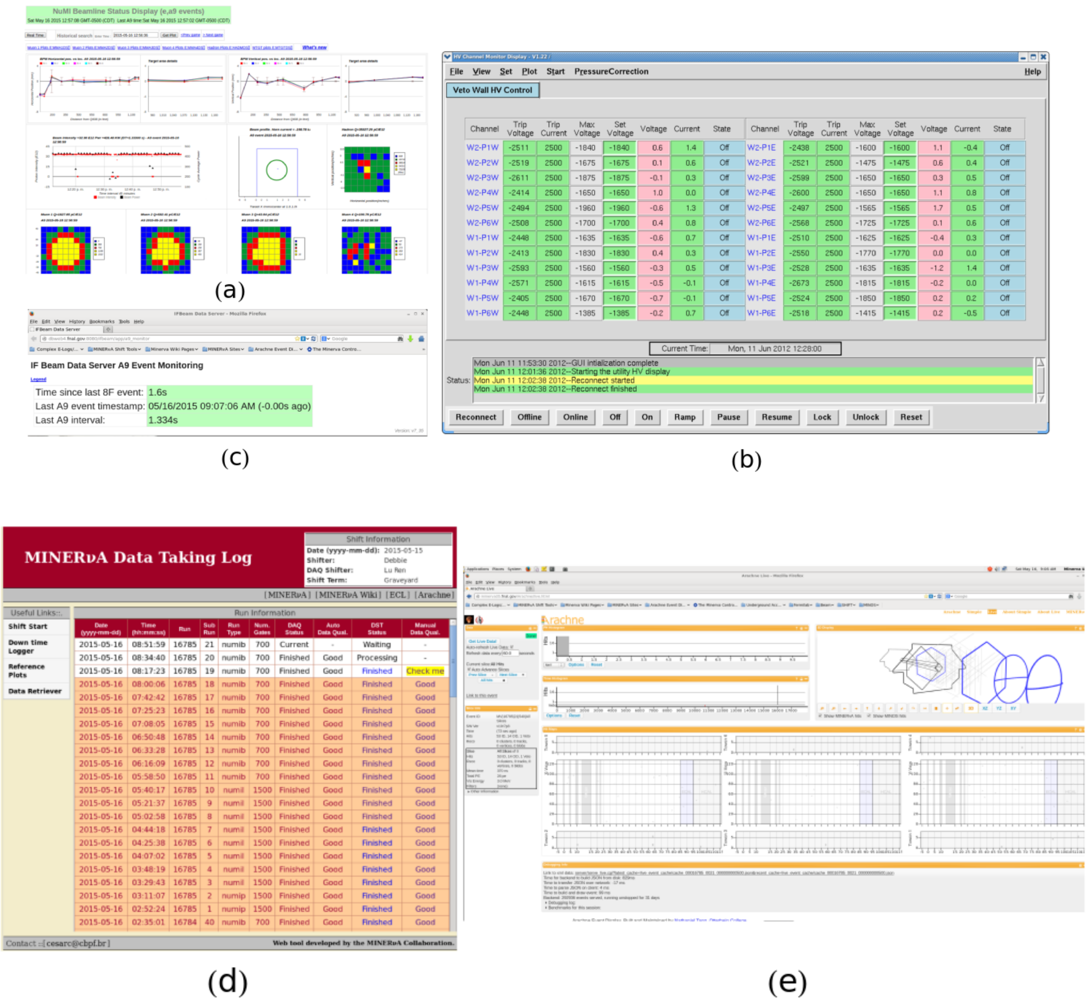

Figure B.2: (a) Up left. NuMI Beamline Status Display which shows the status of the beam. (b) Up right. MINERvA Veto Wall control. (c) IF Beam Data Server A9 event monitoring. (d) Bottom left. MINERvA Quality Checklist. (e) Bottom right. Live event display for neutrino interactions in the Main Detector.

Checklist and the *MINOS OM Checklist* Near at the middle of the shift and *Summary Plots* at the end of the shift. The shifts ends when the next shifter take control of the Run Control.

B.2 Detector Expert Training

We have talked about shifts, as the process of monitoring the data readout in the Main Detector. But as any machine, it will face problems during the data taking that even a trained shifter will no be able to resolve. A Detector Expert is a person who has more training and knowledge that will resolve these problems or at least call the right person to do it. Time is critical, and neutrinos interactions passing our detector without been detected means money spent without any result.

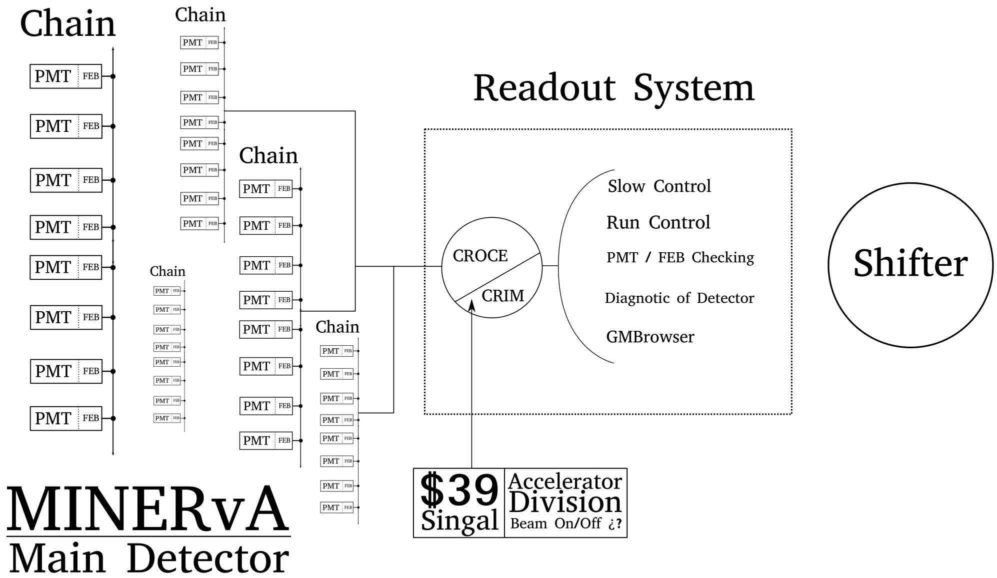

Figure B.3: Diagram of the MINERvA DAQ System. The Detector Expert training include a deeper knowledge in these areas.

The Detector Expert Training included:

- Replacement of malfunction FEB reported by the shifter
- Turn on and off the Main Detector in order to remove some critical parts of them
- DAQ Firmware update
- Use the RunControl and SlowControl in order to check the voltage or any error. Usually a shifter is not allow to change parameters.
- Return to Service the DAQ after any random event
- Change, Replacement of FEB

B.3 PMT Cross Talk problem

One important element in the DAQ and Optical System (3.1.2) of the Main Detector is the PMT. The Hamamatsu Photonics PMT model number H8804MOD-2 was chosen in order to transform photons into photoelectrons using a low quantum efficiency photosensor with a timing resolution of 5ns that avoid overlapping events within a single spill of the NuMI beamline. The photosensor has a 8×8 array of pixels laid out on a $2cm2cm$ grid. The 64 pixels have a spectral response between 300 - 650 nm and can work between -30 to 50 ℃ . B.4.

Each of the pixels correspond to one scintillator strip from the Main Detector, having more than 320000 channels. All the channels have been carefully oriented in one and only one pixel. The problem of **"Cross Talk"** arise when for unknown reasons the photons that reach one pixel also illuminate the one of the four other pixels around it. The task in which I participated was to help measuring if two pixels showed response when one of them was illuminated, i.e. measure the cross talk. In (b) fig. B.4 it can be seen two peaks on different x positions, are a hint that cross talk is happening there.

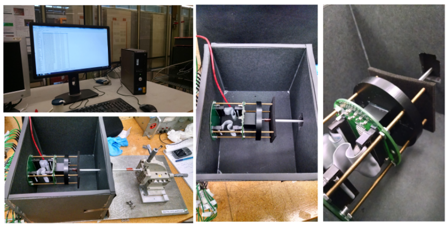

(a) Equipment use for checking the Cross Talk problem on PMTs.

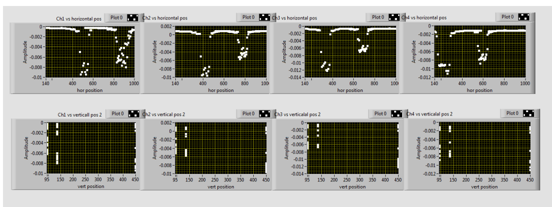

(b) Usual data that shows that there are a problem of Cross Talk.

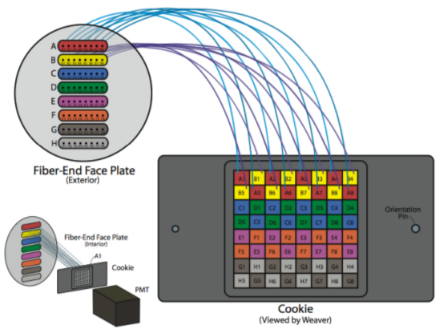

(c) Fiber optic pattern weave within each PMT Box. Image from [2].

Figure B.4: Cross Talk tasks

B.4 PMTs Testings

Also, I participate in the process of checking the quality of the PMTs that have problems in the Main Detector. The fig. B.5 shows the equipment, which is a replica of the DAQ system in the Main Detector. There are 8 CROCE (Chain ReadOut Controller) connected to one custom VME module (Versa Module Europa, a computer bus standard). Each CROCE, one in the image, can support at least 10 FEB (Front End Board) which controls the PMT and digitalize the analogic charge through the TripP Chips that is place on each FEB. Then the CROCE is chained with the CRIM (the CROC Interface Module)which distributes timing to up to four CROCEs (3.1.2).

The work did included the diagnostic of the bad PMTs, to removed from the Main Detector and the confirmation if the problem was becaus bad quality HV delivery, light leak or something else. The methodology included to use the Run and Slow control, to main components of the DAQ MINERvA, change the high voltage, frequency, looking for specific behaviour on a specific pixel (from the 64 that contains one PMT box).

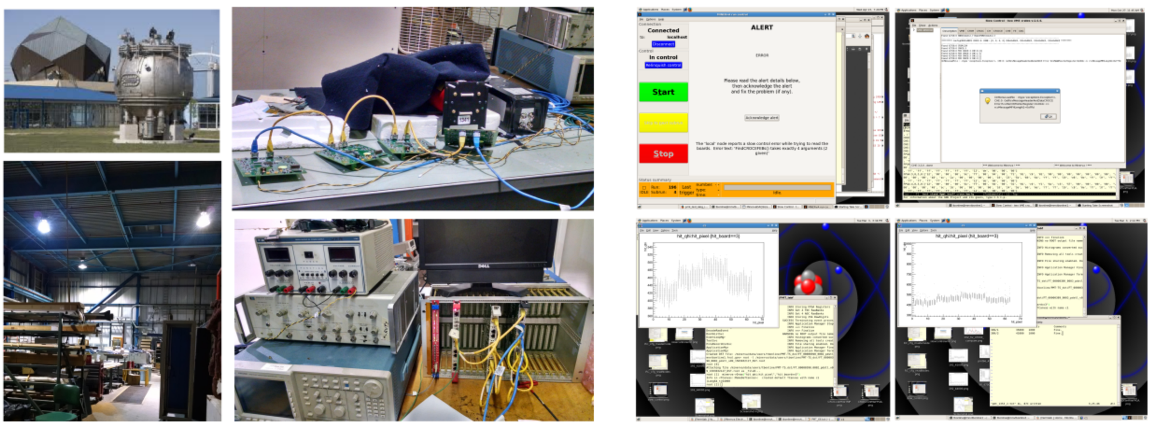

(a) (b)

Figure B.5: (a) Left. Some photos the Sillicon Detector Facility and the equipment where the PMTs' tests were done. (b) Right. Run and Slow Control and some histograms which confirmed the presence of cross talk.

B.5 Data and MonteCarlo Rock Muon eye scanning

This task was designed in order to confirm if the conditions or cuts imposed on the Main Detector's algorithms actually removed the rock muons events from the data samples, leaving the muons produced by neutrino interactions.

We were given two sets of data (around 500 events): real data and Monte Carlo simulated data. According with the nature of the charged particle, the energy lost on a specific material is different for each one, as well as the visual trail in the event viewer. For example fig. B.6 correspond to Monte Carlo simulated data. In this event it can be seen one neutrino interaction, but a lot of activity in the upstream part of the detector even thought eliminating crosstalk that usually makes messy the vertex of interaction that includes other charged particles that produces other vertex. By checking the trails, the time slices of interaction (two events at 4041ns upstream and 4028ns) and the point of vertex we are able to discard this events as a rock muon event, which in theory was one of them.

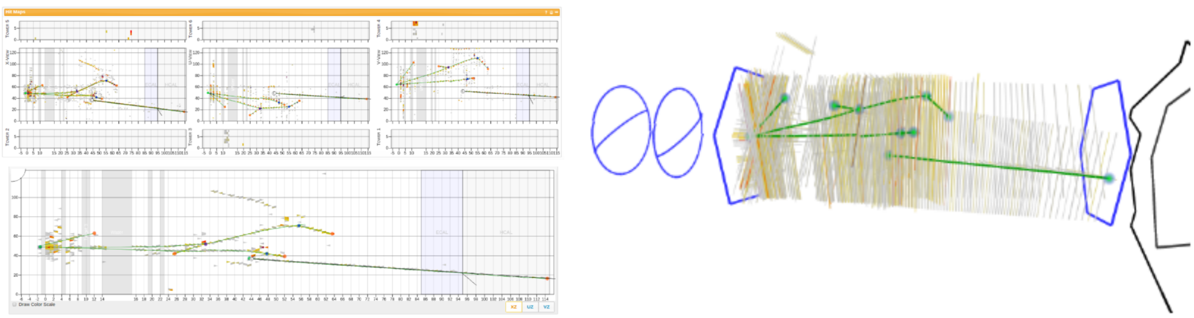

Figure B.6: Monte Carlo simulated Rock Muon interaction with the detector.

In fig. B.7, real data shows two events: one rock moun at 3800 ns comming in front of the veto wall and a neutrino interaction at 3732 ns.

The confirmation that for the last event was a rock muon, as well as the former one was not, helped the collaboration to improve the cuts imposed in the algorithms and clean the real data from rock muons.

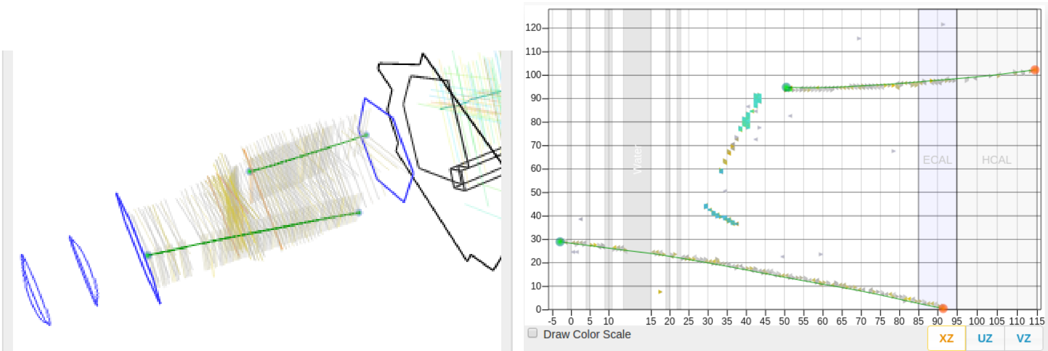

(a) (b)

Figure B.7: Real interaction of Rock Muons with the detector.

B.6 Participation in published articles during 2015

(a) Physical Review Letters Vol 116 (2016) 081802.

Title: Measurement of Electron Neutrino Quasielastic and Quasielastic like Scattering on Hydrocarbon at $E_\nu = 3.6$ GeV

Authors: G. Salazar, A. Zegarra, C. J. Solano Salinas MINERvA colaboration

In this paper, one of the most important analysis in the lower energy carried out by MINERvA, the first direct measurement of electron-neutrino quasielastic and quasielastic-like scattering on hydrocarbon in the few-GeV region of incident neutrino energy.

The results presented (flux-integrated differential cross section in electron production angle, electron energy and Q^2) will help current and future oscillation experiments improve the detection process of CP violation measurements in the neutrino sector (which is done by precise measurements of $\nu e(\bar{\nu e})$ appearance in predominantly $\nu_{\mu(\bar{\nu}_\mu)}$ beams like NuMI at Fermilab).

To maximize the rate of neutrino interactions, these neutrino oscillation experiments like NOvA, T2K and DUNE use detectors of heavy nuclei (e.g. carbon, oxygen, argon). By comparing the observed energy spectrum distribution with the predictions based on different oscillation hypotheses, confirm or deny oscillation parameter values that constrains the mass and the amplitude of the oscillation. This paper reports precise measurements of the charged-current quasielastic (CCQE) interactions $\nu_e n \to e^- p$ and $\bar{\nu}_e p \to e^+ n$ on ¯ep → e +n) on nucleons in a hydrocarbon target at an average e energy of 3.6 GeV, in order to enhance the correct prediction of the observed energy spectrum for ν_e interactions.

(b) Physical Review Letters Vol 116 (2016) 081802

Title: Charged Pion Production in ν_μ Interactions on Hydrocarbon at $E_\nu = 4.0$ GeV

Authors: G. Salazar, A. Zegarra, C. J. Solano Salinas MINERvA colaboration

Current and future long baseline neutrino oscillation experiments rely in study of charged pion production via charged-current ν interactions since the nuclear medium (the detectors themself) impact in the production and propagation of hadrons produced in neutrino-nucleus interactions. Cross sections distorsions which are absent in scattering from free nucleons and affect event rates and final state kinematics, are examples of the impact of nuclear targets.

T2K and MiniBooNE oscillation experiments rely on well understood the CCQE reaction $\nu_e n \rightarrow e^- p$ and the reconstruction of the energy on those events, but the presence of nuclear medium introduce distorsions on the reconstruction and interpretation of the events, as mentioned before. For example if the charged-current interaction produces a single π^+, the if in the process $\nu_e N \rightarrow e^- p \pi^+$, the pion is absorbed by the target nucleus, the event will mimic the CCQE topology. Reconstructed neutrino energy may be underestimated, leading a bias in the measured oscillation parameters. It is expected that analysis in the medium energy are been running, where the new improved models for selection of muon and pion events will include the results of UNI master students.

Appendix C

Radiofrequency Cavities theory

C.1 Electromagnetic Waves

We begin with a review of electromagnetic waves in vacuum and matter propagate throught RF cavities RF are made in order to store electromagnetic energy and kick the particles, increase the kinetic energy conductors have the ability to reflect all the waves wave guides allow the propagation of waves throught hollow cylinders Resonant Cavities have ends, which reflect and create stading waves the maximun efficiency is reach when Q is high and depende of the geometry

throught this section we will explain this concepts applied to RF cavities

C.1.1 Electromagnetic waves in Vacuum

A electromagnetic wave equation is a **disturbance of the electric and magnetic fields that propagates with a fixed shape and at a constant velocity**. In a region where there are no charges or currents, the Maxwell's equations are:

$$
\begin{aligned}
&(i)\nabla \cdot \mathbf{E} = 0, \qquad &&(iii)\nabla \times \mathbf{E} = -\frac{\partial \mathbf{B}}{\partial t} \\
&(ii)\nabla \cdot \mathbf{B} = 0, \qquad &&(iv)\nabla \times \mathbf{B} = \mu_0 \epsilon_0 \frac{\partial \mathbf{E}}{\partial t}
\end{aligned} \tag{C.1}
$$

as we know we can derive two 3D-wave equations for the electric and magnetic field, using eq. C.1 operator relations, after all the mathematics:

$$
\begin{aligned}
\nabla^2 E &= \mu_0 \epsilon_0 \frac{\partial^2 E}{\partial^2 t} \\
\nabla^2 B &= \mu_0 \epsilon_0 \frac{\partial^2 B}{\partial^2 t}
\end{aligned} \tag{C.2}
$$

Maxwell's equations imply that empty space supports the propagation of electromagnetic waves at speed of $\sqrt{1/\epsilon_0 \mu_0}$, since the contribution of Maxwell's term to Ampere's law allow it.

Monochromatic Plane Waves

The most basic expresion for a wave is to be a monochromatic wave (where we only include one frequency) and aslo a plane wave, where the direction of the propagation will be perpendicular to the fields (transverse). Considering the complex expression. These wave are transverse, from (i) in C.1:

$$
\begin{aligned}
\bar{\nabla} \cdot \bar{E} = 0 \rightarrow \bar{\nabla} \cdot (\mathbf{E} e^{i(k \cdot r - \omega t)}) &= 0 \\
\mathbf{E}(ik \cdot r) e^{i(k \cdot r - \omega t)} &= 0 \\
k \cdot r &= 0,
\end{aligned} \tag{C.3}
$$

both fields **E** and **B** are perpendicular to each other. Also they are in phase:

$$
\mathbf{B}(r,t) = \frac{k}{\omega}(\hat{k} \times \bar{E}), \tag{C.4}
$$

and the monochromatic planes waves can be expressed as:

$$
\begin{aligned}
E(\boldsymbol{r},t) &= E_0 e^{i(k \cdot \boldsymbol{r} - \omega t)} \hat{n} \\
B(\boldsymbol{r},t) &= \frac{1}{c} E_0 e^{i(k \cdot \boldsymbol{r} - \omega t)} (\hat{k} \times n) = \frac{1}{c} k \times E
\end{aligned} \tag{C.5}
$$

where $\hat{n}$ is the polarization of the electric field. We can have a number of quantities as the energy density (energy per volume) stored in the EM wave, the flux of energy (Poynting vector) and the density of momentum($\wp$):

$$u = \frac{1}{2}(\epsilon_0 E_0^2 + \frac{1}{\mu_0}B_0^2) \rightarrow = \frac{\epsilon_0}{2}E^2$$
$$\vec{S} = \frac{1}{\mu_0}(\bar{E} \times \bar{B}) \rightarrow = cu\hat{k} \tag{C.6}$$

The flux of energy over a time Δt is th density of energy that passes throught a volume in the time Δt with velocity c. Particles are accelerated in RF systems by the transversal TM or TE waves where energy is transfered to them.

C.1.2 Electromagnetic waves in Matter

RF cavities are not hollow, they use dielectrics for example in order to tune the magnetic field inside them. That is why we describe quickly the EM waves in matter. The EM formalism make simple the study this subject, by just replacing $\epsilon_0, \mu_0 \rightarrow \epsilon, \mu$ we get the former results.

$$\begin{aligned} &(i)\nabla \cdot \mathbf{D} = 0, \qquad &(iii)\nabla \times \mathbf{E} = -\frac{\partial \mathbf{B}}{\partial t} \\ &(ii)\nabla \cdot \mathbf{B} = 0, \qquad &(iv)\nabla \times \mathbf{H} = \mu_0\epsilon_0\frac{\partial \mathbf{D}}{\partial t} \end{aligned} \tag{C.7}$$

with no charge and no currents, again we have the 3D equation but considering the linearity of the fields $\bar{D} = \epsilon\bar{E}$ and $\frac{1}{\mu}\bar{B} = \bar{H}$, the explict expresion for the electric and magnetic field are:

$$E(\boldsymbol{r}, t) = E_0 e^{i(k\cdot\boldsymbol{r} - \omega t)}\hat{n}$$
$$B(\boldsymbol{r}, t) = \frac{1}{v}E_0 e^{i(k\cdot\boldsymbol{r} - \omega t)}(\hat{k} \times n) = \frac{1}{v}k \times E \tag{C.8}$$

The index of refraction is defined as:

$$n = \sqrt{\frac{\epsilon\mu}{\epsilon_0\mu_0}} = \frac{c}{v} \tag{C.9}$$

usually the $\mu_0 \simeq \mu$ so $n \simeq \sqrt{\epsilon_r}$.

C.1.3 Electromagnetic Waves in Conductors

So far we know that EM in vacuum or matter accept monochromatic plane waves that propagate along the space with a well define velocity. In both cases, when there reach a surface, the EM wave will have a reflected, transmitted and incident wave. EMW in conductors consider the existence of free charges and currents, that we don't control ρ_f and $\mathbf{J} = \sigma\mathbf{E}$(which follows) the Ohm's Law so the Maxwell's equation are:

$$\begin{aligned} (i)\nabla\cdot\mathbf{E} &= \frac{1}{\epsilon}\rho_f & (iii)\nabla\times\mathbf{E} &= -\frac{\partial\mathbf{B}}{\partial t} \\ (ii)\nabla\cdot\mathbf{B} &= 0, & (iv)\nabla\times\mathbf{B} &= \mu_0\epsilon_0\frac{\partial\mathbf{E}}{\partial t} + \mu_0 J_f \end{aligned} \tag{C.10}$$

working the math in the solution, we get two partial differential equation that resembles the 3D wave equation but with the add of the third term $\mu_0\epsilon_0\frac{\partial}{\partial t}$. Monochromatic waves are still solutions of theses equations but now k is complex. The imaginary part represent the attenuation that the material exert over the wave.

$$\bar{E}(\bar{r},t) = \bar{E}e^{-\kappa z}e^{i(\bar{r}\cdot\bar{k}-\omega t)} \tag{C.11}$$

Reflection at a Conducting Surface

Consider that in the region of study, there are free charge ρ_f and free current density J_f electric and magnetic fields in both boundaries (in the last section we did not consider that). From the Mawxell's equations, the boundaries conditions are:

$$\begin{aligned} \bar{E}_1^{\parallel} &= \bar{E}_2^{\parallel} & \bar{B}_1^{\perp} &= \bar{B}_2^{\perp} \\ \epsilon_1\bar{E}_1^{\perp} - \epsilon_2\bar{E}_2^{\perp} &= \sigma_f & \frac{1}{\mu_1}\bar{B}_1^{\parallel} - \frac{1}{\mu_1}\bar{B}_2^{\parallel} &= \bar{K}_f\times\hat{n} \end{aligned} \tag{C.12}$$

The surface will produce from an incident monochromatic, a reflected and transmitted wave in defined ratios[1].

[1] The ratios are:

$$E_{O_R} = (\frac{1-\beta}{1+\beta})E_{O_R}, \qquad E_{O_T} = (\frac{2}{1+\beta})E_{O_R}$$

where $\beta = \frac{\mu_1 v_1}{\mu_2 v_2}$ is a complex number (since the number propagation for a linear media is also

In the case of a perfect conductor β is infinite and the incident wave will be totally reflected, with a -180 phase shift.

C.2 Guide Waves and Resonant Cavities

The generation and transmission of electromagnetic radiation involves metallic structures with dimensions comparable to wavelengths (meters) that we are working with. Hollow metallic cylinders that produce the propagation or excitation of electromagnetic waves are called **wave guide**. Maxwell's equations for this case are (we assume a perfect conductor):

$$\begin{array}{ll} (i)\nabla\cdot\mathbf{E}=0 & (iii)\nabla\times\mathbf{E}=-\dfrac{\partial\mathbf{B}}{\partial t} \\ (ii)\nabla\cdot\mathbf{B}=0, & (iv)\nabla\times\mathbf{B}=\mu\epsilon\dfrac{\partial\mathbf{E}}{\partial t} \end{array} \tag{C.13}$$

The cylinder is filled with a uniform nondissipative medium having diaelectric constant ϵ and permeability μ, both **E** and **B** satisfy:

$$(\nabla^2+\mu\epsilon\frac{\omega^2}{c^2})\begin{Bmatrix}\mathbf{E}\\ \mathbf{B}\end{Bmatrix}=0 \tag{C.14}$$

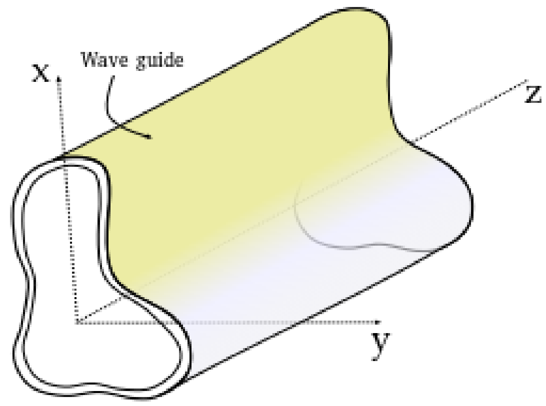

(a) A simple wave guide, with a specific transversal shape where the EM wave enters.

(b) Five-resonator triple-post waveguide band-pass filter made by Ferranti. Source Wikipedia CC1.0.

Figure C.1: Examples of wave guides.

complex taking account the attenuation of the wave).

The general solution will include a the sinusoidal dependece $e^{-i\omega t}$ from the monochromatic plane waves and a cylindrical symmetry:

$$\begin{aligned} \mathbf{E}(x,y,z,t) &= \mathbf{E}(x,y)e^{\pm ikz-i\omega t} \\ \mathbf{B}(x,y,z,t) &= \mathbf{B}(x,y)e^{\pm ikz-i\omega t} \end{aligned} \tag{C.15}$$

$\pm$ describe the appropiate combination for standing or travelling waves in the z direction. The wave number k is unknow. Making explicit the z-dependence eq. C.14 takes the form:

$$[\nabla_t^2 + (\mu\epsilon\frac{\omega^2}{c^2} - k^2)]\begin{Bmatrix}\mathbf{E}\\ \mathbf{B}\end{Bmatrix} = 0 \tag{C.16}$$

Manipulating the eq. C.13 to C.16, for the simple case of the x-component we have:

$$\begin{aligned} \nabla\times\mathbf{E} &= -\frac{\partial B}{\partial t} \\ &= (\frac{\partial E_z}{\partial y} - \frac{\partial E_y}{\partial z})\hat{i} + (\frac{\partial E_x}{\partial z} - \frac{\partial E_z}{\partial x})\hat{j} + (\frac{\partial E_y}{\partial x} - \frac{\partial E_x}{\partial y})\hat{k} \\ &= i\omega B_x\hat{i} + B_y\hat{j} + B_z\hat{k} \end{aligned} \tag{C.17}$$

with similar expression for $B_{x,y,z}$. Since $\partial E_x/\partial z = E_{0x}e^{i(kz-\omega t)} = ikE_x$, after doing the math we get for the particular case:

$$E_x = \frac{i}{(\omega/c)^2 - k^2}(k\frac{\partial E_z}{\partial x} + \omega\frac{\partial B_z}{\partial y}) \tag{C.18}$$

and for the general case:

$$\mathbf{B}_t = \frac{1}{(\mu\epsilon\frac{\omega^2}{c^2} - k^2)}[\nabla_t(\frac{\partial B_z}{\partial z}) + i\epsilon\mu\frac{\omega}{c}\hat{k}\times\nabla_t E_z] \tag{C.19}$$

$$\mathbf{E}_t = \frac{1}{(\mu\epsilon\frac{\omega^2}{c^2} - k^2)}[\nabla_t(\frac{\partial E_z}{\partial z}) - i\epsilon\mu\frac{\omega}{c}\hat{k}\times\nabla_t B_z] \tag{C.20}$$

We assumed a perfect conductor in the surface of the wave guide so: $E^{||} = 0$ and $B^{\perp} = 0$ inside the material itself and the inner wall, or:

$$\mathbf{n}\cdot\mathbf{B} = 0, \qquad \mathbf{n}\times\mathbf{E} = 0 \tag{C.21}$$

the vanishing tangential electric field **E** at the surface means $E_z|_S = 0$), while the perpendicular component of **B** equal to zero implies: $\frac{\partial B_z}{\partial n}|_S = 0$ where $\partial/\partial n$ is the normal derivative at a point on the surface.

This two boundary conditions can not generally be satisfied simultaneously, therefore we have two distinct categories of EMW that can exist in the wave guide: a **tranverse magnetic** mode (TM) and a **transverse electric** mode (TE).

$$\begin{array}{ll} & \text{Transverse Magnetic (TM)} \\ B_z = 0, \text{ everywhere. Boundary condition:} & E_z|_S = 0 \\ & \text{Transverse Electric (TE)} \\ E_z = 0, \text{ everywhere. Boundary condition:} & \frac{\partial B_z}{\partial n}|_S = 0 \end{array} \tag{C.22}$$

From eq. C.19 and C.20 we see that if we find the Ez or Bz we can determine the appropiate solutions for the two-dimesional transverse wave equation. A special case when both conditions are met is call TEM mode, and in this case the wave number $k = \sqrt{\mu\epsilon}\omega/c$

From eq. C.19 and C.20 and considering a dependece in z of e^{ikz}

TM waves:

$$E_t = \frac{ik}{\gamma^2}\nabla_t E_z, \quad B_t = \frac{\mu\epsilon\omega}{ck}\hat{k} \times \nabla_t E_z$$

TE waves:

$$E_t = \frac{ik}{\gamma^2}\nabla_t B_z, \quad E_t = \frac{\omega}{ck}\hat{k} \times \nabla_t B_z$$

As mentioned before for TM mode it is enough to know E_z and for TE; B_z. $\psi = (E_z, B_z)$ has to satisfies the two-dimesional wave equation C.14 for the z component:

$$(\nabla_t^2 + \gamma^2)\psi = 0 \tag{C.23}$$

with the boundary conditions C.22 correspondingly for TM(TE) waves.

$$\psi|_S = 0 \quad \text{, or} \quad \frac{\partial \psi}{\partial n}|_S = 0 \tag{C.24}$$

From this, it is clear that constant γ is not negative and will take a spectrum of eigenvalues γ_λ^2, and the differents solutions for $\lambda = 1, 2, 3, ...$ will be *modes of the guide*. For a frequency ω the wave number is determined according to the values that λ takes:

$$k_\lambda^2 = \mu\epsilon(\frac{\omega^2}{c^2} - \gamma_\lambda^2), \tag{C.25}$$

ω_λ is defined as the cutoff frequency:

$$\omega_\lambda = c\frac{\gamma_\lambda}{\sqrt{\mu\epsilon}} \tag{C.26}$$

and the wave number can be written as:

$$k_\lambda = \frac{1}{c}\sqrt{\mu\epsilon}\sqrt{\omega^2 - \omega_\lambda^2} \tag{C.27}$$

it can be seen that, for $\omega > \omega_\lambda$ the wave number is real and the wave propagates throught the wave guide. When it is not positive, k_λ is imaginary, and it is attenuated while it propagates.

C.2.1 Resonant Cavities

A special type of cylindrical wave guides with end faces are called cavities, as can be seen in the fig. C.2. The cavity's wall are taken to have infinite conductivity, while the cavity is filled with a lossless diaelectric with constants μ, ϵ.

Now we have to take into account the full reflections on the ends of z as a additional boundary conditions for eq. C.19 and C.19, which means that the waves will be reflected, an appropiate choose for standing waves are:

$$\psi \propto A \sin kz + B \cos kz \tag{C.28}$$

where the wave number is $k = p\frac{\pi}{d}$, and d the height of the cavity . For TM fields the, $E_t = 0$ for $z = 0$ and $z = d$ means:

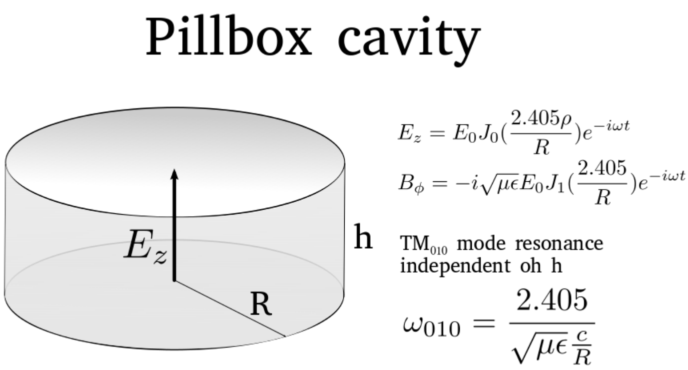

Figure C.2: A pillbox cavity. The lower mode frequency does not depend from the height of the cavity.

$$E_z = \psi(x,y)\cos(\frac{p\pi z}{d}) \tag{C.29}$$

While for TW fields, $B_z = 0$ for $z = 0$ and $z = d$ requires:

$$B_z = \psi(x,y)\sin(\frac{p\pi z}{d}) \tag{C.30}$$

The general solutions for E_t and B_t, for the transverse fields are:

$$\begin{aligned} &\text{TM waves} \\ E_t &= -\frac{p\pi}{d\gamma^2}\sin(\frac{p\pi z}{d})\nabla_t\psi \\ B_t &= -\frac{i\epsilon\mu}{c\gamma^2}\cos(\frac{p\pi z}{d})\hat{k}\times\nabla_t\psi \\ &\text{TM waves} \\ E_t &= -\frac{i\omega}{c\gamma^2}\sin(\frac{p\pi z}{d})\hat{k}\times\nabla_t\psi \\ B_t &= -\frac{i\epsilon\mu}{c\gamma^2}\cos(\frac{p\pi z}{d})\nabla_t\psi \end{aligned} \tag{C.31}$$

From C.25 the eigenvalue problem reads:

$$\gamma^2 = \mu\epsilon\frac{\omega^2}{c^2} - (\frac{p\pi}{d})^2, \tag{C.32}$$

for each value of p the eigenvalue $\gamma^2\lambda$ determines an eigenfrequency of resonance frequency $\omega\lambda p$ and the resonance frequency $\omega_{\lambda p}$ is:

$$\omega_{\lambda p}^2 = \frac{c^2}{\mu\epsilon}[\lambda_\gamma^2 + (\frac{p\pi}{d})^2] \tag{C.33}$$

A practical resonant cavity is the right circular cylinder (pillbox). Choosing cylinder coordinates in the TM mode the transverse equation has a solution that use the Bessel functions and an angular dependence in the ϕ. For $\psi = E_z$ and with the boundary conditions $E_z = 0$ at $\rho = R$, the proposed solution:

$$\psi(\rho, \phi) = J_m(\gamma_{mn}\rho)e^{\pm im\phi} \tag{C.34}$$

where, the independent variable for the Bessel functions, has a factor that depends proportionaly to the n-th root ($J_m(x) = 0$) and R, the inner radius of the cylinder:

$$\gamma_{mn} = \frac{x_{mn}}{R} \tag{C.35}$$

The resonance frequencies depend on three indexes one from the perodicity of the cavity and two from Bessel's solution It has the same structure.

$$\omega_{mnp} = \frac{c}{\sqrt{\epsilon\mu}}\sqrt{\frac{x_{mn}^2}{R^2} + \frac{p^2\pi^2}{d^2}} \tag{C.36}$$

The explicit expresions for the lowest resonance frequency in TM mode (m=0,n=1,p=0) are:

$$\omega_{010} = \frac{2.405}{\sqrt{\mu\epsilon}\frac{c}{R}} \tag{C.37}$$

$$\begin{aligned} E_z &= E_0 J_0(\frac{2.405\rho}{R})e^{-i\omega t} \\ B_\phi &= -i\sqrt{\mu\epsilon}E_0 J_1(\frac{2.405}{R})e^{-i\omega t} \end{aligned} \tag{C.38}$$

which are independent of d.

C.2.2 Power Losses in Cavity: Q of Cavity

Resonant cavities have definite field configuration for each resonance discrete frequency of oscillation. Fields will not built up unless the exciting frequency matches the resonance frequency in reality there is a narrow band of frequencies around the eigenfrequencies where excitation occurs. a measure of the sharpness of response of the cavity to external excitation is Q value of the cavity defined as:

$$Q = \omega_0 \frac{\text{Stored energy}}{\text{Power loss}} \tag{C.39}$$

definition of Q the ratio of the stored energy and the power loss times per cycle the frequency of excitation assuming ohmic losses, the behavior of the stored energy is

$$\frac{dU}{dt} = -\frac{\omega_0}{Q}U \qquad U(t) = U_0 e^{-\omega_0 t/Q} \tag{C.40}$$

for the stored energy the change of energy in time is proportional to the energy stored at that moment. This time dependence implies that the electric field is also damped

$$E(t) = E_0 e^{-\omega_0 t/2Q} e^{-i\omega_0 t} \tag{C.41}$$

but accepting that there is no single frequency but a superposition of frequency around $\omega = \omega_0$, the Fourier decomposition regarding the energy's frequency will be:

$$E(t) = \frac{1}{\sqrt{2\pi}} \int_{-\infty}^{\infty} E(\omega) e^{-i\omega t} d\omega$$
$$E(\omega) = \frac{1}{\sqrt{2\pi}} \int_{0}^{\infty} E_0 e^{-\omega_0 t/2Q} e^{-i(\omega-\omega_0)t} dt \tag{C.42}$$

And the frequency distribution for the energy in the cavity can be calculated from

$$|E(\omega)|^2 \propto \frac{1}{(\omega-\omega_0)^2+(\omega_0/2Q)^2} \tag{C.43}$$

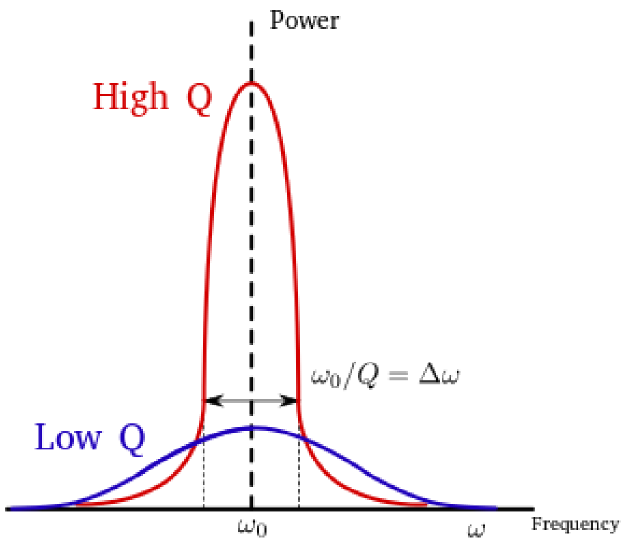

Figure C.3: The resonance curve's full width is equal to the central frequency ω_0 dived by Q.

which has a Lorentz line shape shown in the fig. C.3 with a full width at half-maximun equalto to ω_0/Q. The energy of oscillation in the cavity will follow the resonant curve in the neighborhood of the particular resonant frequency. $\Delta\omega$, the frequency separation between half-power points, so Q os the cavity can be defined as:

$$Q = \frac{\omega_0}{\Delta\omega} \tag{C.44}$$

having Q values of severald hundreds for microwave cavities.

C.3 ToF basic physics

The momentum can be determined if we know the time of flight and the path lenght with the following equation,

$$p = \frac{1}{c}\frac{L(m_0c^2)}{\sqrt{t^2c^2-L^2}} \tag{C.45}$$

with an error propagation depending on time and lenght.

$$\sigma_p^2 = \frac{t^2c^4m^2}{(t^2c^2 - L^2)^3}[L^2\sigma_t^2 + t^2\sigma_L^2] \tag{C.46}$$

also it can be derived that, two particles with the same momentum but different masses have different time of flight.

$$T_1 - T_2 = \frac{L}{c}(\sqrt{1 + \frac{m_1^2}{p^2}} - \sqrt{1 + \frac{m_2^2}{p^2}}) \tag{C.47}$$

Appendix D

Documentation of Code

D.1 Subroutines

D.1.1 Numbers of events in one subrun

Command name: `NumberEventsInSpill()`

Description: This function calculate the numbers of events in one subrun or one root file. With D.1.2 we can calculate the total number of events in a set of file, including the numbers of events for all the data set that we are analyzing.

Table D.1: Calculation of the number of events in one subrun.

Input	Description	output	Description
`char* file_name`	path of the root file to be calculated	`values_NumberEventsInSpill[r]`	numbers of the $r-th$ spills in the input file `"file_name"`
`int value_NumberSpills`	fixed value of spill number in the root files. for Run 2 (6)m for Run 3 (11)		
`int r`	number of subrun's spill that will be calculated		

D.1.2 Numbers of events for a Run

Command name: `NumberEventsInSpillForRun()`

Dependencies: D.1.1

Description: This function calculate all the events in a set of files, usually a "run". A run is a collection of subruns (usually 74 of them). The total number of subruns is defined by the tool input's limits (`file_begin` and `file_end`). Since there is no dependence in energy, this subroutine do not classify the results into energy or polarity. Each subrun is an element of the array `name_file[1000]` now set to be 1000 of file.

Table D.2: Calculation of number of events for a set of root files.

Input	Description	output	Description
`int file_begin`	first root file path to be calculated	`NumberEventsInSpillForRun.txt`	txt file with the number of events for all the files
`int file_end`	path of the last root file to be calculated		

D.1.3 Extracting the timestamp of one subrun

Command name: BeginTimeOneSubRun()
Description: Calculate the timestamp of the subrun or root file, by getting the first value that was recorded by the CAMAC TDC (that passes all the Veto conditions).

Table D.3: Getting the unix timestamp for one subrun.

Input	Description	Output: `t_begin` Description
`char* file_name`	path of the root file to be use	timestamp for the `$file_name` root file. If it is not calculated the value is set as `t_begin = -404`
`int file_end`	path of the last root file to be calculated	

D.1.4 Extracting the timestamp for the first event of all spills inside one subrun

Command name: BeginTimeOfSpillsForOneSubRun()
Description: This subroutine calculate the timestamp for the first event of all spills inside one subrun. The time is returned in Chicago local time.

Table D.4: Getting the unix timestamp for the beginning all the spills in one subrun.

Input	Description	output	Description
`char* file_name`	path of the root file to be use	`BeginTimeOfSpillsForOneSubRun[m]`	timestamp value of the beginning of the spill number m
`int m`	Spill number to be used		
`Long64_t nentries`	numbers of entries in the root file `nentries=fChain->GetEntries()`		

D.1.5 Calculation of the Kick-Off of One Subrun

Command name: KickOffOneSubRun()

Description: This subroutine calculate timestamp of the first event inside the first non-zero event spill within a subrun.

Table D.5: Return one timestamp for the real beginning of one subrun.

Input	Description	output	Description
`char* file_name`	path of the root file to be use	`value_KickOffOneSubRun`	Kick-off of the subrun
`Long64_t nentries=0`	numbers of entries in the root file `nentries=fChain->GetEntries()`		

D.1.6 Generation of txt file with timestamps of beginning of the subrun

Command name: BeginTimeForRun()

Dependencies: D.1.5 and D.1.4

Description: Create a txt file with the timestamps for two cases. If the `which_tbegin=0`, the function will record the timestamp of the beginning of the subrun using `BeginTimeOneSubRun()` (D.1.4); if `which_tbegin=0`, the data saved will be the timestamp of the first event in the subroot using `KickOffOneSubRun()` (D.1.5).

Table D.6: Function that create a txt file with beginning timestamps of root files.

Input	Description	output	Description
`int i_begin`	index of the first root file		
`int i_final`	index of the last root file		
`int which_tbegin= 0`	if we use Run 2 (0) or Run 3 (1)		

D.1.7 Matching the two closest timestamps

Command name: MatchTwoPoints()

Description:

From two set of points, this subroutine matches the closets ones. In this case, `e39time[k]` is the set of points that we need to match with `BeginTimeForRun()` time of the root file. Also, it gives the distances and both points in time.

Table D.7: Function that matches a set of two points.

Input	Description	output	Description
`int r`	index of the result	`value_MatchTwoPoints[0]`	e39time matched value
`Double_t t_begin`	input time to be matched	`value_MatchTwoPoints[1]`	delta time for the matched values
		`value_MatchTwoPoints[2]`	tbegin as an input

D.1.8 Matching two points for a set of subruns during a data run

Command name: MatchTwoPoints()

Dependencies: D.1.7

Description: Same as D.1.7 but for a set of root files. The output is txt file that is use to feed `Double_t e39times[50000]` array in `TbTaTool_files.h`.

Table D.8: Function that matches a set of two points for various root files.

Input	Description	output	Description
`int i_index =0`	beginning file index	Loop for creating a root file	`int f_index =0`
end file index			
`int fenergy = -404`	energy		
`int fpolarity=-404`	polarity		
`int which_tbegin=0`			

D.1.9 Generate a matched times analysis

Command name: GenerateMatchedTimesAnalysis()

Dependencies:D.1.7 and D.1.8

Description: Generate a analysis root file using D.1.7 and D.1.8 in order to study if the set of points given as inputs to be matched have a average delta time acceptable for the study.

Table D.9: Function that generate the plots that shows the interval between all the matched points.

Input	Description	output
`int which_tbegin`	Same condition for this input as D.1.6	Root file with the analysis of time for matched points

D.1.10 Plotting one variable against all energies of the data set

Command name: PlotOneVariableOverAllEnergies()

Description:

Generate histograms for the variable `variable1` for all `category1 = energies` and `category2 = polarities`.

Table D.10: Function that plots the histograms of one variable.

Input	Description	output
`int variable_a_analizar =0`	Since there are three types of results, this parameter indicates what tree is opened in TbTaTool::Init()	Plots of the variable for all the energies and polarities
`char* variable1="delta_time"`	variable to plot	
`char* restriction_var ="delta_time = 0”!`	restrictions to be applied to the variable	
`char* char* label_hist_result1 = "Title"`	title of the histogram	
`int nbins = 100`	numbers of bins for the histograms	
`float xmin=0`	bottom limit for the histogram	
`float xmax=200`	upper limit for the histogram	

D.1.11 Plotting stacked histograms for all energies

Command name: PlotStackAllEnergiesPionsTimeProfile()

Description:

Generate stacked histograms for the `variable1 = Time` for all the values of a `category == spills`.

Table D.11: Plotting stacked histograms for all energies

Input	Description	output
`int r =1`	Since there are three types of results, this parameter indicates tree is opened in TbTaTool::Init()	Plots of the variable for all the energies and polarities stacked (r=1)

D.1.12 Plotting one variable for polarities

Command name: PlotOneVariableOnlyPolarity()

Description:

Generate all the plots for energy and polarity for a variable (e.g. `duration_spill`).

Table D.12: Plotting one variable for polarities

Input	Description	output
`int variable_a_analizar`	Since there are three types of results, this parameter indicates tree is opened in TbTaTool::Init()	Plots for both polarities
`char* variable1="my_cycle"`	variable to plot	
`char* restriction_var ="my_cycle = 0"!`	restrictions to be applied to the variable	
`char* char* label_hist_result1 = "Title"`	title of the histogram	
`int nbins = 250`	numbers of bins for the histograms	
`float xmin=60.2`	bottom limit for the histogram	
`float xmax=60.9`	upper limit for the histogram	

D.1.13 Generating histograms for one variable for all energies and stacked them in one plot

Command name: PlotOneVariableAllEnergiesStacked()

Description:

Generate histograms for the variable `variable1` in all the energies and polarities and then stack them into one plot.

Table D.13: Generating histograms for one variable for all energies and stacked them in one plot

Input	Description	output
`int variable_a_analizar =2`	Since there are three types of results, this parameter indicates tree is opened in TbTaTool::Init()	Plots of the variable for all the energies and polarities stacked in one plot
`char* variable1="delta_time"`	variable to plot	
`char* restriction_var ="delta_time = 0"!`	restrictions to be applied to the variable	
`char* char* label_hist_result1 = "Title"`	title of the histogram	
`int nbins = 250`	numbers of bins for the histograms	
`float xmin=60.2`	bottom limit for the histogram	
`float xmax=60.9`	upper limit for the histogram	

D.1.14 GetValuesHistograms

Command name: GetValuesHistograms()

Description:

Gets the value of the events according with the conditions that generate the histograms.

Table D.14: Match of to points.

Input	Description	output
`int variable_a_analizar =0`	Since there are three types of results, this parameter indicates tree is opened in TbTaTool::Init()	Plots of the variable for all the energies and polarities
`char* variable1="delta_time"`	variable to plot	
`char* restriction_var ="delta_time = 0"` !	restrictions to be applied to the variable	

D.1.15 Production of all the analysis

Command name: GenerateDataPions()

Description:

Create, cut and plot all the variables that are presented in this thesis. This is the analogous `main()` function in a usual C++ program, which contains all the definitions and subrutines.

Appendix E

Developed Code

In this appendix I am showing the most important parts of code of the tool and some auxiliary codes. For access to the full code, please go to `https://github.com/gsalazarq/TbTaTool/tree/master/TbTaTool`

E.1 TbTaTool Time Profile (for only one subrun)

```
const char* name_file[1000] = { "/path/to/subrun1234.root" }

//Value of $39 that match the begining of the subrun 1234
const Double_t* t_begin[1000] = { 1429844171}

void TimeToolForRun::Loop()
{
TString label ="profile_spills_pions_run_2.root";
char * name_results = label;

//Creation of the ROOT File
TFile f_spill(name_results,"RECREATE");
TTree *tree_spill = new TTree("tree_spill","Tree␣Spill");

Double_t Time_spill_1b, Time_spill_2b, Time_spill_3b,
Time_spill_4b, Time_spill_5b, Time_spill_6b;
```

```
Int_t energyb, polarityb, Spill_numberb, file;

TBranch *b_Time_spill_1b = tree_spill->Branch("Time_spill_1b",
 &Time_spill_1b, "Time_spill_1b/D" );
TBranch *b_Time_spill_2b = tree_spill->Branch("Time_spill_2b",
 &Time_spill_2b, "Time_spill_2b/D" );
TBranch *b_Time_spill_3b = tree_spill->Branch("Time_spill_3b",
 &Time_spill_3b, "Time_spill_3b/D" );
TBranch *b_Time_spill_4b = tree_spill->Branch("Time_spill_4b",
 &Time_spill_4b, "Time_spill_4b/D" );
TBranch *b_Time_spill_5b = tree_spill->Branch("Time_spill_5b",
 &Time_spill_5b, "Time_spill_5b/D" );
TBranch *b_Time_spill_6b = tree_spill->Branch("Time_spill_6b",
 &Time_spill_6b, "Time_spill_6b/D" );
TBranch *b_file = tree_spill->Branch("file", &file, "file/I");
TBranch *b_Spill_numberb = tree_spill->Branch("Spill_numberb",
 &Spill_numberb, "Spill_numberb/I" );
TBranch *b_energyb = tree_spill->Branch("energyb", &energyb, "energyb/I" );
TBranch *b_polarityb = tree_spill->Branch("polarityb", &polarityb, "polarityb/I" );
1
// Definition of auxiliary variables

Double_t duration_spill_1, duration_spill_2, duration_spill_3,
duration_spill_4, duration_spill_5, duration_spill_6;
Double_t t_o_spill_absolute,code_spill_1, code_spill_2,
code_spill_3, code_spill_4, code_spill_5, code_spill_6;
Double_t exists_spill_1, exists_spill_2, exists_spill_3,
 exists_spill_4, exists_spill_5, exists_spill_6;
Double_t signal1_t_begin_spill_1, signal1_t_begin_spill_2,
 signal1_t_begin_spill_3, signal1_t_begin_spill_4, signal1_t_begin_spill_5,
 signal1_t_begin_spill_6;
Double_t Time_spill, Time_spill_1, Time_spill_2, Time_spill_3,
Time_spill_4, Time_spill_5, Time_spill_6;
Double_t Time_begin_spill, Time_begin_spill_1, Time_begin_spill_2,
Time_begin_spill_3, Time_begin_spill_4, Time_begin_spill_5, Time_begin_spill_6;
Float_t interval_between_spills = 60.53333333;
```

```
TFile *f[10000];
TTree *tree[10000];

if (fChain == 0) return; Long64_t nentries = fChain->GetEntries();
Long64_t nbytes = 0, nb = 0;

signal1_t_begin_spill_1 = 0; signal1_t_begin_spill_2 = 0;
signal1_t_begin_spill_3 = 0; signal1_t_begin_spill_4 = 0;
signal1_t_begin_spill_5 = 0; signal1_t_begin_spill_6 = 0;
Time_begin_spill_1 = -404; Time_begin_spill_2 = -404;
Time_begin_spill_3 = -404; Time_begin_spill_4 = -404;
Time_begin_spill_5 = -404; Time_begin_spill_6 = -404;

for (Long64_t jentry=0; jentry<nentries;jentry++) {
Long64_t ientry = LoadTree(jentry);                //if (ientry < 0) break;
nb = fChain->GetEntry(jentry);   nbytes += nb;

if (In_spill > 0.5 ){ if (Spill_number == 1  && exists_spill_1 != 0
){
Time_begin_spill_1 = (Double_t) Time - t_begin[i];
signal1_t_begin_spill_1 = 1;
break ;                  }                  }


for (Long64_t jentry=0; jentry<nentries;jentry++) {
Long64_t ientry = LoadTree(jentry);                 //if (ientry < 0) break;
nb = fChain->GetEntry(jentry);   nbytes += nb;
if (In_spill > 0.5 ){ if (Spill_number == 2 && exists_spill_2 != 0
){
Time_begin_spill_2 = (Double_t) Time - t_begin[i];
signal1_t_begin_spill_2 = 1;
break ;                    }                   }
}


for (Long64_t jentry=0; jentry<nentries;jentry++) {
Long64_t ientry = LoadTree(jentry);                 //if (ientry < 0) break;
nb = fChain->GetEntry(jentry);   nbytes += nb;
```

```
if (In_spill > 0.5 ){ if (Spill_number == 3  && exists_spill_3 != 0
){
Time_begin_spill_3 = (Double_t) Time - t_begin[i];
signal1_t_begin_spill_3 = 1;
break ;                      }                    }
}


for (Long64_t jentry=0; jentry<nentries;jentry++) {
Long64_t ientry = LoadTree(jentry);
//if (ientry < 0) break;
nb = fChain->GetEntry(jentry);   nbytes += nb;
if (In_spill > 0.5 ){ if (Spill_number == 4  && exists_spill_4 != 0
){
Time_begin_spill_4 = (Double_t) Time - t_begin[i];
signal1_t_begin_spill_4 = 1;
break ;                       }                    }
}


for (Long64_t jentry=0; jentry<nentries;jentry++) {
Long64_t ientry = LoadTree(jentry);
//if (ientry < 0) break;
nb = fChain->GetEntry(jentry);   nbytes += nb;
if (In_spill > 0.5 ){ if (Spill_number == 5 && exists_spill_5 != 0
){
Time_begin_spill_5 = (Double_t) Time - t_begin[i];
signal1_t_begin_spill_5 = 1;
break ;                        }                     }
}


for (Long64_t jentry=0; jentry<nentries;jentry++) {
Long64_t ientry = LoadTree(jentry);
//if (ientry < 0) break;
nb = fChain->GetEntry(jentry);   nbytes += nb;
```

```
if (In_spill > 0.5 ){ if (Spill_number == 6 && exists_spill_6 != 0
){
Time_begin_spill_6 = (Double_t) Time - t_begin[i];
signal1_t_begin_spill_6 = 1;
break ;                          }                          }
}

cout << "."; 	t_o_spill_absolute = 0;

code_spill_1 = - 404;                              code_spill_2 = - 404;
code_spill_3 = - 404;                              code_spill_4 = - 404;
code_spill_5 = - 404;                              code_spill_6 = - 404;

// = choose the absolute time considering the actual first spill that exist
if( Time_begin_spill_1 != -404 ){ t_o_spill_absolute =  Time_begin_spill_1;
 code_spill_1 =100;  }
else if( Time_begin_spill_2 != -404 ){ t_o_spill_absolute =  Time_begin_spill_2;
code_spill_2 =100; }
else if( Time_begin_spill_3 != -404 ){ t_o_spill_absolute =  Time_begin_spill_3;
code_spill_3 =100; }
else if( Time_begin_spill_4 != -404 ){ t_o_spill_absolute =  Time_begin_spill_4;
code_spill_4 =100; }
else if( Time_begin_spill_5 != -404 ){ t_o_spill_absolute =  Time_begin_spill_5;
 code_spill_5 =100; }
else if( Time_begin_spill_6 != -404 ){ t_o_spill_absolute =  Time_begin_spill_6;
code_spill_6 =100; }

// = Loop for cutting the Spills
if (fChain == 0) return;  Long64_t nentries = fChain->GetEntries();
 Long64_t nbytes = 0, nb = 0;

for (Long64_t jentry=0; jentry<nentries;jentry++) {
Long64_t ientry = LoadTree(jentry);
//if (ientry < 0) break;
nb = fChain->GetEntry(jentry);   nbytes += nb;

//Conditions for Spill has actual values
```

```
Time_spill_1b = -404; Time_spill_2b = -404; Time_spill_3b = -404;
Time_spill_4b = -404; Time_spill_5b = -404; Time_spill_6b = -404;

if (In_spill > 0.5 )
{
if (Spill_number == 1 && exists_spill_1 != 0  )
{
Time_spill_1 = (Double_t) Time -t_begin[i];
Time_spill_1b = (Double_t) Time  -t_o_spill_absolute - t_begin[i] ;
Spill_numberb = 1;
tree_spill->Fill();
}

else if (Spill_number == 2 && exists_spill_2 != 0 )
{
if(code_spill_1 != -404 ){
Time_spill_2= (Double_t) Time -t_begin[i];
Time_spill_2b = (Double_t) Time - interval_between_spills*1
- t_begin[i] - t_o_spill_absolute;
Spill_numberb = 2;
tree_spill->Fill();
}
else{
Time_spill_2= (Double_t) Time -t_begin[i];
Time_spill_2b = (Double_t) Time - interval_between_spills*0
- t_begin[i] - t_o_spill_absolute;
Spill_numberb = 2;
tree_spill->Fill();
}
}
else if (Spill_number == 3 && exists_spill_3 != 0 )
{
if(code_spill_1 != -404){
Time_spill_3= (Double_t) Time -t_begin[i];
Time_spill_3b = (Double_t) Time  - interval_between_spills*2
- t_begin[i] - t_o_spill_absolute;
Spill_numberb = 3;
tree_spill->Fill();
```

```
}
else if(code_spill_2 != -404){
Time_spill_3= (Double_t) Time -t_begin[i];
Time_spill_3b = (Double_t) Time  - interval_between_spills*1
- t_begin[i]- t_o_spill_absolute;
Spill_numberb = 3;
tree_spill->Fill();
}
else{
Time_spill_3= (Double_t) Time -t_begin[i];
Time_spill_3b = (Double_t) Time  - interval_between_spills*0
- t_begin[i]- t_o_spill_absolute;
Spill_numberb = 3;
tree_spill->Fill();
}
}
else if (Spill_number == 4 && exists_spill_4 != 0 )
{
if(code_spill_1 != -404){
Time_spill_4= (Double_t) Time -t_begin[i];
Time_spill_4b = (Double_t) Time - interval_between_spills*3
- t_begin[i] - t_o_spill_absolute;
Spill_numberb = 4;
tree_spill->Fill();
}
else if(code_spill_2 != -404){
Time_spill_4= (Double_t) Time -t_begin[i];
Time_spill_4b = (Double_t) Time - interval_between_spills*2
- t_begin[i]- t_o_spill_absolute;
Spill_numberb = 4;
tree_spill->Fill();
}
else if(code_spill_3 != -404){
Time_spill_4= (Double_t) Time -t_begin[i];
Time_spill_4b = (Double_t) Time - interval_between_spills*1
- t_begin[i]- t_o_spill_absolute;
Spill_numberb = 4;
tree_spill->Fill();
```

```
}
else{
Time_spill_4= (Double_t) Time -t_begin[i];
Time_spill_4b = (Double_t) Time - interval_between_spills*0
- t_begin[i]- t_o_spill_absolute;
Spill_numberb = 4;
tree_spill->Fill();
}
}
else if (Spill_number == 5 && exists_spill_5 != 0 )
{
if(code_spill_1 != -404){
Time_spill_5= (Double_t) Time -t_begin[i];
Time_spill_5b = (Double_t) Time  - interval_between_spills*4
- t_begin[i]- t_o_spill_absolute;
Spill_numberb = 5;
tree_spill->Fill();
}
else if(code_spill_2 != -404){
Time_spill_5= (Double_t) Time -t_begin[i];
Time_spill_5b = (Double_t) Time  - interval_between_spills*3
- t_begin[i]- t_o_spill_absolute;
Spill_numberb = 5;
tree_spill->Fill();
}
else if(code_spill_3 != -404){
Time_spill_5= (Double_t) Time -t_begin[i];
Time_spill_5b = (Double_t) Time  - interval_between_spills*2
- t_begin[i]- t_o_spill_absolute;
Spill_numberb = 5;
tree_spill->Fill();
}
else if(code_spill_4 != -404){
Time_spill_5= (Double_t) Time -t_begin[i];
Time_spill_5b = (Double_t) Time  - interval_between_spills*1
- t_begin[i]- t_o_spill_absolute;
Spill_numberb = 5;
tree_spill->Fill();
```

```
}
else {
Time_spill_5= (Double_t) Time -t_begin[i];
Time_spill_5b = (Double_t) Time  - interval_between_spills*0
- t_begin[i]- t_o_spill_absolute;
Spill_numberb = 5;
tree_spill->Fill();
}
}
else if (Spill_number == 6 && exists_spill_6 != 0 )
{
if(code_spill_1 != -404){
Time_spill_6= (Double_t) Time -t_begin[i];
Time_spill_6b = (Double_t) Time - interval_between_spills*5
- t_begin[i]- t_o_spill_absolute;
Spill_numberb = 6;
tree_spill->Fill();
}
else if(code_spill_2 != -404){
Time_spill_6= (Double_t) Time -t_begin[i];
Time_spill_6b = (Double_t) Time - interval_between_spills*4
 - t_begin[i]- t_o_spill_absolute;
Spill_numberb = 6;
tree_spill->Fill();
}
else if(code_spill_3 != -404){
Time_spill_6= (Double_t) Time -t_begin[i];
Time_spill_6b = (Double_t) Time - interval_between_spills*3
- t_begin[i]- t_o_spill_absolute;
Spill_numberb = 6;
tree_spill->Fill();
}
else if(code_spill_4 != -404){
Time_spill_6= (Double_t) Time -t_begin[i];
Time_spill_6b = (Double_t) Time - interval_between_spills*2
- t_begin[i]- t_o_spill_absolute;
Spill_numberb = 6;
tree_spill->Fill();
```

```
}
else if(code_spill_5 != -404){
Time_spill_6= (Double_t) Time -t_begin[i];
Time_spill_6b = (Double_t) Time - interval_between_spills*1
 - t_begin[i]- t_o_spill_absolute;
Spill_numberb = 6;
tree_spill->Fill();
}
else {
Time_spill_6= (Double_t) Time -t_begin[i];
Time_spill_6b = (Double_t) Time - interval_between_spills*0
 - t_begin[i]- t_o_spill_absolute;
Spill_numberb = 6;
tree_spill->Fill();
}
} // end of else if (Spill_number == 6 && exists_spill_6 != 0 )
} // end of:  if (In_spill > 0.5 )
}//end of: for (Long64_t jentry=0; jentry<nentries;jentry++)
cout << "." << endl;
}
```

E.2 TbTaTool Spill Frequency and Spill Duration (for only one subrun)

```
// ## 1
duration_spill =  duration_spill_1;
category = 1;
mi_cycle = 0;
spill_global->Fill();
// ## 2
if(signal1_t_begin_spill_1 == 1 && signal1_t_begin_spill_2 == 1){
duration_spill =  duration_spill_2;
mi_cycle = t_o_spill_2 - t_o_spill_1;
category = 1;
//myfile << mi_cycle << endl;
```

```
//myfile4 << duration_spill << endl;
spill_global->Fill();
}
else {
duration_spill =  duration_spill_2;
mi_cycle = 0;
category = 1;
spill_global->Fill();
}
```

E.2.1 Cut a variable of time into different parts according to a criteria

```
for (Long64_t jentry=0; jentry<1;jentry++) {
Long64_t ientry = LoadTree(jentry); if (ientry < 0) break;
nb = fChain->GetEntry(jentry);   nbytes += nb;
t_begin[i] = (Double_t) Time;
//myfile2 << "t_begin: "<< t_begin[i] << endl;    }
//  LOOP 1 : Begin Time for the Spill_number == 1 //
for (Long64_t jentry=0; jentry<nentries;jentry++) {
Long64_t ientry = LoadTree(jentry);
nb = fChain->GetEntry(jentry);   nbytes += nb;

if (In_spill > 0.5 ){if (Spill_number == 1 && exists_spill_1 != 0 ){
//jentry_array= (Double_t) jentry;

Time_begin_spill_1 = (Double_t) Time - t_begin[i];
t_o_spill_1 = (Double_t) Time;
signal1_t_begin_spill_1 = 1;
break ; } } }
```

E.2.2 Calculation of different variables regarding time

```
for (Long64_t jentry=0; jentry<nentries;jentry++) {
```

```
Long64_t ientry = LoadTree(jentry);
nb = fChain->GetEntry(jentry);   nbytes += nb;
//Conditions for Spill has actual values

Time_spill_1b = -1; Time_spill_2b = -1; Time_spill_3b = -1;
Time_spill_4b = -1; Time_spill_5b = -1; Time_spill_6b = -1;
mi_cycle = 0;

if (In_spill > 0.5 )                {
if (Spill_number == 1  )                   {
Time_spill_1 = (Double_t) Time -t_begin[i];
duration_spill_1 = Time_spill_1 - Time_begin_spill_1;
Time_spill_1b = (Double_t) Time - t_o_spill_1;
Spill_numberb = 1;
tree_spill->Fill();
}
else if (Spill_number == 2 )
{
Time_spill_2= (Double_t) Time -t_begin[i];
duration_spill_2 = Time_spill_2 - Time_begin_spill_2;
Time_spill_2b = (Double_t) Time - t_o_spill_2;
Spill_numberb = 2;
tree_spill->Fill();
}
```

E.3 Auxiliary Tools

E.3.1 Tool for match the $39 signal and the corresponding root file

```
if (tree_e39 == 0) return;
```

```
Long64_t nentries_e39 = tree_e39->GetEntries();
Long64_t nbytes_e39 = 0, nb_e39 = 0;

for (Long64_t jentry_e39=0; jentry_e39<nentries_e39;jentry_e39++) {
Long64_t ientry_e39 = LoadTree(jentry_e39);
//if (ientry_e39 < 0) break

nb = tree_e39->GetEntry(jentry_e39);   nbytes_e39 += nb_e39;
// if (Cut(ientry) < 0) continue;
delta_time =  t_begin[i] - unixtime_e39;

if(delta_time > 0 ){ }
else {
//myfile << delta_time_old << endl;
tree_diff->Fill();
break;
}

delta_time_old = delta_time; time_root_file = t_begin[i];
last_jentry_e39 = jentry_e39;
}
file = i ;
//tree_diff->Fill();
cout <<  i  << "." << endl  ;
```

E.3.2 Conversion between Unixtime into readable human time

Unix machines use the unixtime as the way to tag the events. This tools is useful since e39 data come into date-like format, while time in the data is in unixtime. The time of the ROOT files are 5 hours before the Central Time, which is the time at Fermilab. This correction was introduce in the data.

This code convert unixtime into human-readable date:

```
#!/usr/bin/python

import datetime
f = open("MINERVA_E39.txt","a+")
f_converted = open("unixtime_MINERVA_E39.txt","a+")
print "File␣opened"
array_months = ["MAR","APR"]
#for reading lines from a file
i = 0
for line in f:
  day = line[0:2]
  month = line[3:6]
  year = line[7:11]
  mi_cicle_line_1 = line[25:27]
  mi_cicle_line_2 = line[28:]
  mi_cicle_line = mi_cicle_line_1 + "." + mi_cicle_line_2
d = int(day)
y = int(year)

if month == array_months[0]:
  month_n = 3
else:
  month_n = 4

m = int(month_n)
time_line = datetime.datetime(y,m,d,0, 0, 0)
unix_reference = datetime.datetime(1970,1,1, 0, 0, 0)
delta_time = time_line-unix_reference
days_delta = delta_time.days

hours= line[12:14]
```

```
h=float(hours)
minutes = line[15:17]
m=float(minutes)
seconds = line[18:24]
s=float(seconds)

#calculation of the seconds
#unixtime_line = s + m*60 + h*3600 + days_delta*86400
unixtime_line = s + m*60 + h*3600 + days_delta*86400 + 5*3600
f_converted.write("%s␣\n" % str(unixtime_line) )
i=i+1
print i

#f_converted.write("%s" % mi_cicle_line)
```

The output of this code show the unixtime and the date in UCT

```
  UNIX Time             Date
1426939223        23-APR-2015_20:00:09.669
1426956777        23-APR-2015_20:01:10.234
1426957317        23-APR-2015_20:02:10.799
continues ....
```

E.4 Election of the reference point for time profile

```
// == Computing Delta Interval e39 ==

if (tree_e39 == 0) return;
Long64_t nentries_e39 = tree_e39->GetEntries();
Long64_t nbytes_e39 = 0, nb_e39 = 0;
```

```
for (Long64_t jentry_e39=0; jentry_e39<nentries_e39;jentry_e39++) {

Long64_t ientry_e39 = LoadTree(jentry_e39);
nb = tree_e39->GetEntry(jentry_e39);   nbytes_e39 += nb_e39;
delta_time =  t_begin[i] - unixtime_e39;

if(t_begin[i] != -404){
if(delta_time > 0 ){ }
else {
tree_diff->Fill();
break;}}
else{
delta_time = -404;
tree_diff->Fill();}
delta_time_e39 = delta_time;
time_root_file = t_begin[i];
time_unixtimee39 = unixtime_e39;
file = i ;}
```

E.5 Creation of ROOT Files from TXT files

```
// reading a text file
#include <iostream>
#include <fstream>
#include <string>
using namespace std;
void ReadAsciiCreateRootFile(){
TFile *f = new TFile("temp.root","RECREATE");
TTree *tree_mi_cycle = new TTree("tree_mi_cycle","Tree MI Cycle");
Double_t time_mi_cycle = 0, mi_cycle = 0 ;
TBranch *b_time_mi_cycle = tree_mi_cycle->Branch("time_mi_cycle",
&time_mi_cycle, "time_mi_cycle/D" );
```

```
TBranch *b_mi_cycle = tree_mi_cycle->Branch("mi_cycle", &mi_cycle,
"mi_cycle/D" );
string line;
ifstream myfile ("data2");
if(myfile.is_open()){
while(getline (myfile, line))
{
cout << line << "\n";
in >> time_mi_cycle >> mi_cycle; //format of the data
tree_mi_cycle->Fill();
}
myfile.close()
}
else cout << "Unable␣to␣open␣the␣file" << endl;
for(Int_t i; i<nlines; i++){
if (!in.good())
//if(nlines<5) printf("time_mi_cycle=%8f,
mi_cycle=%8f",␣time_mi_cycle,mi_cycle);
}
printf("found %d points \n",␣nlines);
in.close();
f->Write();
}
```

Bibliography

[1] E. Kh. Akhmedov. The neutrino magnetic moment and time variations of the solar neutrino flux. page 22, may 1997.

[2] L Aliaga and MINERvA Collaboration. Design, Calibration, and Performance of the MINERvA Detector. *Nucl. Instrum. Methods A*, may 2013.

[3] L Aliaga and MINERvA Collaboration. MINERvA neutrino detector response measured with test beam data. *Nuclear Instruments and Methods in Physics Research Section A: Accelerators, Spectrometers, Detectors and Associated Equipment*, 789:1–44, jan 2015.

[4] Ilka Antcheva, Maarten Ballintijn, Bertrand Bellenot, Marek Biskup, Rene Brun, Nenad Buncic, Philippe Canal, Diego Casadei, Olivier Couet, Valery Fine, Leandro Franco, Gerardo Ganis, Andrei Gheata, David Gonzalez Maline, Masaharu Goto, Jan Iwaszkiewicz, Anna Kreshuk, Diego Marcos Segura, Richard Maunder, Lorenzo Moneta, Axel Naumann, Eddy Offermann, Valeriy Onuchin, Suzanne Panacek, Fons Rademakers, Paul Russo, and Matevz Tadel. ROOT - A C++ Framework for Petabyte Data Storage, Statistical Analysis and Visualization. (September 2015):1–33, aug 2015.

[5] Michael Backfish, Leo Bellantoni, Anne Norrick, and Geoff Savage. Time Of Flight for MINERvA Testbeam II. Technical report, 2014.

[6] N. J. Baker, P. L. Connolly, S. A. Kahn, M. J. Murtagh, R. B. Palmer, N. P. Samios, and M. Tanaka. otal cross sections for $_{} n$ and $_{}p$ charged-current interactions in the 7-foot bubble chamber. *Physical Review D*, 25(3):617–623, feb 1982.

[7] D Casper. The nuance neutrino physics simulation, and the future. *Nuclear Physics B - Proceedings Supplements*, 112(1-3):161–170, nov 2002.

[8] J. Chadwick. Possible Existence of a Neutron. *Nature*, 129(3254):402–402, mar 1932.

[9] Daniel Cherdack and Elizabeth Worcester. Summary of long-baseline systematics session at CETUP*2014. page 030001, jan 2015.

[10] Bruce T. Cleveland, Timothy Daily, Raymond Davis, Jr., James R. Distel, Kenneth Lande, C. K. Lee, Paul S. Wildenhain, and Jack Ullman. Measurement of the Solar Electron Neutrino Flux with the Homestake Chlorine Detector. *The Astrophysical Journal*, 496(1):505–526, mar 1998.

[11] Super-Kamiokande Collaboration. A Measurement of Atmospheric Neutrino Oscillation Parameters by Super-Kamiokande I. *Physical Review D*, 71(11):112005, jan 2005.

[12] Accelerator Division. Concepts Rookie Book. 2013.

[13] J. a. Formaggio and G. P. Zeller. From eV to EeV: Neutrino Cross Sections Across Energy Scales. *Reviews of Modern Physics*, 84(3):1307–1341, may 2013.

[14] Y. Fukuda, T. Hayakawa, and SuperKamiokande Collaboration. Evidence for Oscillation of Atmospheric Neutrinos. *Physical Review Letters*, 81(8):1562–1567, aug 1998.

[15] Thomas K Gaisser. Atmospheric Neutrino Fluxes. *Physica Scripta*, T121:51–56, feb 2005.

[16] David J. Griffiths. Introduction to Elementary Particles, 2008.

[17] Deborah a. Harris. The State of the Art of Neutrino Cross Section Measurements. *Prospects in Neutrino Physics Conference*, page 11, jun 2015.

[18] K. S. Hirata, K. Inoue, T. Ishida, T. Kajita, K. Kihara, M. Nakahata, K. Nakamura, S. Ohara, A. Sakai, N. Sato, Y. Suzuki, Y. Totsuka, Y. Yaginuma,

M. Mori, Y. Oyama, A. Suzuki, K. Takahashi, M. Yamada, M. Koshiba, K. Nishijima, T. Kajimura, T. Suda, T. Tajima, K. Miyano, H. Miyata, H. Takei, Y. Fukuda, E. Kodera, Y. Nagashima, M. Takita, H. Yokoyama, K. Kaneyuki, Y. Takeuchi, T. Tanimori, E. W. Beier, E. D. Frank, W. Frati, S. B. Kim, A. K. Mann, F. M. Newcomer, R. Van Berg, and W. Zhang. Observation of a small atmospheric v??/ve ratio in Kamiokande. *Physics Letters B*, 280(1-2):146–152, apr 1992.

[19] Edward Kearns. Experimental measurements of atmospheric neutrinos. *Nuclear Physics B - Proceedings Supplements*, 70(1-3):315–323, jan 1999.

[20] T. Leitner. *Neutrino Interactions with Nucleons and Nuclei*. Diplomat, Justus-Liebig-Universität Gießen, 2005.

[21] Andrew John Lowe. Neutrino Physics & The Solar Neutrino Problem. page 40, jul 2009.

[22] Marco Martini. Recent developments in neutrino-nucleus scattering theory. In Morfín J. da Motta H., editor, *NuFact15 : XVII International Workshop on Neutrino Factories and Future Neutrino Facilities*, Rio de Janeiro, 2015.

[23] R. N. Mohapatra, S. Antusch, K. S. Babu, G. Barenboim, M-C Chen, A de Gouvêa, P. de Holanda, B. Dutta, Y. Grossman, A. Joshipura, B. Kayser, J. Kersten, Y. Y. Keum, S. F. King, P. Langacker, M. Lindner, W. Loinaz, I. Masina, I. Mocioiu, S. Mohanty, H. Murayama, S. Pascoli, S. T. Petcov, A. Pilaftsis, P. Ramond, M. Ratz, W. Rodejohann, R. Shrock, T. Takeuchi, T. Underwood, and L. Wolfenstein. Theory of neutrinos: a white paper. *Reports on Progress in Physics*, 70(11):1757–1867, nov 2007.

[24] Mihoko M. Nojiri. Beyond the Standard Model. jun 2014.

[25] Anne Norrick. The Minerva Detector. In *MINERVA 101*, 2015.

[26] K.A. Olive. Review of Particle Physics. *Chinese Physics C*, 38(9):090001, aug 2014.

[27] Cheryl Patrick. Calculation cross-sections. 2015.

[28] Carlos Pena-Garay and Aldo Serenelli. Solar neutrinos and the solar composition problem. page 5, nov 2008.

[29] G N Perdue, L Bagby, and MINERvA Collaboration. The data acquisition system and infrastructure. *Nuclear Instruments and Methods in Physics Research Section A: Accelerators, Spectrometers, Detectors and Associated Equipment*, 694(0):179–192, 2012.

[30] M. L. Perl, G. S. Abrams, A. M. Boyarski, M. Breidenbach, D. D. Briggs, F. Bulos, W. Chinowsky, J. T. Dakin, G. J. Feldman, C. E. Friedberg, D. Fryberger, G. Goldhaber, G. Hanson, F. B. Heile, B. Jean-Marie, J. A. Kadyk, R. R. Larsen, A. M. Litke, D. L??ke, B. A. Lulu, V. L??th, D. Lyon, C. C. Morehouse, J. M. Paterson, F. M. Pierre, T. P. Pun, P. A. Rapidis, B. Richter, B. Sadoulet, R. F. Schwitters, W. Tanenbaum, G. H. Trilling, F. Vannucci, J. S. Whitaker, F. C. Winkelmann, and J. E. Wiss. Evidence for anomalous lepton production in e+-e- annihilation. *Physical Review Letters*, 35(22):1489–1492, dec 1975.

[31] Frederick Reines and Clyde L. Cowan. The Neutrino. *Nature*, 178(September):3, 1956.

[32] U Tokyo and Particle Data Group Group. Neutrino mass, mixing, and oscillations, 2014.

[33] Geralyn P. Zeller, Jorge G. Morfin, and F. (Flavio) Cavanna. *Neutrino-nucleus interactions in the few-gev region : NuInt07, the 5th International Workshop on Neutrino-Nucleus Interactions in the Few-GeV Region, Batavia Illinois, 30 May-3 June 2007*, volume 967. American Institute of Physics, 2007.